UNIVERSIDAD DE LA RIOJA

TESIS DOCTORAL

Título
Applications of computer vision techniques in precision viticulture

Autor/es
Borja Millán Prior

Director/es
Javier Tardáguila Laso

Facultad
Facultad de Ciencia y Tecnología

Titulación

Departamento
Agricultura y Alimentación

Curso Académico

Facultad de Ciencia y Tecnología

Departamento de Agricultura y Alimentación

TESIS DOCTORAL

CON MENCIÓN DE DOCTOR INTERNACIONAL

Applications of computer vision techniques in precision viticulture

BORJA MILLÁN PRIOR

SEPTIEMBRE 2017

Javier Tardáguila Laso, Profesor Titular de Producción Vegetal de la Universidad de La Rioja, como Director de esta Tesis Doctoral

INFORMA:

Que la presente Memoria de Tesis Doctoral titulada *"Applications of computer vision techniques in precision viticulture"* ha sido realizada bajo mi dirección en el Departamento de Agricultura y Alimentación de la Universidad de La Rioja por D. Borja Millán Prior.

Esta tesis reúne los requisitos propios de este tipo de trabajo: rigor científico, aportaciones novedosas y aplicación adecuada de la metodología. Asimismo, esta tesis cumple los requisitos necesarios para obtener la Mención Internacional.

Logroño, 29 de junio de 2017

Dr. Javier Tardáguila Laso
DIRECTOR DE LA TESIS DOCTORAL

Tesis por compendio de artículos según la normativa para defensa de Tesis doctoral en la Universidad de La Rioja, compuesta por los siguientes trabajos publicados:

En acceso abierto:

Aquino, A., Millan, B., Gaston, D., Diago, M.-P. & Tardaguila, J. (2015). vitisFlower®: Development and testing of a novel Android-smartphone application for assessing the number of grapevine flowers per inflorescence using artificial vision techniques. *Sensors*. 15 (9). p. 21204. DOI: 10.3390/s150921204

Diago, M., Correa, C., Millán, B., Barreiro, P., Valero, C. & Tardaguila, J. (2012). Grapevine yield and leaf area estimation using supervised classification methodology on RGB images taken under field conditions. *Sensors*. 12 (12). pp. 16988–17006. DOI: 10.3390/s121216988

Sujetos a copyright:

Diago, M.P., Sanz-Garcia, A., Millan, B., Blasco, J. & Tardaguila, J. (2014). Assessment of flower number per inflorescence in grapevine by image analysis under field conditions. *Journal of the Science of Food and Agriculture*. 94 (10). pp. 1981–1987. DOI: 10.1002/jsfa.6512

Millan, B., Aquino, A., Diago, M.P. & Tardaguila, J. (2017). Image analysis-based modelling for flower number estimation in grapevine. *Journal of the Science of Food and Agriculture*. 97 (3). pp. 784–792. DOI: 10.1002/jsfa.7797

Diago, M., Krasnow, M., Bubola, M., Millan, B. & Tardaguila, J. (2016). Assessment of vineyard canopy porosity using machine vision. *American Journal of Enology and Viticulture*. 67 (2). pp. 229–238. DOI: 10.5344/ajev.2015.15037

A mis padres

Well, I suggest you gentlemen invent a way to put

a square peg in a round hole. Rapidly.

From the film Apollo XIII (Ron Howard, 1995)

Agradecimientos

Quiero mostrar mi agradecimiento a mi director de Tesis, el profesor Javier Tardáguila Laso por su confianza, apoyo y dirección. Gracias a Javier he podido realizar esta Tesis, en un camino lleno de retos, instructivo y emocionante.

Asimismo, quiero mostrar mi agradecimiento a mis compañeros del grupo Televitis: María Paz, Arturo, Ignacio, Daniel, Juan, Salvador, Víctor y muchas más personas que durante estos años han sido soporte e impulso. Sin vosotros no hubiera sido posible.

Me gustaría agradecer especialmente a todos los compañeros y amigos del IVIA. Especialmente a José Blasco por ser mucho más que un director durante mi estancia. También todo mi agradecimiento a Sergio, Rosana, Rafa, Santiago y tantos otros por acogerme desde el principio, apoyarme, enseñarme y hacerme tan dura la vuelta.

No puedo sino agradecer a los componentes del Centro de Morfología Matemática de MINES ParisTech por su gran impacto, tanto a nivel formativo como personal. Quiero expresar mi gratitud a Santiago Velasco y Jesús Angulo por dirigir mi estancia e integrarme en "la familia CMM". Asimismo, mi más sincero agradecimiento para todos los compañeros con los que tuve la suerte de coincidir en mi estancia: gracias especialmente a Sébastien, Pierre, Gianni, Théodore y Vaïa por haberme hecho pasar tan buenos momentos.

A mi familia, por acompañarme cuando todo va bien y levantarme cuando todo parece ir mal. Esta Tesis es en buena parte vuestra.

Gracias a todos los amigos que me han impulsado con sus ánimos, y consejos apoyo y cariño.

Gracias a todos los que me habéis ayudado y mostrado el camino.

Table of contents

Figure Index

Resumen

La viticultura de precisión permite mejorar la calidad y producción de la uva, al mismo tiempo que optimiza el uso de los recursos, reduciendo el impacto ambiental. Para su correcta implementación es necesaria la medida precisa y georreferenciada del estado del viñedo, de forma que se represente la variabilidad intra e inter parcela. Los recientes progresos en sistemas de geo-posicionamiento y sensores capaces de monitorizar el viñedo de forma rápida, no invasiva y precisa han impulsado el desarrollo e implementación de la viticultura de precisión, aunque su uso comercial es limitado. Entre los diferentes tipos de sensores disponibles, destacan los basados en análisis de imagen, que están experimentando un fuerte desarrollo en los últimos años gracias a su bajo coste y amplio rango de aplicaciones. Debido a sus características, el análisis de imagen es una tecnología clave para la viticultura de precisión y su implantación comercial.

El objetivo principal de este trabajo es el desarrollo de nuevas metodologías de monitorización del viñedo mediante el análisis de imagen. Con esta finalidad se han desarrollado y evaluado nuevas técnicas para: i) estimación del número de flores por inflorescencia; ii) predicción de la cosecha; y iii) evaluación del estado de la "canopy". Para ello se han utilizado diferentes métodos de adquisición de imagen, incluyendo la captura manual, el uso de "smartphones" y la utilización de plataformas móviles que realizan la adquisición de forma automática.

La precisión del algoritmo para el conteo de flores por inflorescencia fue superior al 90% en todas las variedades evaluadas. Con el fin de facilitar el uso de esta metodología en el viñedo, se desarrolló una versión mejorada del algoritmo compatible con "smartphones" de sistema operativo Android. La aplicación fue capaz de identificar correctamente el 84% de las flores presentes por imagen, obteniendo una precisión del 94% y un error cuadrático medio (RMSE) de 37,1 en la estimación del número total de flores por inflorescencia.

La predicción de la cosecha se realizó mediante dos enfoques distintos: a partir de imágenes capturadas de forma manual utilizando un fondo blanco o con una plataforma móvil capaz de realizar la captura de forma automatizada. En el primer caso se logró la clasificación correcta del 98%

y 92% de los píxeles correspondientes a racimos y hojas respectivamente, obteniéndose la estimación de la producción con alta precisión (R^2=0,73). En el segundo caso se utilizó el modelo Booleano para mejorar la precisión de la estimación frente a oclusiones y errores de segmentación, obteniéndose un error (RMSE) de 203g por cepa.

La capacidad de medida del estado de la "canopy" mediante análisis de imagen se ha evaluado con experimentos ejecutados en Nueva Zelanda, Croacia, y España, de forma que se pudo valorar la robustez del sistema frente a diferentes variedades y sistemas de manejo. Se obtuvo un coeficiente de determinación superior a 0,90 para la relación entre el método de referencia ("point quadrat analysis") y el algoritmo de análisis de imágenes (capturadas manualmente utilizando un fondo blanco) para cada uno de los experimentos y de R^2=0,93 cuando todos los datos se analizaron de forma conjunta. Para aumentar la aplicabilidad comercial de la metodología, se modificó un "quad" de forma que la captura de las imágenes se realizara de forma automática y continua a una velocidad en torno a 7 km/h. Con esta metodología se pudo evaluar la porosidad del viñedo (R^2>0,85) y hojas expuestas (R^2>0,71), y gracias a la alta densidad de muestreo se pudieron realizar mapas representativos de la variabilidad del viñedo. Finalmente, también se evaluó la capacidad de estimar el peso de la madera de poda, que es un indicador del vigor del viñedo. Mediante el análisis de las imágenes capturadas de manera manual se obtuvo una estimación (R^2=0,91) con un error (RMSE) de 87,7g por cepa. Cuando la captura de imágenes se realizó de forma automatizada y en continuo, la precisión descendió ligeramente (RMSE=115,7; R^2=0,85), pero con una importante reducción en el esfuerzo requerido para la obtención de las imágenes.

Los resultados obtenidos muestran que el análisis de imagen es una tecnología de gran interés para la viticultura de precisión. El bajo coste de los sensores, la captura rápida y no destructiva y la alta precisión y variedad de los parámetros que pueden ser medidos representa importantes ventajas frente a los métodos clásicos. Los algoritmos desarrollados permiten la estimación del número de flores por inflorescencia, predicción de la producción y evaluación de la "canopy" con gran precisión. La posibilidad de captura de imágenes desde plataformas móviles reduce el esfuerzo de captura y permite la generación de mapas, facilitando el uso de estas técnicas a nivel comercial en el sector vitícola.

6

Palabras clave: análisis de imagen, sensores no-invasivos, estimación del número de flores, estimación de la producción, evaluación de la *canopy*, vid*Vitis vinifera* L.

Abstract

Precision viticulture is a technique that aims at improving grapevine production and quality while reducing the environmental impact by optimising resource use. For its implementation, the correct, georeferenced, precise measurement of the vine status which represent the inter- and intra-field variability is mandatory. The development of the geo-positioning systems and sensing technologies, capable of monitoring vine status in a non-invasive, fast and reliable way has stimulated the development and implementation of precision viticulture. Image analysis techniques are currently of increased interest to agricultural monitoring. Their low costs and wide range of applications make them ideal for crop status evaluation.

The main goal of this PhD thesis is to provide new reliable, objective and simple methodologies for vineyard status monitoring using image analysis. To this end, different procedures have been developed to do so: i) assessment of flower number per inflorescence; ii) estimation of the yield before harvest; and iii) evaluation of canopy status. The use of different capturing procedures (manual, smartphone based and on-the-go) was also taken into account, tested and analysed.

The algorithm developed for the assessment of flower number per inflorescence provided estimations with over 90% precision for all the studied varieties. When an improved version of this algorithm was implemented for use in an Android smartphone, the precision rose to the 94%. The new version identified 84% of the flowers present in the image correctly. The number of flower that were visible per image (not all the flowers are visible in the image due to occlusions) was used to estimate the total flower number using a non-lineal model with a root mean square error (RMSE) of 37.1.

The yield assessment before harvest was carried out using two approaches: firstly, a series of vine images were captured manually using a white screen as background, resulting in a classification performance of 98% for clusters and 92% for leaves, this allowed the assessment of the yield with $R^2 = 0.73$. Not all the berries are visible in a vine image due to occlusion from clusters or other parts of the vine. Secondly, the use of a Boolean model was used to reduce the error associated to the occlusion

and segmentation errors, resulting in an error in the yield estimation of RMSE = 203g per vine from images captured on-the-go.

Canopy status assessment was carried out with a multi-site experiment conducted in New Zealand, Croatia and Spain. The comparison between the reference method (point quadrat analysis) and the results obtained by analysis of manually captured images (taken on the field using a white screen as background) yielded a determination coefficient over 0.90 on every evaluated site and R^2=0.93 when all the data was analysed together. The following experiment was carried out using a modified all-terrain vehicle (ATV) for the automatic image capture at a speed of approximately 7 km/h. This setup permitted high sampling rate data capture and thus vine status map generation. The correlations obtained for the canopy porosity and exposed leaves showed a R^2>0.85 and R^2>0.71 respectively. Finally, the pruning wood weight is a classic vine vigour indicator. The use of manually captured images (with white screen as background) resulted in RMSE=87.7g and R^2=0.91. When the images were captured with a modified ATV the precision slightly dropped to RMSE=115.7 and R^2=0.85 but with a significant reduction in the capturing effort.

The results show how computer vision can provide valuable information on vineyard status for precision viticulture. The low cost of the sensor, its non-destructive and fast capturing process offers a great advantage over classical manual reference methods. Image analysis showed high precision in the assessment of flower number per inflorescence, yield estimation and canopy status assessment. The possibility to capture the images on-the-go greatly increases its applicability reducing the effort for data capturing and allowing map generation.

Keywords: image analysis, non-invasive sensing technologies, flower number estimation, yield estimation, canopy status assessment, grapevine, *Vitis vinifera* L.

List of abbreviations

CMOS	complementary metal-oxide-semiconductor
DGPS	differential global positioning system
EGNOS	European geostationary navigation overlay service
EU	European Union
GNSS	global navigation satellite systems
GIS	geographic information systems
GPR	ground-penetrating radar
GPS	global positioning system
HPLC	high performance liquid chromatography
LED	light emitting diode
LIDAR	light detection and ranging
NIRS	near infrared spectroscopy
NMEA	national marine electronics association
OCR	optical character recognition
PQA	point quadrat analysis
QTL	quantitative trait locus
r	correlation coefficient
R^2	determination coefficient
RGB	red, green and blue, additive colour model
RMSE	root mean square error
SSM	site specific management
SVM	support vector machine

UAV	unmanned aerial vehicle
VRA	variable rate application
VRT	variable rate technology
VSP	vertically shoot-positioned

1 Introduction

1.1 Precision viticulture

1.1.1 Definition and origin

Precision agriculture is a new term used for a technique that has been applied since the early stages of agriculture, and one of the first references of intra-field heterogeneity can be read in the Parable of the Sower[1] from the Bible (Matthew 13 v 8). Subsistence farmers noticed that the development of cultivars was not uniform in a given plot. To increase productivity, they divided their lands into smaller areas with heterogeneous characteristics that are more appropriate to the farming of a particular crop. In this sense, precision agriculture was encouraged by the need to get enough food to ensure the survival of the family (Oliver, 2010). In the second half of the XIX century the introduction of mechanization and intensive production drove the change of merging small fields into larger ones. This increase in plot area was motivated by the use of tractors that allow managing wider areas, which were also preferred to avoid the need for continuous manoeuvre. This resulted in an increase of the intra-plot variability and complexity with the management of new bigger plots.

The term precision agriculture appears to be first used in 1990 in a seminar held in Montana State University, but the same techniques were previously referred to as "site specific crop management" (Oliver, 2010). The modern concept of precision agriculture has been boosted by the development of new sensors, GPS technology and the use of differential corrections (DGPS), which has allowed for precise geo-localization. Furthermore, the development of geographical information systems (GIS), software used to combine the data obtained and generate maps, has

---

[1]Hearken; Behold, there went out a sower to sow: And it came to pass, as he sowed, some fell by the way side, and the fowls of the air came and devoured it up. And some fell on stony ground, where it had not much earth; and immediately it sprang up, because it had no depth of earth: But when the sun was up, it was scorched; and because it had no root, it withered away. And some fell among thorns, and the thorns grew up, and choked it, and it yielded no fruit. And other fell on good ground, and did yield fruit that sprang up and increased; and brought forth, some thirty, and some sixty, and some a hundred. And he said unto them, He that hath ears to hear, let him hear.

made possible the practical implementation of precision agriculture (Zhang et al., 2002).

Precision viticulture is a branch of precision agriculture and is stimulated by vineyard variability. The management of this variability in a uniform way reduces the quality of berries and increases management costs (Proffitt et al., 2006). Even though the results of applying precision viticulture have become quite obvious, it is a only field of study despite the fact that in the coming years a huge increase in the use of these techniques is foreseen (Schrijver, 2016).

Due to ever growing competition in the wine market, increasing grape quality and yield have become of utmost importance while reducing production costs. In this way, the viticulturist can compete better in such an environment. These objectives require a revision of the classic viticulture techniques and the application of new ones, which allows an increase in the quality and sustainability of the agricultural procedures. The optimization of field/crop inputs such as water, fertilizers and chemicals to reduce costs and ensure environmental preservation (Matese & Di Gennaro, 2015). The concept of precision viticulture pursues these objectives, providing the required information to meet the existent needs of each homogeneous and non-homogenous area within the vineyard.

Vineyards are considered to be a high value crop with an important focus on quality. Over 3 million hectares of vineyards were managed in EU during 2017 of which almost 80% were for quality wine. In 2015 Spain contained the largest area of all the EU countries devoted to grapes for wine (941,000 ha or 30% of EU total area), followed by France (803,000 ha or 25%), Italy (610,000 ha in 2010 or 19%) and, at a distance, Portugal (199,000 ha or 6%) (Eurostat, 2017). The grape production is mainly dedicated to quality, governmentally certified wine. Spain and France together accounted for about two-thirds of the total quality wine area in the EU (Eurostat, 2017).

Spatial variability of the vineyard is linked to many causes such as the heterogeneity of the field (topography elevation, slope, aspect, proximity to plot boundary and streams), soil (soil fertility, depth, water holding capacity, texture, electrical conductivity or pH), crop variability (crop density, height), anomalous factors (weed infestation, plagues, diseases,

wind or other weather event damage) and management variability (tillage, fertilizer application, cultural practices) (Zhang et al., 2002), which determines the differential response of the vineyard (Ferreira et al., 2010; Proffitt et al., 2006). However, understanding the iterations between the different factors generating this variability and the vineyard is a difficult task, which depends on the specific conditions of each plot. This can be perceived not only in the different characteristics found in wines produced in different regions, but also can be observed at the intra-plot scale (Proffitt et al., 2006). Figure 1 shows an image of a vineyard located in La Rioja's appellation (Spain) at the beginning of the season. A zone with lower vine vigour can be observed in the centre of the image, also affecting the under-vine vegetation cover. Without the information about this heterogeneity, the viticulturist has to treat the variability as "noise" (Cook & Bramley, 1998) and manage the vineyard as an homogeneous field resulting in inadequately covering the needs of all the vines or in a waste of inputs.

Figure 1: Image of vineyard at the beginning of the season located in La Rioja's appellation (Spain) where the spatial variability is visible: a low vigour zone in the centre of the image surrounded by vines with stronger vegetative development.

The re-parcelling processes carried out in developed countries has led to larger plots resulting in the rise in intra-plot variability due to different soil or topographic properties that were intrinsic to the same plot. Because of the management necessities and the development of the available technologies, the concept of precision viticulture has evolved into intra-plot management. This site-specific management (SSM) requires two components to be deployed (Proffitt et al., 2006): firstly, the development of sensors that can obtain dense sampling of the variables in a non-invasive way as not to alter the normal development of the vineyard during the season; and secondly: the geo-localization of the data under study to allow the creation of maps or zoning of the vineyard.

Precise positioning of the data obtained by means of global navigation satellite systems (GNSS) has been available since 1999. GNSS technology (of which GPS is the most widely used at present) provides current, highly accurate 3D position (x, y, z) information. The available precisions is to the centimetre when differential correction techniques are applied using a network of fixed ground-based reference stations (Matese & Di Gennaro, 2015).

The first applications of precision viticulture were conducted in the USA (Wample et al., 1999) and Australia (Bramley & Proffitt, 1999) almost simultaneously. This initial test was based on the use of load cells installed in automated harvesters to generate yield maps. The increased interest in precision viticulture techniques spurred more research works in Australia (Bramley et al., 2000; Bramley, 2001; Bramley & Lamb, 2003), France (Tisseyre et al., 2001; Ojeda et al., 2005), Italy (Matese et al., 2009) and Spain (Arnó et al., 2005; Arnó, 2005).

Research in precision viticulture is currently being performed around the world, Australia being the most advanced country (Hall et al., 2011; Liu et al., 2015, 2017), followed by USA (Nuske et al., 2011a, 2014). New world wine regions are also contributing to the development of precision viticulture: Canada (Reynolds, 2010; Marciniak et al., 2017); Chile (Sepúlveda-Reyes et al., 2016; Poblete-Echeverría et al., 2017); and South Africa (Smit et al., 2010). In Europe, the main contributions were made by France (Cerovic et al., 2012), Italy (Palliotti et al., 2011; Matese & Di Gennaro, 2015), Germany (Roscher et al., 2014; Kicherer et al., 2015a) and Spain (Bellvert et al., 2014; Diago et al., 2016a).

Apart from the first studies using load cells, other sensors utilised at the beginning of precision viticulture were soil sensors (Adamchuk et al., 2004), radiometric sensors (Zhang et al., 2002), and remote sensing (Montero et al., 1999; Flexas et al., 2000). In 2006 Proffitt et al. published a book summarising the application of these new technologies. A review article containing the techniques used for the implementation of precision viticulture was released by Arnó et al. (2009) and more recently by Matese & Di Gennaro (2015).

Image analysis techniques are especially applicable to viticulture, because of the high crop value in addition to the quality being the key to obtain a high sale price (Zarco-Tejada et al., 2014). Moreover, due to its consumer use, there is a strong interest in the development of high quality image sensors at a reduced price. Capturing good images is the first step, but it is also necessary to create algorithms that can analyse them to extract useful data. This task is known as image analysis. The applications of image analysis in precision viticulture include yield prediction at different vine development stages: pre-flowering (Liu et al., 2017); flowering (Millan et al., 2017); pre-veraison (Nuske et al., 2014; Aquino et al., 2017); and at harvest (Diago et al., 2012b; Font et al., 2015). Other applications currently being developed are canopy status assessment (Gatti et al., 2016; Kicherer et al., 2017) and plague/pest assessment (Kole et al., 2014).

The information obtained by sensors must be used for designing a management plan. Thus aiming at satisfying the specific requirements of the crop in relation to the spatial variability within the vineyard (Proffitt et al., 2006). The integration of the management plan and modern machinery create the concept of site specific vineyard management (SSM) allowing the application of inputs according to the needs of the vines instead of average quantities per hectare (Matese & Di Gennaro, 2015). This management is carried out by specialised machinery, identified as variable-rate technologies (VRT), that can be applied for the regulation of input usage such as water (Matese et al., 2009), fertilizers and pesticides (Berenstein et al., 2010).

The use of robotics in farming has become a strong development field, with many agricultural robots (agbots) already in the final stage of development, and some of which have already been put on the market (Matese & Di Gennaro, 2015). Agbots will be autonomous and able to perform various task via a reconfiguration of its structure (Schrijver, 2016).

The research on these devices is not only limited to arable land crops, but includes robots for monitoring vineyard status as VineRobot (Diago et al., 2016b), which can be seen in Figure 2, vineyard pruning robots (Botterill et al., 2016) and vineyard spraying robots (Ogawa et al., 2006).The use of such devices will have huge impact in a high value crop as vineyards, and thus the development of these technologies is expected to increase in future years. The use of agbots will transform agriculture practices, speeding up the energy transition to electricity as a power source for the machinery, minimizing soil compaction and erosion thanks to the use of lighter equipment that will be used only where and when needed. Labour requirements and resource inputs will be reduced at the same time as yield and quality are increased, resulting not only in cost optimization but also in reduced environmental impact (Schrijver, 2016).

Figure 2: VineRobot prototype for autonomous vineyard monitoring.

1.1.2 Implementation and benefits

The application of precision agriculture permits optimisation of the production steps. It is widely accepted that better decision making in agriculture practices should provide an array of benefits (Zarco-Tejada et

al., 2014). From the economic point of view, a review of 234 studies published from 1988 to 2004 revealed that the implementation of precision agriculture was profitable in an average of 68% of the cases (Griffin et al., 2004). The wine market is very competitive, and the opportunity to increase benefits provides an important advantage to the grape-growers. In contrast to other crops, quality is key in grape production. For example, in the EU, 80% of grapes produced are designated to quality wine elaboration (Eurostat, 2017).

The environmental degradation associated with agriculture is reduced by the application of precision agriculture (Zarco-Tejada et al., 2014). Environmental impact reduction was assessed by Schrijver (2016), and will include the reduction of the soil erosion (from 17 T/ha per year to 1 T/ha per year) and fuel consumption (10%) due to the use of automatic machine guidance. Schrijver (2016) also pointed out that inputs usage will be optimised, including a reduction in the cost of pesticides (up to 30%). When the vine architecture is used to optimise treatments, there can be a reduction up to 84.5% if early and localised pest or disease detection is combined with VRA. The fine tuning in the use of fertilizers will also decrease environmental impact with a reduction of the residual nitrogen in soils up to 50%, along with a reduction in soil and fertilizers run-off by controlled irrigation and soil texture maps. The use of patch herbicide spraying instead of homogeneous application can reduce herbicide needs to 20% of their current usage.

The combination of precision agriculture and the inclusion of IT in agriculture production will also contribute to food safety by improving tracking, tracing and documenting (Schrijver, 2016). The food chain will be easier to monitor by authorities, producers and consumers.

The implantation of precision agriculture also presents benefits for society and working conditions, reducing work fatigue and labour requirements (Zarco-Tejada et al., 2014).
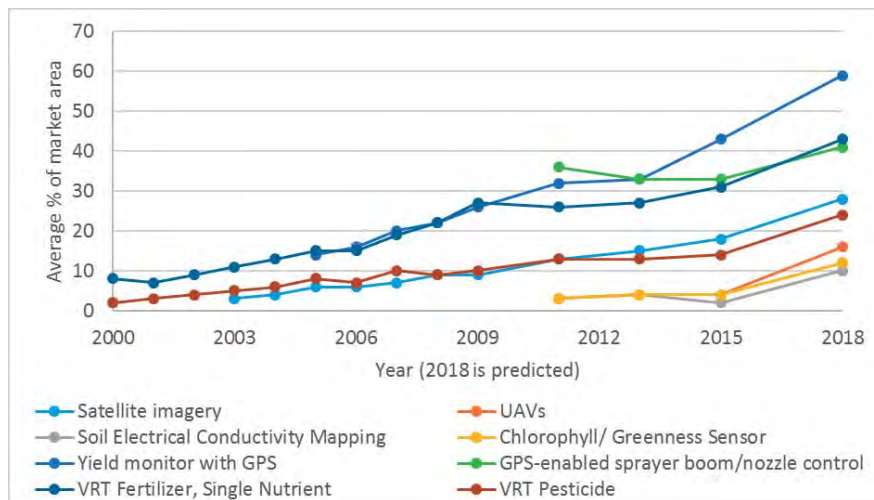
Figure 3: Producers use of precision agriculture technologies over time in USA. Data elaborated from that of Erickson & Widmar (2015). Data for 2018 is estimated.

A survey by Erickson & Widmar (2015) on the use of precision agriculture in EEUU showed an increase especially associated to VRT technologies (Figure 3). The implantation of yield monitoring systems, which are expected to be used by 60% of the producers is important to note.

The precision farming market is also expected to rise (Figure 4) up to 4.5 billion euros in 2020. The increase in the market is currently sustained, and there are no evidences of a plateau in the market size in the coming years. This is associated to a stage of introduction/growth in the product life cycle that agrees with the current stage of development of precision agriculture. The leaders in market sales are currently North America and Europe as shown in Figure 5. This leadership is expected to drive the development of new technologies these regions (Dressler et al., 2015).
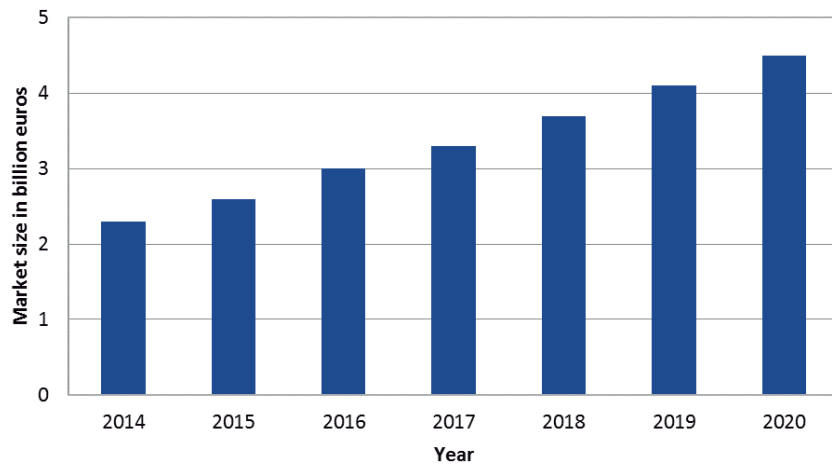
Figure 4: Estimated global precision farming market size from 2014 to 2020 (in billion euros). Data elaborated from that of Dressler et al. (2015).
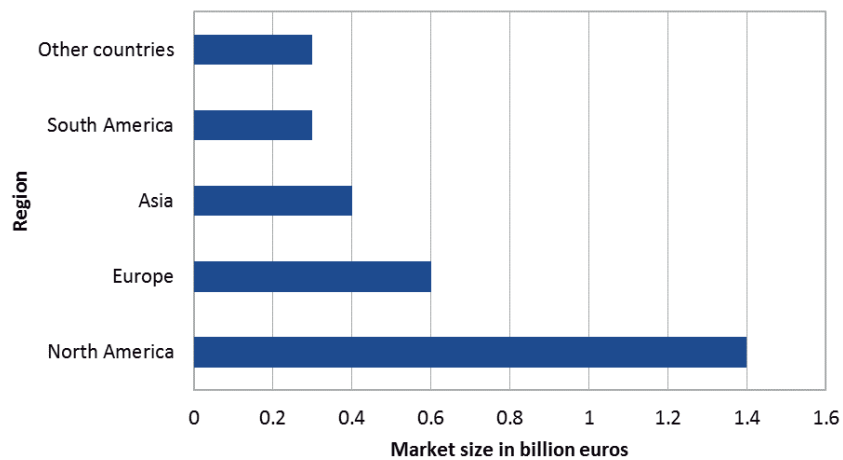
Figure 5: Estimated global precision farming market size in 2016 by region (in billion euros). Data elaborated from that of Dressler et al. (2015).

Even though the application of precision agriculture is increasing, there are barriers to its use. A report from the European Commission (Zarco-Tejada et al., 2014) identified a lack of technical expertise and knowledge,

deficiency in the infrastructures and institutional restrictions as well as high investment costs. Meanwhile, the principal impediments identified by Erickson & Widmar (2015) from the final users point of view are shown in Figure 6. The economic cost greatly limits the application, along with the stabilization in confidence by farmers over time, showing how the results of the precision agriculture are not obvious to farmers. It must be noted that this survey does not only focus on precision viticulture, but on precision agriculture as a whole. The demand for high quality in the case of grape production will probably induce the expansion of the application of precision viticulture in the future.
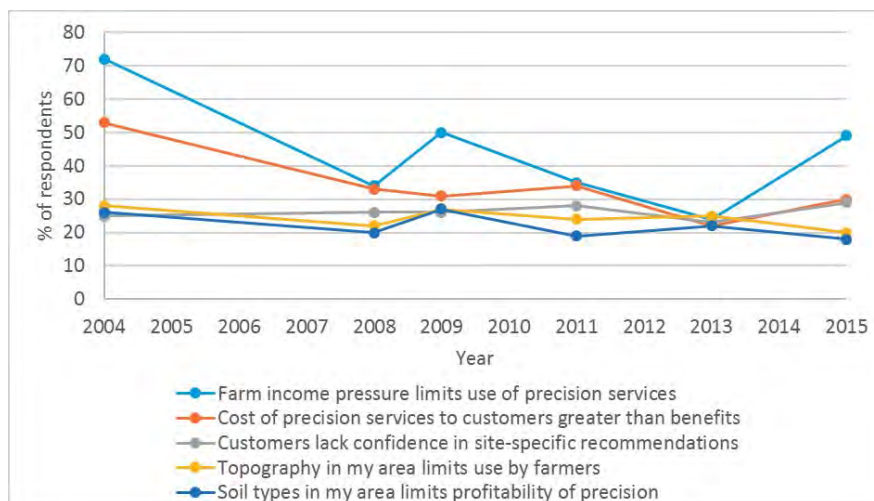
Figure 6: Barriers to the expansion of precision agriculture over time in USA. Data elaborated from that of Erickson & Widmar (2015).

On the other hand, an evaluation of the barriers faced by dealers (Figure 7), found the inadequate costs or fees to customers to be the prominent cause (related to the excessive cost perceived by the clients) and the rapid change of technologies that require constant investment. This is associated to the phase of development that is experimenting precision agriculture, which has not yet reached the plateau associated to other well-established technologies (Erickson & Widmar, 2015).
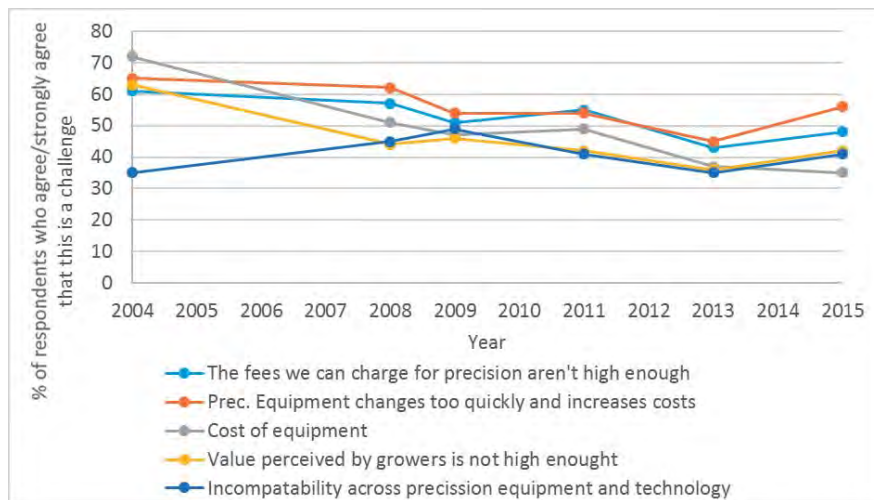
Figure 7: Dealer barriers to the expansion of precision agriculture over time in USA. Data elaborated from that of Erickson & Widmar (2015)

1.1.3 Vegetative status and yield assessment

Grapevine, as a perennial ligneous plant, has an annual growth cycle composed of vegetative and reproductive cycle (Keller, 2015). It begins with bud break (buds are the small part of the vine that rest between the vine's stem and the petiole) in the spring and ends with the leaf fall in autumn followed by winter dormancy. The fruit production cycle is comprised of 2 years: the buds that sprout in the first year give rise to shoots bearing buds which will fruit during the second season.

The transition from winter dormancy to active growth is marked by the exude of xylem sap from pruned surfaces and others wounds. This sap flow or "bleeding" is associated with the restoration of the metabolic activity in the root system and it seems to be related to soil temperature, starting when it rises above 7 °C (Keller, 2015). The initial growth of the shoots depends on the reserves stored in the roots and the wood of the vine from the previous season until the leaves start to develop, allowing the energy and the carbohydrate to be obtained from photosynthesis. In warm climates, after about 4 weeks shoots growth starts to rapidly accelerate with the shoots growing in length an average of 3 cm a day (Robinson & Harding, 2015). The shoot growth continues as the temperature rises until the onset of fruit ripening at which time the lignification occurs,

23

transforming shoots into canes. During this period the latent buds that will evolve into shoots during the next season enter a dormant state.

The flowering stage takes place 40-80 days after bud break. The vines, as other woody perennials, have a juvenile phase of 2 to 4 years before they are able to produce flowers. This phase guarantees that the reserves of the plant will be enough to support fruit production (Keller, 2015). The inflorescences are formed during the bloom the year that precedes the flowering, so the future number of inflorescences is determined the year before.

The fruit set takes place after the flowering stage. The fertilized flowers begin to develop the berry and seeds. Not every flower becomes fertilized, and the non-fertilized fall from the inflorescence. After fruit set, the grape berries are green with low sugar content; they grow until near half its final size when they enter in the veraison phase. The colour of the grape evolves to red/black or yellow/green depending on the grape varieties. This colour change corresponds to the chlorophyll in the skin being replaced by anthocyanin (red varieties) or carotenoids (white varieties) (Robinson & Harding, 2015) and marks the change from partly photosynthetic to wholly dependent on the vine for nutrient generation (Keller, 2015). After the complete ripeness of the grapes, the clusters can be harvested.

Accurate yield prediction is essential for successful yield regulation and thus to improve and maintain wine quality (Martin et al., 2003; Dunn, 2010). Traditional yield components determination is carried out by counting the number of clusters per vine and then detaching and counting the berries in the lab. This method is destructive and labour demanding, so it is difficult to increase the number of data points to accurately represent the vineyard variability. Also, the manual sampling procedure is subjective and prone to errors in yield forecasting (Clingeleffer, 2001).

The yield components are defined as the number of clusters per vine (representing 60% of yield variation), number of berries per cluster (30% of yield variation) and berry size (10% of yield variation) as studied by (Clingeleffer, 2001). The average yield can be obtained by combining these three components.

It must be noted that the 60% of the yield variability is associated to the number of cluster per vine, and this is determined during the previous season and is clearly visible during the flowering stage. The measurement

of the number of inflorescences during the flowering phase will account for a high variability; moreover, if the number of berries can be estimated from the flower number, 90% of the variation in yield is accounted for at the flowering stage, providing data with plenty of time to perform corrective management practices on the vine, if necessary.

1.2   Sensing technologies in precision viticulture

Traditional vineyard monitoring requires a lot of man-work and labour, because of the use of manual procedures (Smart & Robinson, 1991). For example, evaluation of vine vigour and vegetative growth has been traditionally done using indicators as shoot length, pruning weight, leaf area and porosity that are manually measured. Similar problems are encountered when the soil characteristics are measured, requiring labour intensive sampling as ground pits (Rossi et al., 2013). Moreover, for the assessment of plant status, the measurement of chemical compounds such as nitrogen or chlorophyll require the destructive processing of some samples and its analysis using wet chemistry, high performance liquid chromatography (HPLC) or near-infrared spectroscopy (NIRS) (Ghozlen et al., 2010). These laboratory analyses are expensive, require trained personnel and specialized equipment and are limited by the concern of the representativeness of the samples. Conversely, the use of non-invasive sensing require less time and workforce than the reference methods (Tregoat et al., 2001), thus is ideal for precision agriculture purposes.

The spatial variability associated to the vineyard requires site-specific management to obtain the best quality and yield from the vineyard. The use of fast, non-invasive sensors that can be mounted on mobile platforms for continuous measurements on-the-go (Arnó et al., 2009; Zerger et al., 2010; Matese & Di Gennaro, 2015) allows the accurate measurement of intra-vineyard variability. The next step in vineyard monitoring will be the use of robots for autonomous monitoring.

There are two basic sensor types that can be applied from a distance: active and passive sensors. Active sensors emit some sort of energy and its reflection from the surface is perceived by the sensor (Jones & Vaughan, 2010). Passive sensors measure the reflected energy originated from an external source as the sun and can measure in many ranges of the electromagnetic spectrum depending on the application. Passive sensor applications include visible range (Nuske et al., 2011a; Kicherer et al., 2017), near infrared (Fernandes et al., 2014) and short wave infrared for thermal measurements (Bellvert et al., 2014; Pou et al., 2014). Active sensors have more wide application and technologies, such as ultrasonic sensors (Palleja & Landers, 2017), LIDAR (Grocholsky et al., 2011; Mack et al., 2017; Tagarakis et al., 2017), soil sensors (Rossi et al., 2013),

fluorescence sensors (Rey-Caramés et al., 2016) or active spectral sensors (Rossi et al., 2013; Fernández-Novales et al., 2017).

The continuous advances in sensor devices, data processing and information technologies have facilitated the measurement of diverse plant status indicators. Different reviews of their application in precision viticulture have been published. It is worth mentioning the ones by Arnó et al., (2009), Zerger et al. (2010) and more recently Matese & Di Gennaro (2015).

The data obtained by using sensors must be associated to their geographical position to be able to establish vineyard variability. The geo-referencing of the data can be achieved by using the Global Navigation Satellite Systems (GNSS) technology. The GPS is the most widely used (Zarco-Tejada et al., 2014), but the European geostationary navigation overlay service (EGNOS) from the EU, Russian GLONASS or Chinese BeiDou can also be used to increase accuracy.

The analysis of the geo-referenced data recorded by different sensors is carried out using geographic information systems (GIS). GIS is a computer software that associates a database with its position, allowing for the analysis, display and storage of spatially referenced data (Proffitt et al., 2006). This software is used for mapping information in different layers, including terrain data such as slope or altitude, climatic variables, or data acquired by sensors. The layers can be represented alone or combined to determine the different management zones within a vineyard and thus enabling the use of precision viticulture.

Described and discussed below are some of the more prominent sensor technologies that are applied in precision agriculture and more specifically in precision viticulture.

1.2.1 Fluorescence sensors

Fluorescence is the rapid re-emission of absorbed radiative energy, usually at characteristic wavelengths, which corresponds to energy transitions of pigments (Jones & Vaughan, 2010). Chlorophyll fluorescence is one of the most widely used indicators of the plant health. Two types of pigments can be assessed with fluorescence sensors when applied to grapevines: leaf chlorophyll content (Rey-Caramés et al., 2016) and epidermal flavonols (Diago et al., 2012a). The Multiplex 3 (Force A) is a device composed by

light emitters and sensors and is able to measure the fluorescence without direct contact in the field (Ghozlen et al., 2010). This device can be used manually operated or vehicle mounted (Figure 8) for on-the-go monitoring (Diago et al., 2016b).

Figure 8: Multiplex sensor (Force A) mounted on an ATV.

1.2.2   Spectral sensors

The electromagnetic spectrum provides information about the chemical characteristics of an object. Certain chemical compounds have unique spectral "fingerprints" known as spectral signatures, which can be identified using spectral sensors. The applications include alterations in photosynthetic activity, nutritional status, plant health and vigour (Matese & Di Gennaro, 2015).

There are two principal sensor types: punctual radiometers and spectral cameras. The first provide spectral information for one sample point, while the cameras measure the spectrum of every pixel in the image.

The principal descriptors of these sensors are the wavelength resolution (also known as radiometric resolution) and range defining the compounds that can be identified.

Figure 9: Manually operated punctual radiometer.

There are commercial handheld radiometer devices (Figure 9) and vehicle mounted versions have recently become available on the market (Figure 10).

Figure 10: Adjustment of an ATV mounted experimental spectrometer for non-destructive assessment of berry composition.

Spectral cameras generate a hypercube containing the spectra corresponding to every pixel in the image. This hypercube can be

visualized also as composed by multiple images, each one corresponding to one waveband. The advantage of these sensors in contrast to radiometers is that dimensional information is also acquired, every pixel spectra can be easily compared with its neighbourhood, allowing the comparison between different regions. A spectral camera designed for unnamed aerial vehicle (UAV) integration is showed in Figure 11.

Figure 11: Multispectral camera with four spectral bands (Red, Green, Red edge and NIR), RGB camera, solar light spectra calibration and GPS designed for UAV integration.

1.2.3   Thermal sensors

Thermal sensors have also been used in precision viticulture to assess plant water status in the vineyard. Thermal sensors assess the surface temperature of an object from the emitted infrared radiation in a non-invasive fast way.

Leaf temperature increases with stomatal closure, interrupting the cooling effect of evapotranspiration, which occurs as a result of water stress in an attempt to reduce water consumption (Costa et al., 2010). As a result, the canopy temperature can be used as an indicator of plant water status (Jones & Vaughan, 2010; Baluja et al., 2012) and thus to regulate irrigation scheduling optimising water usage (Jones, 1999).
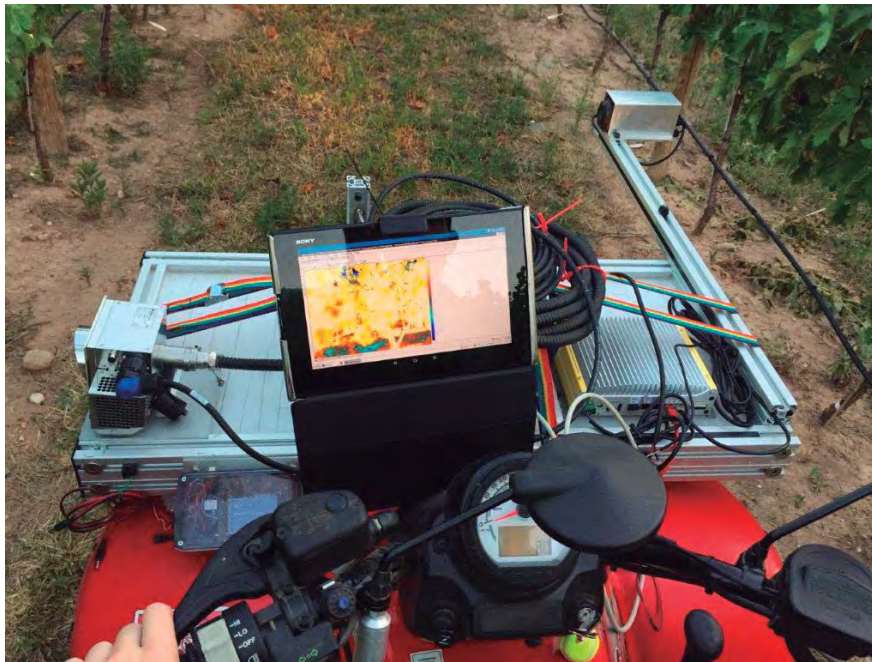
Figure 12: Thermal camera mounted on an ATV for on-the-go canopy temperature measurement. The thermal image of the canopy is shown on the tablet screen.

Applications in viticulture include punctual sensors, which only provide one value per measurement (Sepúlveda-Reyes et al., 2016), and thermal cameras (Figure 12), where temperatures corresponding to every pixel are visualised (Pou et al., 2014).

1.2.4   Electrical resistivity soil sensors

There is quite a lot of research on the relationship between soil properties, topography, vigour and plant and grape composition (Arnó, 2005; Reynolds, 2010; Tardaguila et al., 2011).

Electrical resistivity soil and inductive sensors are used to find the depth of bed rock, thickness of bands of clay, groundwater and to evaluate soil salinity. These sensors measure the electrical conductivity of the soil that is determined by the relative amounts and types of clay, salts, rock and water (Proffitt et al., 2006). The use in the vineyard includes on-the-go sensors (Figure 13) that permit fast and extensive soil mapping for site specific management (Rossi et al., 2013).

Figure 13: A resistivity soil sensor for on-the-go operation in a vineyard located in La Rioja appellation. The four rolling electrodes enabled measurements on approximately 0.5, 1 and 2 m depths.

1.2.5 RGB sensors

RGB sensors are increasingly being used in precision viticulture, mainly because of their reduced cost as a consumer technology, availability and range of applications. As opposed to other sensors, the image does not provide information by itself and must be analysed to extract it. Image analysis consist of a set of techniques that allows extracting meaningful information from images and it is a field of pertinent research and development.

RGB sensors can be operated manually, mounted in agricultural vehicles (Grocholsky et al., 2011; Gatti et al., 2016) or UAVs (Arnó et al., 2009; Matese et al., 2015). Moreover, the increase in the use of smartphones with high quality cameras and processing capabilities has permitted the development of apps that can not only take images in the field, but also analyse them (Fuentes et al., 2012b, 2012a; Aquino et al., 2015a).

A revision of the applications of RGB sensors in precision viticulture is provided in section 1.3.4.

1.3 Computer vision

1.3.1 Origin and evolution

Computer vision is a set of techniques associated to artificial intelligence, whose objective is to allow a computer to "understand" an image or more precisely "the construction of explicit, meaningful description of physical objects from images" (Ballard & Brown, 1982). It is a relatively new field with its origins back in the late 1960s. At the beginning, it was believed by some pioneers of artificial intelligence and robotics, that solving the "visual-input" problem will be an easy step to go forward with more complicated problems such as higher-level reasoning and planning (Szeliski, 2011). An anecdote that corroborated with this perception took place in MIT in 1966: the artificial intelligence group proposed a summer project for his undergraduate students. The objective was to link a camera to a computer and get the computer to describe what "it" saw (Papert, 1966).

Computer vision tries to resolve an inverse problem, attempting to discover some unknowns given insufficient information to fully identify the solution (Szeliski, 2011). Humans and animals can solve this problem effortless, while computer vision algorithms are unable to reach the performance of a two-year old baby (Szeliski, 2011). The difficulties of the "vision problem" are analysed in the next section.

David Marr created a paradigm of how vision work in his posthumous book "Vision" (Marr, 1982). In image analysis this work was probably the most influential ever produced (Huang, 1996); it set up a bottom-up approach for scene understanding (Cipolla et al., 2014): the application of low-level image processing algorithms generates the "primal sketch"; from this sketch a 2.5D one is obtained using binocular image; and, finally, high-level techniques are used to obtain 3D representation of the scene (Huang, 1996). The inherent ambiguities of optical structure greatly limit the applicability of the bottom-up representation. The generation of complete 3D models of the objects in an image is not necessary for most of the computer vision applications, therefore algorithms should be goal driven, and in many cases, can be qualitative.

In recent years, computer vision has become key technology in a wide variety of real world applications (Szeliski, 2011), which include (but is not limited to): medical imaging; photogrammetry; optical character

recognition (OCR); in-line quality inspection and control; surveillance; fingerprint recognition/biometrics; and autonomous driving.

Even when the design of computer vision algorithms is highly application dependant, there are some typical functions which are common to many setups (Sonka et al., 2008; Szeliski, 2011):

- Image acquisition: many types of sensors and capturing setups (i.e.: illumination, scene control, optics) can be used depending on the application.
- Pre-processing: includes noise reduction, contrast enhancement and other transformations to enhance the image and simplify its processing.
- Detection/segmentation: some parts of the image are selected as relevant for further processing.
- Feature extraction: different features such as lines, edges, interest points or shape/texture can be extracted.
- High-level processing: this processing is limited to segmented objects and includes the estimation of specific parameters or recognition of parameters.
- Decision making: the final decision required for the application can be generated from the extracted data.

1.3.2 Complexity of the computer vision problem

The vision problem is a very complicated task. Almost no research problem has been properly solved, and the solutions are brittle: the application of an algorithm for solving a problem can be successful in one situation but not in other (Huang, 1996). As stated in the previous section, the lack of information prevents the obtention of a solution; an overview of the problem is given below. A revision of the complex landscape of the computer vision can be viewed in Sonka et al. (2008)

The first simplification is associated to the representation of a 3d scene on a 2d image (Sonka et al., 2008). A small object close to the camera is represented in same way as a big one positioned far away, so it is not possible to solve this problem without extra information as binocular cameras or active sensors (i.e. time of fly or structured light). Also, the image capturing process is not precise and noise is inherently present in the images. Mathematical tools can be used to attenuate the effect of the noise, but at the cost of the use of more complex analysis.

34

In general, the analysis of images corresponds to the analysis of a huge amount of data (Sonka et al., 2008), which is increased if video is used. Even though technical advances in memory and computer power over the last decades has been spectacular, the amount of data limits the possibilities of real time analysis and limits the imposed use of algorithms, which utilise local windows to process the image. The analysis of regions of the image limits the capacity of context establishing and thus image understanding (Sonka et al., 2008).

The expectations of the performance of a computer vision are high because of the comparison with that of the human visual system. The human vision complexity is usually underestimated, but it is comprised by a very complex image acquisition system associated to the capacity to apply previous knowledge and experience (Huang, 1996). For example, face recognition is a task that humans can realise under all kinds of variations in illumination, viewpoint, face expression or even when the reference image was taken many years ago. Also, the "faces databank" seems also to have no limit in our brain. There appears to be little hope in building a computer vision system that can get close to this performance (Huang, 1996).

Perceptual psychologist have studied the anthropological visual procedure for decades and a complete solution to this problem was not founded yet (Szeliski, 2011). The human vision system is indeed very complex and the mind perceives more information than the raw stimulus, which is somehow processed. A clue of how the system works was tested using optical illusions. Figure 14 left shows the Kanizsa's Triangle (Kanizsa, 1997). In this illusion, a white triangle that does not exist is seen. The mind seems to perceive forms from edges and then visualises the white triangle. The Müller-Lyer optical illusion is shown in Figure 14 right, in this illusion the perceived length of the lines appears different, probably due to perspective corrections of the human visual system.
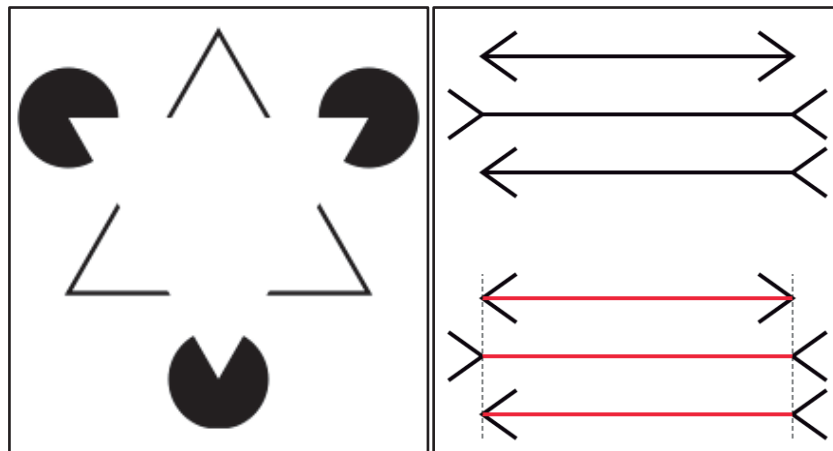
Figure 14: Left: Kanizsa's Triangle (Kanizsa, 1997) *in this optical illusion an inexistent white triangle is perceived over the rest of the figures. Right: The Müller-Lyer optical illusion where equal segments look bigger or smaller depending on whether the arrow ends point inwards or outwards. Fibonacci / Wikimedia Commons /* CC-BY-SA-3.0 */* GFDL*.*

Optical illusions prove that the human vision system is very complex and that the image analysis has a great weight in human image understanding.

1.3.3   Computer vision in precision agriculture

Computer vision-based systems are being increasingly applied to automate inspection tasks in agriculture and food processing. The use of this technology makes it feasible to monitor plant and crop development in a much faster way than any manual non-destructive procedure, allowing supervising with objectivity and repeatable criteria. The growing interest in this research topic is represented by the increase in the number of publications related to the field (Figure 15).
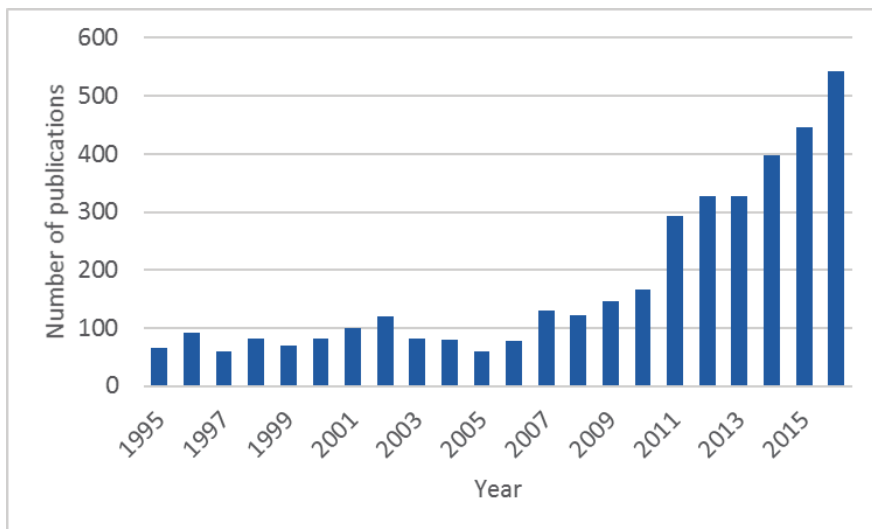
Figure 15: Number of publications listed in the web of science for the terms "computer vision and agriculture" during the last two decades. Data elaborated from that of the Web of Science.

One of the most important applications of computer vision in agriculture is the post-harvest in-line inspection and classification of fruit and vegetables. These measurements were usually done manually, in subjective, slow, expensive and tedious procedures, which was undoubtedly prone to human errors (Paulus et al., 1997). Nowadays, several manufacturers around the world produce sorting machines capable of pre-grading fruits by its characteristics, such as size, colour, texture and weight. Machine vision systems can automate these tasks increasing the repeatability, the inspection speeds, while decreasing costs. An extensive study of the different technologies and techniques was made by Sun (2016) showing not only their actual and current use, but also depicting their future challenges.

Contrary to the quality inspection of manufactured goods, vegetable and fruit inspection has great variability in its characteristics due to its biological nature. Moreover, the colour and texture of goods can evolve during time. It is necessary to generate computer vision algorithms capable of working with this variability and at the same time produce precise and repeatable measurements.

Infield monitoring also is a current field of research where computer vision can be applied to measure the status of plants. These applications added the difficulties of uncontrolled illumination and scene when compared to in-line inspection. The light conditions may change (e.g. from direct sunshine to cloudy sky) during the same capturing stage altering the colours and conditions for image formation. One of the first applications of infield computer vision was weed control and a prototype is described in Lee et al. (1996). The detection of weeds will help reduce the use of herbicides, optimising cost and environmental impact. The automatic and real-time detection of weeds is the foundation for VRA herbicide application.

Infield and pre-harvest fruit detection is another major application of computer vision. Manual yield predictions are coarse, imprecise, labour demanding and destructive. Rapid, accurate and infield fruit crop yield predictions based on computer vision will allow for managing crops, optimising harvest operations and will help growers with storing, selling and shipping decision-making.

Apart from the previous considerations and limitations with infield operations, in the case of fruit detection, the partial occlusion of fruits from other parts of the vegetation or other fruit is common; therefore, algorithms must be able to detect the fruit even when it is partially visible. Fruit detection has been applied to numerous cultivars such as mangos (Qureshi et al., 2017), apples (Wang et al., 2012), citrus fruits (Bansal et al., 2013; Sengupta & Lee, 2014), tomatoes (Schillaci G et al., 2012) and pineapples (Chaivivatrakul et al., 2010).

Given the rapid development of plant genomic technologies, the manual determination of plant phenotype limits the possibility to dissect the genetics of quantitative traits. Computer vision, as a fast and reliable tool for monitoring a high number of samples is perfect for the quantification of plant phenotypes. The development of new genotype editing techniques has driven the development of numerous applications, many of which are listed in a recent review by Li et al. (2014).

1.3.4 Computer vision in precision viticulture

The use of computer vision in viticulture is increasing owing to the advantages of vine monitoring over manual assessment. Vine status evaluation is a requisite for applying precision viticulture, whose use

improves the economic profitability, fruit quality and environmental sustainability. Although image analysis and computer vision have the potential of enhancing the speed and accuracy of many parameters assessment in precision viticulture, the task is challenging, mainly for the unstructured environment and the scarcity of stable features, which can be applied collectively in grapevines. The terrain, vegetation, visibility, illumination and atmospheric conditions are not well defined, unpredictable and variable over time. Furthermore, indicators to be measured correspond to objects with variable and non-uniform characteristics such as size, colour, shape, texture and location.

The use of inspection chambers allows obtaining images under controlled and defined conditions, including uniform illumination and structured background. Images of clusters in an inspection chamber (Figure 16) were used for the assessment of cluster yield components (berry weight, berry number and cluster weight) (Diago et al., 2015; Liu et al., 2015; Ivorra et al., 2015), and cluster compactness (Cubero et al., 2015). Individual berry weight and size can also be estimated using image analysis algorithms (Cubero et al., 2014; Kicherer et al., 2015b), reducing considerably the measuring time in some experiments such as plant phenotyping.

Figure 16: Inspection chamber for berry image acquisition. The berries were placed in a plate for proper image acquisition, the camera and the illumination were positioned in top of the chamber.

 The assessment of vineyard infection and diseases is a very subjective task, greatly affected by operator bias. Image processing of in-lab captured pictures has a great potential in the objective assessment of plant resistance and phenotype. Boso et al. (2004) conducted an experiment evaluating infection severity and evolution over leaf disks in different *cv.* Albariño clones. In a similar study, Peressotti et al. (2011) developed a semi-automatic image analysis algorithm for assessing of downy mildew sporulation on vine leaf disk to perform quantitative trait locus (QTL) analysis of infection resistance. A fully automated methodology based on fuzzy set theory was presented by Kole et al. (2014), obtaining a success rate of over 87% for the infected area segmentation. Although these methods offer important advances in plant health monitoring, they require cutting the leaves to be processed in the laboratory. A step further on this procedure was presented in Meunkaewjinda et al. (2008). They developed a methodology able to work in field, but with some restrictions in the scene (no complex background and only one leaf being examined with controlled light, orientation and size), for the analysis of manually acquired images using hybrid intelligent system.

The application of infield computer vision techniques to monitor vineyard status is an important step for site specific management. One of the most interesting techniques associated with on-site monitoring is VRA technique, which can be applied for fertilizer, pesticide and herbicide dosage optimisation. An automated vineyard foliage analysis algorithm was developed by Braun et al. (2010). The system is composed of a wide-angle camera and a distinctively coloured canvas placed behind the vineyard row, both mounted on a vehicle. The canopy is segmented using a Bayesian colour classifier and the spray flow is adapted to the canopy surface. A similar system was developed by Berenstein et al. (2010) with the advantage of not needing to place a canvas behind the vineyard row. The proposed methodology was capable of segmenting grape and foliage to guide the application of hormones and pesticides precisely. Nutritional deficiencies can also be monitored and quantified using image analysis. Potassium deficit was assessed by Rangel et al. (2016) on vine leaves using KNN-based image segmentation. The proposed methodology consisted of the analysis of images of leaves taken under controlled conditions.

Canopy monitoring is used not only for VRA but also as an indicator of vineyard status and variability. The detection of non-productive vine is a key factor in reducing the drain on infrastructure and was addressed by

green pixel thresholding in video frames by Tang et al. (2016). The assessment of manually captured images (Figure 17) to segment clusters, gaps, canes and leaves (Diago et al., 2016c) is currently being employed.

Figure 17: Manual vine imager acquisition using a tripod mounted digital camera, controlled background and semi-controlled illumination (use of a diffuser to avoid direct-sunlight).

Recently, thanks to the advance in the computing capabilities and the use of improved imaging sensors in smartphones, the development of applications for precision viticulture has become an option(Fuentes et al., 2012a, 2013; De Bei et al., 2015; Aquino et al., 2015a). Figure 18 shows the image capturing process with one of these smartphone applications.
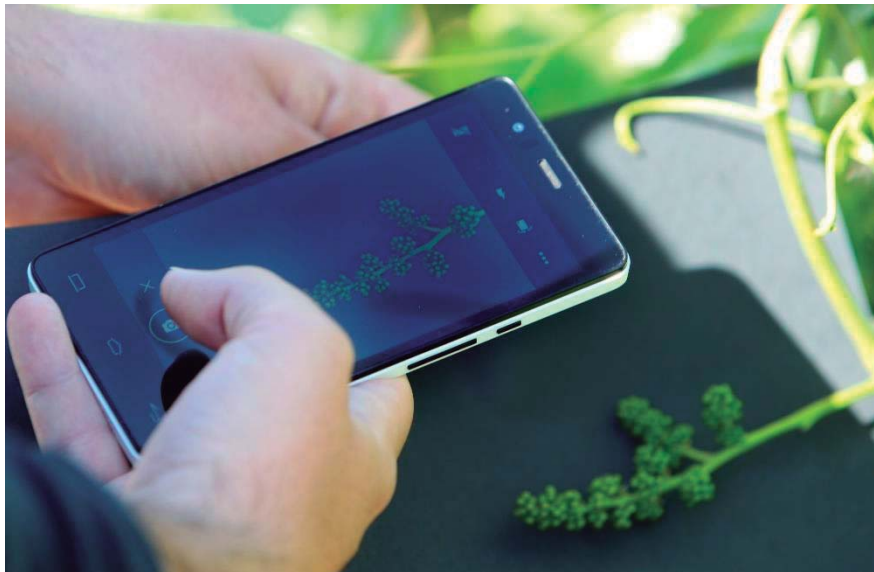
Figure 18: Infield image capture and analysis using a smartphone app (VitisFlower) for number of flower per inflorescence estimation.

Cluster detection is one of the main applications of computer vision in precision viticulture, as it allows yield forecasting and quality assessment. One of the first research projects in this field was carried out by Dunn & Martin (2004). In this study, a series of images of the canopy from Cabernet Sauvignon grapevines were manually captured, using a white screen as background. Threshold values were manually set over the RGB components to segment the fruit pixels from the images. Different image analysis techniques have been applied to grape and cluster detection: Zernike moments and SVM (support vector machine) were used by Chamelat et al. (2006) to detect grapes on images captured manually in the field. Reflection points on grapes surface generated by the artificial illumination on images captured at night was used to identify the berries by (Font et al., 2014). 3D reconstruction of bunches from images captured manually was tested by Herrero-Huerta et al. (2015).

Figure 19: Modified ATV for on-the-go RGB image capture. The vehicle is equipped with automatic triggering, camera and GNSS receiver.

The use of automated and on-the-go capturing platforms (Figure 19) reduces labour requirements and allows dense vineyard sampling. One of the first use of this capturing devices is described in Nuske et al. (2011 & 2014), who developed a computer vision algorithm based on a set of descriptors for shape, texture and colour to detect grape berries and estimate the yield from berry number. Automated image capture was also used by Font et al. (2015) to estimate the yield from the area of the segmented clusters, Liu & Whitty (2015) used it to segment cluster using SVM combining colour and texture information.

Vineyard yield can also be estimated in early stages of vine development providing more time to adjust the managing practices. Liu et al. (2017) used a shoot detection system to estimate yield from images captured with a vehicle mounted low cost camera. Manually captured images of inflorescences in conjunction with mean berry weight and berry set were also tested for yield estimation by Millan et al. (2017).

Due to the perennial nature, the acquisition of phenotypic data is mainly realized infield and by manual methods. The application of computer

vision for field phenotyping offers the advantage of the objective evaluation of the descriptors and reduces the necessary time for data acquisition. Initial research in this field was documented in Herzog et al. (2014), highlighting the importance of this field to meet the fast development of genotyping method to support grapevine breeding. A method for grapevine growth assessment using dense reconstruction was presented by Klodt et al. (2015). The presented algorithm allows monitoring leaves, stems and grapes. Winter canes also provided information about the vigour of the plant, e.g., Kicherer et al. (2017) used RGB cameras to manually capture infield images with a white screen as background to measure the potential vine balance. Other descriptors can be assessed using computer vision, such as winter grapevine buds (Pérez et al., 2017), berry number per cluster (Aquino et al., 2017) or flower number per inflorescence (Diago et al., 2014; Aquino et al., 2015b). Moreover, the automation of the image acquisition procedure to measure more than 250 vines per hour was presented in Kicherer et al. (2015a).

2 Objectives

The main objective of this PhD Thesis was to develop and apply new sensing technologies and algorithms based on computer vision to assess vineyard status (*Vitis vinifera* L.) in the scope of precision viticulture.

Along with this main goal, other specific objectives have been pursued:

- To assess flower number per inflorescence
- To estimate yield components before harvest under field conditions.
- To evaluate on-the-go canopy status, including cluster exposure, porosity and pruning weight within a vineyard.
- To develop a mobile platform for on-the-go vineyard status assessment using RGB sensors.
- To map yield components and canopy status of the vineyard.

3   Experimental section

3.1   Assessment of flower number per inflorescence

The assessment of flower number per inflorescence is a great example of the applicability of image analysis techniques to precision viticulture. The first article included in this section describes a computer vision algorithm that is capable of automating this task, with a process that does not destroy the inflorescence, and avoids interferences in the flowering process that permits studying the reproductive performance.

The applicability of image analysis algorithms for flower count has greatly increased with the development of an Android-based smartphone application. This application, reviewed in the second article included in this section, allows for rapid, non-destructive and on-the-field flower number per inflorescence assessment.

The relation between the number of flowers that are visible in an image, and the total number of flowers per inflorescence was assessed using linear and non-linear models in a wide number of varieties. Moreover, the number of flowers, as the first visible indicator of yield, was tested for yield estimation, obtaining a R^2=0.79 when combined with the fruit set value and if the average berry weight is available, the coefficient of determination rises to 0.91.

3.1.1 Number of flower per inflorescence assessment

Resumen:

El número de flores y la tasa de cuajado son factores clave que determinan la producción de la vid. Actualmente, los métodos prácticos utilizados para la determinación del número de flores por inflorescencia (un proceso necesario para el cálculo de la tasa de cuajado) son muy laboriosos y lentos. El trabajo que se presenta a continuación propone el uso de una metodología basada en el análisis de imágenes RGB para la estimación del número de flores por inflorescencia de forma automática.

Se adquirieron un total de noventa imágenes de inflorescencias de *Vitis vinifera* L. correspondientes a las variedades Tempranillo, Graciano y Mazuelo utilizando una cámara compacta. Estas imágenes se utilizaron para ajustar y evaluar los algoritmos de análisis de imagen para el conteo del número flores.

El algoritmo desarrollado fue capaz de estimar el número total de flores por inflorescencia con una precisión superior al 90% para todas las variedades evaluadas.

Contribución del autor de la Tesis:

La contribución de Borja Millán fue determinante para la realización del artículo, e incluye el diseño experimental y la generación de los algoritmos de análisis de imagen que permiten la estimación del número de flores por inflorescencia. Además, Borja Millán realizó el análisis de los resultados y la generación de modelos para el documento final.

The Publisher and copyright holder corresponds to Journal of the Science of Food and Agriculture. The online version of this journal is the following URL:

http://onlinelibrary.wiley.com/journal/10.1002/(ISSN)1097-0010

3.1.2 Smartphone app for number of flower assessment

Título de la publicación: vitisFlower® Development and testing of a novel android-smartphone application for assessing the number of grapevine flowers per inflorescence using artificial vision techniques

Autores: AQUINO, A., **MILLAN, B.**, GASTON, D., DIAGO, M.P., TARDAGUILA, J.

Resumen:

La floración y la tasa de cuajado de la vid son los factores más determinantes de la producción. En esta investigación se presenta una aplicación desarrollada para "smartphones" que permite el conteo de flores por inflorescencia de forma no invasiva a partir de imágenes capturadas en el viñedo.

La aplicación, llamada vitisFlower, guía al usuario durante la captura de la imagen, que se realiza con la cámara del propio dispositivo. La fotografía es analizada para identificar y contar las flores presentes. La aplicación es compatible con "smartphones" con sistema operativo Android y está implementada utilizando las librerías OpenCV.

VitisFlower ha sido evaluada en 140 imágenes de inflorescencias correspondientes a 11 variedades de *Vitis vinifera* L., siendo capaz de identificar correctamente más del 84% de las inflorescencias con una precisión superior al 94%. También se evaluó el rendimiento en cuatro "smartphones" que representan un amplio rango en de capacidad de procesamiento. Los análisis mostraron diferencias importantes en el tiempo necesario para el análisis de las imágenes, pero sin ser excesivo en ningún caso, por lo que la aplicación puede usarse con dispositivos de gama baja.

Contribución del autor de la Tesis:

El autor de esta Tesis realizó el diseño experimental, implementación de los algoritmos de la aplicación vitisFlower y testeo con datos de campo. Además, participó en la redacción del documento final.

OPEN ACCESS

sensors

ISSN 1424-8220
www.mdpi.com/journal/sensors

Article

vitisFlower®: Development and Testing of a Novel Android-Smartphone Application for Assessing the Number of Grapevine Flowers per Inflorescence Using Artificial Vision Techniques

Arturo Aquino [†], **Borja Millan** [†], **Daniel Gaston** [†], **María-Paz Diago** [†] **and Javier Tardaguila** *

Instituto de Ciencias de la Vid y del Vino (University of La Rioja, CSIC, Gobierno de La Rioja), 26006 Logroño, Spain; E-Mails: arturo.aquino@unirioja.es (A.A.); borja.millanp@unirioja.es (B.M.); daniel.gaston@unirioja.es (D.G.); maria-paz.diago@unirioja.es (M.-P.D.)

[†]   These authors contributed equally to this work.

*   Author to whom correspondence should be addressed; E-Mail: javier.tardaguila@unirioja.es; Tel.: +34-941-299-741; Fax: +34-941-299-720.

Academic Editor: Vittorio M. N. Passaro

Abstract: Grapevine flowering and fruit set greatly determine crop yield. This paper presents a new smartphone application for automatically counting, non-invasively and directly in the vineyard, the flower number in grapevine inflorescence photos by implementing artificial vision techniques. The application, called vitisFlower®, firstly guides the user to appropriately take an inflorescence photo using the smartphone's camera. Then, by means of image analysis, the flowers in the image are detected and counted. vitisFlower® has been developed for Android devices and uses the OpenCV libraries to maximize computational efficiency. The application was tested on 140 inflorescence images of 11 grapevine varieties taken with two different devices. On average, more than 84% of flowers in the captures were found, with a precision exceeding 94%. Additionally, the application's efficiency on four different devices covering a wide range of the market's spectrum was also studied. The results of this benchmarking study showed significant differences among devices, although indicating that the application is efficiently usable even with low-range devices. vitisFlower is one of the first applications for viticulture that is currently freely available on Google Play.

55

1. Introduction

Precision agriculture proposes the development and use of new technologies for improving crop management and quality. In the field of viticulture, there has been an increasing interest over the last few years in the development of innovative image-based techniques for objective vineyard monitoring [1–6]. This approach would allow one to increase management efficiency by providing more accurate control of agronomic parameters. Undoubtedly, it would produce an outstanding positive impact on grape-growing sustainability, as well as on grape and wine quality.

Flowering and fruit set (rate of flowers becoming grapes) are two physiological processes that strongly determine grapevine yield [7]. Furthermore, 30% of yield seasonal variation is associated with the number of berries per cluster and 60% with the number of clusters per vine [8,9], impacted by the pruning load and bud fruitfulness. The knowledge of the rate of fruit set at very early stages (prior to bunch closure) is of great value for grape growers, as this variable can be used to estimate or predict the final yield at harvest, provided a historical value of average berry weight, and the average cluster number per vine for each vineyard is available for each vineyard. Flowering and fruit set, together with berry size, have also a great impact on grape and wine quality, since they define the number of berries per cluster and contribute to determining the cluster architecture and compactness, which are a recognized key indicators of grape and wine quality [10]. Due to their importance and multi-factorial variability [7,11,12], there are a great number of viticultural actions aimed at controlling their behavior [7,13–19]. So far, flowering and fruit set cannot be accurately assessed, since manual flower counting is unfeasible, as it is extremely time and labor demanding, besides being mostly destructive.

The huge recent progress of mobile devices (also known as smartphones) has opened a wide range of opportunities that were previously unviable. Their portability, accessibility, computing performance and the high quality of the cameras they currently include are features that have enabled the development of innovative applications in fields, like medicine, sport, geography and agriculture, among others. Specifically, in viticulture, there are still not many examples of smartphone applications. One of them was recently presented by De Bei *et al.* [20,21]. These authors developed an application for measuring grapevine canopy architecture using image analysis techniques on images acquired with the device's camera. The application was developed exclusively for iOS smartphones, not being commercial yet.

The goal of the present work was to develop and to test the reliability and computational efficiency of a novel smartphone application, called vitisFlower®, for automatically, efficiently and non-invasively counting flowers in grapevine inflorescence images taken directly in the vineyard. This application benefits from the fact that the number of flowers in an inflorescence image is strongly correlated to the actual flower number in the real inflorescence [22], to provide the user with a powerful tool for flowering assessment. The application, called vitisFlower®, was developed and implemented for Android devices with the aim of maximizing its availability to users, since this operating system is the most extended

56

worldwide [23]. The application was tested following a double approach. On the one hand, the application was tested by taking and analyzing 140 inflorescence images of 11 grapevine varieties using two different devices: a high-end and a mid-range device. In this way, not only its accuracy in detecting grapevine flowers was evaluated, but also its reliability to properly work on devices of different capabilities. On the second hand, the application's computational efficiency was also evaluated by performing a benchmarking study using four devices covering the whole market spectrum.

2. Experimental Section

2.1. Image Analysis for Flower Counting in Grapevine Inflorescences

vitisFlower® is a newly-developed application for Android devices that allows one to take a photo of a grapevine inflorescence for its analysis. This analysis, based on the methodology proposed and validated in [22], implements artificial vision algorithms aimed at counting the number of flowers per inflorescence in the image.

The methodology for counting grapevine flowers is based on mathematical morphology and statistical techniques. It has a pre-requisite, which involves taking the photo by placing dark cardboard behind the inflorescence for allowing its segmentation from the background. Once the image is correctly acquired, the methodology can be divided into three steps:

- Image pre-processing: this step basically consists of automatically segmenting the inflorescence from the background using color discrimination criteria (invariant to light conditions) for computing a region of interest (ROI).
- Image analysis: in this step, the detection of flower candidates is achieved. Flowers are quasi-spherical in shape, so they produce a point of maximum light reflection. Therefore, flower candidates are identified in the area of the image delimited by the ROI as those connected components being regional maxima in the lightness channel of the Lab color space (concretely the Lab space used was CIE 1976 L*a*b* [24]).
- Image post-processing: this final stage intends to remove those regional maxima not corresponding to real flowers in the image. It is carried out by sequentially applying these two statistical filters:

    1. Region size filter: removal of those candidates with a size larger than expected, taking into account the statistical size distribution of the candidates.
    2. Shape filter: due to the geometry of a flower, the area of maximum light reflection on its surface is expected to describe a quasi-circular shape; therefore, this filter eliminates those candidates describing elongated configurations.

Once flower candidates are filtered, the remaining ones are definitely considered as real flowers and counted. As an example, Figure 1a shows a photo of a grapevine inflorescence on dark cardboard, whereas Figure 1b illustrates the result of its analysis by representing detected flowers with blue crosses.

21207
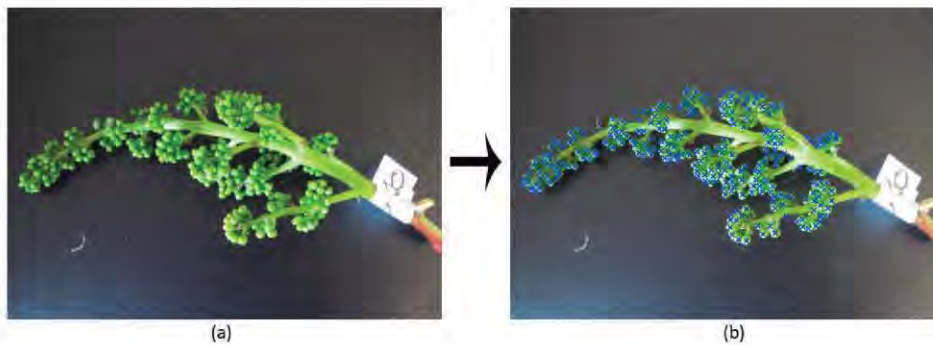
Figure 1. (**a**) Grapevine photo taken in the vineyard using black cardboard as the background; (**b**) result of the image analysis algorithm overviewed in Section 2.1 for automatically detecting flowers. Detected flower centers are marked with blue crosses.

2.2. Application's Technical Overview

The vitisFlower® application integrates the image analysis methodology previously described with the image capture process and the results storage to provide vine growers with a unique and comprehensive tool for counting grapevine flowers in the vineyard. For its implementation, technical and design decisions were taken for finding the best trade-off between accessibility, efficiency and portability.

With the aim of maximizing the availability of the application to potential users, the first technical decision was its development for Android-powered smartphones and tablets, since this operating system is the dominant one in the mobile-device market worldwide [23]. In addition, this accessibility was also favored by guaranteeing the compatibility of its implementation with Android Version 2.3 and above.

As discussed, the selection of Android as the operating system provides outstanding accessibility advantages. On the contrary, it also implies certain limitations in terms of efficiency and versatility for the needs of this work, especially for the implementation of the image analysis algorithms. In this respect, OpenCV is a highly optimized library, written in C/C++, that offers a wide catalogue of image processing and analysis functions. Android applications are mainly developed in Java, with an existing Android version of this library called OpenCV4Android. However, the original C/C++ version was used instead of its Android version to implement the core of the image analysis methodology due to the following reasons:

- The use of OpenCV4Android through Java code introduces limitations in image handling, which influence efficiency. In this respect, C/C++ provides higher versatility than Java, allowing image handling at lower levels.
- The power and versatility that is offered by C/C++ pointers allows one to reduce memory usage by reducing image and other variable copies. This advantage considerably helped to keep the application within the standard Android heap size.

- The implementation of the core using the standard C/C++ OpenCV library instead of its Android version outstandingly increases its portability, since there are OpenCV compilations for numerous operating systems, like iOS and Windows, among others.
- The use of the standard C/C++ OpenCV for implementing the image analysis algorithms facilitates their development and testing, since it can be carried out directly on a PC, avoiding the need for the use of smartphones or emulators to this effect.

The inclusion of the C/C++ OpenCV library for implementing the core of image analysis algorithms highly influenced the application's architecture design, as can be seen in Figure 2.
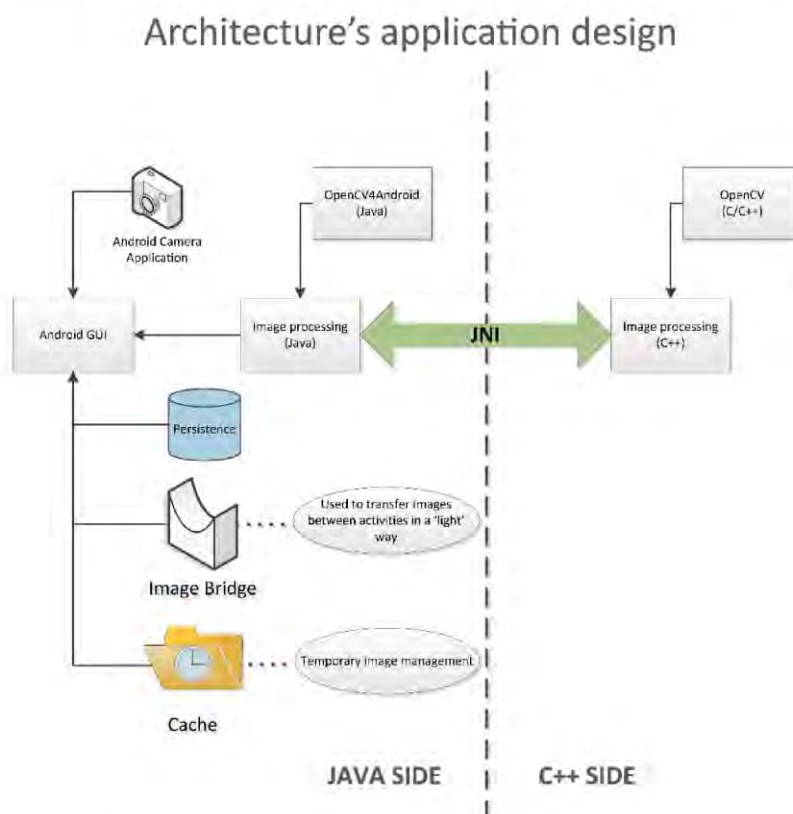
Figure 2. Architecture design of the vitisFlower® Android application.

The application's architecture was basically composed of two blocks, one implemented in Java and the other one in C++. The "C++ side" implements the algorithm described in Section 2.1 using the OpenCV library, offering a ready-to-use compiled library. On the other hand, the "Java side" implements the whole application with the exception of the "*ad hoc*" developed functions. Hence, it implements the main application's body and the graphical user interface; it is in charge of coordinating tasks; it calls the Android camera application for taking an image; it is responsible for appropriately storing the

59

results, *etc.* When an image is captured on the "Java side" and its analysis is required, this is requests the "C++ side". Nevertheless, the direct communication between both blocks was unfeasible, and the use of the Java Native Interface (JNI) for allowing this interaction was required. This way, the "Java side" invokes the desired functionality through JNI, which is really in charge of executing the C++ library and returning the results.

2.3. Application's Performance Description

vitisFlower® was designed to be used by all kinds of smartphone users. It was achieved by means of the following two decisions:

- Implementation of a simple and friendly graphical user interface: the interface shows only the relevant information to the user, preferably by using symbols or illustrations instead of descriptive text.
- Linear execution: the application has a user-independent execution line in which the user is exempted from making any important decision. It allows the user to utilize the application without any knowledge about its internal performance.

Figure 3 shows an illustrated flow-chart diagram of the application, in which the different stages can be described as:

1. Home: the application shows the vitisFlower® logo along with basic information about the aims and authorship.
2. Instructions for image capture: the application briefly informs the user of some basic notions for appropriately taking a photo.
3. Image capture: the camera application available in the user's Android device is invoked to make a capture. If the camera application is properly configured, it shows the captured image and allows one to discard it to take a new one in case the previous one was not properly acquired, for example because of the presence of leaves in the image, or due to the fact that the scene was not correctly focused, or it was overexposed.
4. Image analysis: this state is transparent to the user. It is in charge of analyzing the image taken in the previous state for detecting and counting flowers. For reducing the computational workload, the image is scaled down to a resolution of 2 Mpx prior to its analysis.
5. Results display: the results of the image analysis are presented to the user. On the one hand, the image with the detected flowers marked with red crosses is displayed. It easily allows one to graphically inspect the obtained results. On the other hand, the number of detected flowers is also shown. At this point, the user decides to save the results or to discard them if they are not satisfactory.
6. Image storage: this stage is reached if the user decided to save the results in the previous step. The processed image is saved in a folder called "VitisFlowerImages" created by the application and located in the root folder of the device's internal storage. The image is saved and named as follows [name]_[date]_[detected number of flowers].jpg, where:
   - [name]: a dialog box allowing one to insert an image name. If it is omitted, this field takes the value "image".

- [date]: the complete date of the image capture with the following format and information: day-month-year_hour.minutes.seconds.miliseconds.
- [detected number of flowers]: the number of flowers detected in the image.

Additionally, the user can read the complete information about the application's copyright and technical issues by clicking the icon composed of three white dots located in the upper-right corner of the window (see any application's screenshot in Figure 3 to identify this icon).
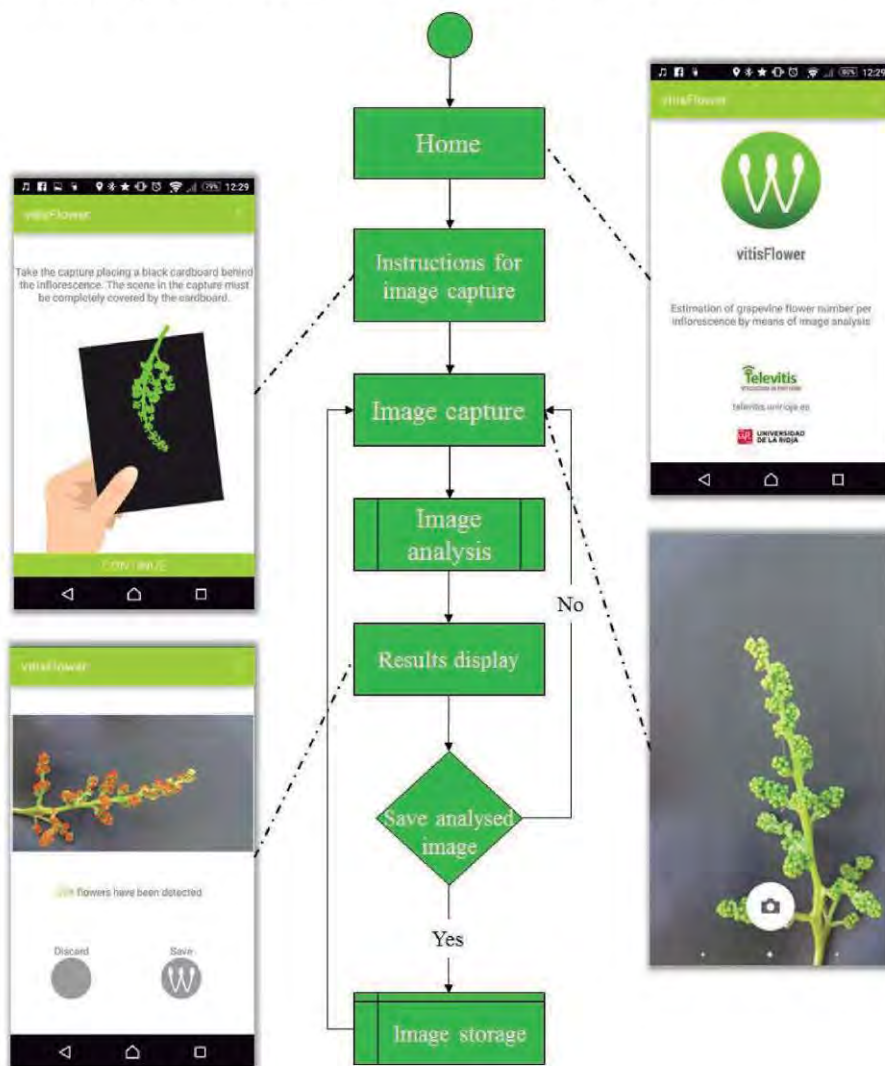

Figure 3. Flow-chart diagram of the vitisFlower® application illustrated with the application's screenshots.

2.4. Testing and Validation of the Application

2.4.1. Application's Performance Evaluation

The application's performance was evaluated with a double purpose: the assessment of its ability to accurately detect flowers and the comparison of its performance using the smartphone's cameras. To achieve these goals, an experiment using 2 devices of different capabilities was designed. The vitisFlower® application was installed on a high-end and a mid-range device; the Sony Xperia Z2 (Sony Corp., Tokyo, Japan) and BQ Aquaris E5 (Mundo Reader S.L., Madrid, Spain), respectively (see Table 1 for the features of both smartphones relevant to this experiment). These devices were separately used to acquire and analyze 70 images of 7 different grapevine varieties (10 images per variety), producing a total of 140 analyzed images. The considered varieties were: Airen, Cabernet Sauvignon, Chardonnay, Grenache, Riesling, Syrah, Tempranillo, Merlot, Chenin Blanc, Sauvignon Blanc and Semillon. The images were taken at pre-flowering stage denoted as BBCH 55, according to the scale of Lorenz *et al.* [25], in a grapevine variety collection located in the experimental vineyards of the "Instituto de Ciencias de la Vid y el Vino" (Logroño, Spain). Then, the produced outcomes were evaluated using the following metrics based on contingency tables for binary classification:

$$RC = \frac{TP}{TP + FN}; PC = \frac{TP}{TP + FP} \tag{1}$$

Table 1. Main relevant features of the 2 devices used for evaluating the performance of the vitisFlower application.

Feature / Device	Price/Release Date	Sensor Model	Resolution	Lens Size	Aperture	ISO
Sony Xperia Z2	549.0 €/2014	Sony IMX220	20.7 Mpx	1/2.3″	f/2.0	50–800
BQ Aquaris E5	209.90 €/2014	Sony IMX214	13 Mpx	1/3.2″	f/2.2	100–1600

Metric *RC* denotes *Recall*, which provides the percentage of actual flowers detected by the algorithm, whereas *PC* stands for *Precision*, which calculates the percentage of flowers correctly detected. For allowing the calculation of these metrics, a gold standard set was created. It was performed by manually labelling flowers on each of the 140 images acquired with both smartphones, making use of a PC software specifically developed in MATLAB (MatlabR2010b, MathWorks, Natick, MA, USA) to this effect. Thus, true positives (*TP*), false positives (*FP*) and false negatives (*FN*) were calculated and annotated per image as follows:

- *TP*: the number of flowers automatically detected corresponding to the actual flowers labelled in the gold standard.
- *FP*: the number of flowers automatically detected that do not correspond to actual flowers in the gold standard. Redundant *TP*s (a redundant true positive is when a flower is detected more than once) were also considered as *FP*s.
- *FN*: the number of actual flowers labelled in the gold standard that were not automatically found.

2.4.2. Application's Computational Efficiency Study

The usability of the application is highly influenced by the time it takes to analyze an image. Moreover, its accessibility is strengthened if this computation time does not exceed reasonably values for a wide range of smartphones. Therefore, to evaluate these attributes, the application was tested from a computational point of view. This study basically consisted of studying the computation time consumed by 4 smartphones with different hardware and software configurations for analyzing the same set of images. The devices were selected to cover a wide range of the market's spectrum in terms of price and performance; the selected ones were: the Sony Xperia Z2, Sony Xperia Z2 Tablet, BQ Aquaris E5 and Motorola Moto G (2013 version) (Motorola Mobility, IL, USA). Table 2 shows the features relevant for this study of the 4 selected devices.

To accomplish a rigorous and accurate comparison, all devices analyzed exactly the same images. Fifty inflorescence images were acquired with the Sony Xperia Z2 using the common Android camera application. Then, a simplified version of the application excluding the image capture and storage features was implemented. Basically, this version only included a simple home page with a single button for running the test. Upon test starting, the application iteratively analyzed the 50 images (stored in the device's internal storage), registering the time taken for each one.

Table 2. Main relevant features of the 4 devices used for evaluating the computational efficiency of the vitisFlower application.

Feature / Device	Price/Release Date	Chipset	CPU	GPU	RAM Memory	Android Version
Sony Xperia Z2	549.0 €/2014	Qualcomm MSM8974AB Snapdragon 801	Quad-core 2.3-GHz Krait 400	Adreno 330	3 GB	5.0.1 Jelly bean
Sony Xperia Z2 Tablet	449.0 €/2014	Qualcomm MSM8974AB Snapdragon 801	Quad-core 2.3-GHz Krait 400	Adreno 330	3 GB	4.4.4 Kit kat
BQ Aquaris E5	209.90 €/2014	MediaTek MT6582	Quad-core 1.3-GHz ARM Cortex-A7	Mali-400 MP2	1 GB	4.4 Kit kat
Motorola Moto G	172.0 €/2013	Qualcomm MSM8226 Snapdragon 400	Quad-core 1.2-GHz Cortex-A7	Adreno 305	1 GB	4.4.2 Kit kat

The acquired set of 50 images and the benchmarking version of the vitisFlower® application were used to compare its computation time running on the devices detailed in Table 2. For standardizing the state of the smartphones and minimizing the interference of other applications or services installed on them, the following testing protocol was defined and followed for carrying out the test:

1. Closing all recent applications in the device.
2. Selection of the flight mode.
3. Re-starting the device.
4. Waiting for 20 s for the operating system to completely load.
5. Starting the benchmarking version of vitisFlower.

6. Running the tests 5 times.

Once the test was finished, the application generated 5 files, including the measured computation time for each image in each of the 5 iterations. Finally, the definitive computation time for an image was calculated as the average time taken for its analysis in the 5 performed iterations.

3. Results and Discussion

3.1. Results of Performance Evaluation

Table 3 shows the results obtained with the 2 smartphones detailed in Table 1 in terms of average *Recall* ($\overline{RC}$) and *Precision* ($\overline{PR}$) following the testing methodology described in Section 2.4.1. Results are given in detail per variety. The overall results obtained with both devices (see Figure 4) indicated that more than 84% of flowers in the images were identified, producing less than 6% of detection errors. Furthermore, the dispersion of $\overline{RC}$ and $\overline{PR}$ values measured per variety and graphically represented in Figure 4 indicated a good stability of the application's behavior for all of them. In this respect, only the $\overline{RC}$ value obtained by the BQ Aquaris E5 on Chenin Blanc was lower than the values achieved for other cultivars, which may be explained by non-optimum acquisition conditions and potentially by the huge degree of compactness of the flower buttons of this cultivar at this phenological stage. In this regard, the usage of the application in the field and the analysis of the acquired images led to delineating the image acquisition settings that yielded the best application behavior. These include:

*   Analyzing inflorescences facing the Sun. The opposite orientation leads to light reflection and refraction patterns that can negatively affect the results.
*   Casting a shadow on the inflorescence to create a homogeneous scene. If the illumination is poor due to low natural-light conditions, the use of the camera flash is recommended.

Table 3. Performance evaluation of vitisFlower® using 2 different devices. The average *Recall* ($\overline{RC}$) and *Precision* ($\overline{PR}$) calculated from the 10 images in each grapevine variety are given.

Sony Xperia Z2			BQ Aquaris E5		
Variety	$\overline{RC}$	$\overline{PR}$	**Variety**	$\overline{RC}$	$\overline{PR}$
Airen	0.8223	0.9787	Merlot	0.9173	0.9517
Cabernet Sauvignon	0.8363	0.9615	Cabernet Sauvignon	0.8855	0.9531
Chardonnay	0.8770	0.9339	Chenin Blanc	0.7987	0.9563
Grenache	0.8045	0.9763	Grenache	0.8391	0.9685
Riesling	0.8411	0.9458	Riesling	0.9035	0.9212
Syrah	0.8889	0.9376	Sauvignon Blanc	0.8664	0.9557
Tempranillo	0.8308	0.9851	Semillon	0.8826	0.9158

The Sony Xperia Z2 comprises a camera sensor and a lens, which are technically more advanced than those of the BQ Aquaris E5. As can be seen in Table 1, the Xperia smartphone offers a sensor with higher image resolution, as well as a lens with a wider size and aperture. These features allow this device to produce less noise and better defined images than those captured by the BQ. Nevertheless, comparing the results obtained with both smartphones, it can be concluded that technical differences between them did not affect the application's performance. Furthermore, the results obtained with the BQ device were

64

slightly higher in terms of $\overline{RC}$ than those obtained with the smartphone from Sony. This outstanding result indicates that the vitisFlower® application can be satisfactorily used, at least with smartphones in the mid-range, like the BQ Aquaris E5 and above. Moreover, since performance degradation has not been detected with this device, good results may be surely obtained, even with more modest smartphones.

(a)   (b)
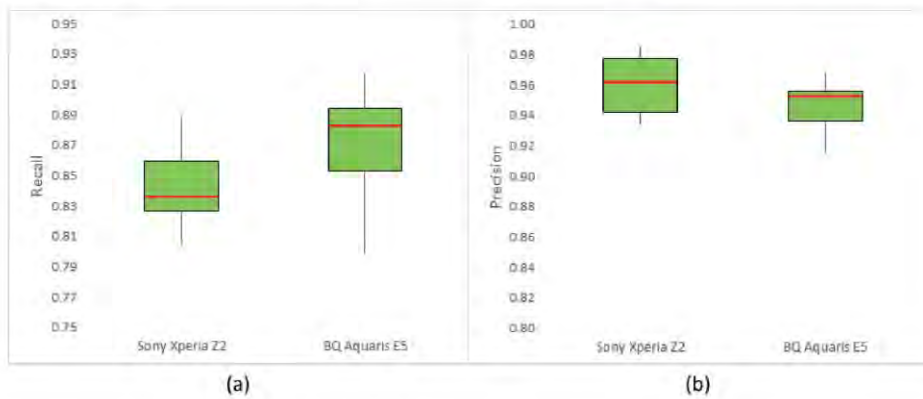
Figure 4. Box and whisker comparison plots for the Sony Xperia Z2 and the BQ Aquaris E5: (**a**) performance in terms of average *Recall* ($\overline{RC}$); (**b**) performance comparison in terms of average *Precision* ($\overline{PR}$).

3.2. Results of the Study of Computational Efficiency

Figure 5 illustrates the results obtained in the experiment specified in Section 2.4.2 for evaluating the computational efficiency of the vitisFlower® application running on the four devices listed in Table 2.

(a)   (b)
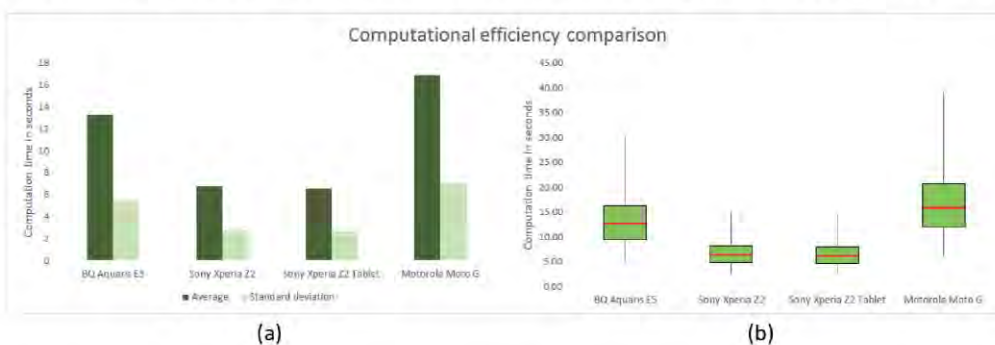
Figure 5. (**a**) Average and standard deviation of computation time for four different devices measured on the analysis of 50 images; (**b**) box and whisker plots for the same experiment shown in (**a**).

As expected, the Sony Xperia Z2 and Sony Xperia Z2 Tablet offered the best computational time distribution. The performance of these devices was high and virtually equal, with an average and standard

deviation time of around 6.5 and 2.6 s, respectively. Since they were equipped with the same computational hardware, but different Android versions, this result reveals that the differences between both versions did not affect the application's efficiency. On the other hand, the performance of the other two devices tested was considerably poorer. Despite this, the measured computational time for both devices (between 10 and 20 s) can be considered acceptable for allowing normal use of the application. Indeed, the BQ Aquaris E5 and Motorola Moto G (2013 version) took 13.27 and 16.83 s on average for analyzing the 50 images with a standard deviation of 5.48 and 7.01 s, respectively. Furthermore, according to the complete outcomes represented in Figure 5b by a box and whisker plot, 75% of the images were analyzed by the BQ Aquaris E5 in less than 16.24 s and by the Motorola Moto G (2013 version) in less than 20.64 s.

3.3. Significance of the vitisFlower® Application for the Wine Industry

Flowering and fruit-set are the main determinants of grapevine yield, and fruit-set rates may be impacted by many viticultural practices, including late pruning [14], shoot tipping [26], topping [15], early defoliation [16] and spray applications of growth regulators and nutrients [19,27]. Despite its importance, limited flower counting and fruit-set estimation are currently carried out in commercial vineyards, as manual flower counting is very laborious and destructive. However, the possibility of doing it in a fast and non-destructive way, such as with the vitisFlower® application, may pave the way for the early estimation of yield by the assessment of the fruit-set rates. The knowledge of this variable can help to estimate the final yield at harvest prior to bunch closure. This yield forecast can be very valuable for making decisions on vineyard management to optimize the grapevine balance between vegetative and reproductive growth and to prepare growers and wineries for the harvest operation, including scheduling and arrangements of shipping, storing, processing and trading the crop [28].

In the last few years, smart devices' user penetration has increased exponentially worldwide, and the development of applications for a wide range of uses has grown in parallel. The user's penetration percentage had surpassed 70% by June 2014 in many wine producing countries [29], where grape growers and farmers have adopted smartphones for their routine duties. For this reason, the development of agriculture-oriented applications, such as vitisFlower®, to provide fast and in-field, non-invasive assessment of agronomical and physiological information of the grapevines may become decision support tools for vineyard management.

4. Conclusions/Outlook

This paper presents an innovative smartphone Android application, called vitisFlower®, that provides the worldwide wine industry with a powerful tool for easily and automatically assessing flowering in the vineyard and providing useful information for yield estimation at early stages. The results of the experimentation developed in this paper demonstrate that even with modest devices, the application can be efficiently and reliably used at high rates of applicability and performance.

vitisFlower® is currently freely available in Spanish, English and French via Google Play [30], being one of the first viticulture smartphone applications available worldwide The development of friendly, non-invasive applications for viticulture and other agricultural fields opens a new and profitable window

66

for the implementation of precision agriculture strategies, aimed at optimizing the management according to the field variability.

Author Contributions

Arturo Aquino, Borja Millan and Daniel Gaston designed, implemented and tested the application. María-Paz Diago, Borja Millan and Javier Tardaguila developed and tested the original image analysis algorithm. Javier Tardaguila led and supervised the group from the beginning of the presented work. The original idea was conceived of by Javier Tardaguila, María-Paz Diago and Borja Millan.

Conflicts of Interest

The authors declare no conflict of interest.

References

1. Nuske, S.; Achar, S.; Bates, T.; Narasimhan, S.; Singh, S. Yield Estimation in Vineyards by Visual Grape Detection. In Proceedings of the IEEE/RSJ International Conference on Intelligent Robots and Systems (IROS), San Francisco, CA, USA, 25–30 September 2011; pp. 2352–2358.
2. Nuske, S.; Wilshusen, K.; Achar, S.; Yoder, L.; Narasimhan, S.; Singh, S. Automated Visual Yield Estimation in Vineyards. *J. Field Robot.* **2014**, *31*, 837–860.
3. Font, D.; Pallejà, T.; Tresanchez, M.; Teixidó, M.; Martinez, D.; Moreno, J.; Palacín, J. Counting Red Grapes in Vineyards by Detecting Specular Spherical Reflection Peaks in RGB Images obtained at Night with Artificial Illumination. *Comput. Electron. Agric.* **2014**, *108*, 105–111.
4. Diago, M.P.; Correa, C.; Millán, B.; Barreiro, P.; Valero, C.; Tardaguila, J. Grapevine Yield and Leaf Area Estimation using Supervised Classification Methodology on RGB Images Taken Under Field Conditions. *Sensors* **2012**, *12*, 16988–17006.
5. Roscher, R.; Herzog, K.; Kunkel, A.; Kicherer, A.; Töpfer, R.; Förstner, W. Automated Image Analysis Framework for High-Throughput Determination of Grapevine Berry Sizes using Conditional Random Fields. *Comput. Electron. Agric.* **2014**, *100*, 148–158.
6. Dunn, G.M.; Martin, S.R. Yield Prediction from Digital Image Analysis: A Technique with Potential for Vineyard Assessments Prior to Harvest. *Aust. J. Grape Wine Res.* **2004**, *10*, 196–198.
7. May, P. *Flowering and Fruitset in Grapevines*; Phylloxera and Grape Industry Board of South Australia: Adelaide, Australia, 2004.
8. Martin, S.R.; Dunn, G.M.; Hoogenraad, T.; Krstic, M.P.; Clingeleffer, P.R.; Ashcroft, W.J. Crop Forecasting in Cool Climate Vineyards. In Proceedings for the 5th International Symposium on Cool Climate Viticulture and Enology, Melbourne, Australia, 16–20 January 2000.

67

9.   Clingeleffer, P.R. Plant Management Research: Status and what it can Offer to Address Challenges and Limitations. *Aust. J. Grape Wine Res.* **2010**, *16*, 25–32.

10. Matthews, M.; Nuzzo, V. Berry Size and Yield Paradigms on Grapes and Wines Quality. *Acta Hortic.* **2007**, *754*, 423–436.

11. Dry, P.R.; Longbottom, M.L.; McLoughlin, S.; Johnson, T.E.; Collins, C. Classification of Reproductive Performance of Ten Winegrape Varieties. *Aust. J. Grape Wine Res.* **2010**, *16*, 47–55.

12. Carbonneau, A.; Deloire, A.; Jaillard, B. *La Vigne: Physiologie, Terroir, Culture*; Dunod: Paris, France, 2007.

13. Coombe, B. The Effect of Removing Leaves, Flowers and Shoot Tips on Fruit-Set in *Vitis Vinifera* L. *J. Hortic. Sci.* **1962**, *37*, 1–15.

14. Friend, A.P.; Trought, M.C.T. Delayed Winter Spur-Pruning in New Zealand can Alter Yield Components of Merlot Grapevines. *Aust. J. Grape Wine Res.* **2007**, *13*, 157–164.

15. Collins, C.; Dry, P.R. Response of Fruitset and Other Yield Components to Shoot Topping and 2-Chlorethyltrimethyl-Ammonium Chloride Application. *Aust. J. Grape Wine Res.* **2009**, *15*, 256–267.

16. Poni, S.; Casalini, L.; Bernizzoni, F.; Civardi, S.; Intrieri, C. Effects of Early Defoliation on Shoot Photosynthesis, Yield Components, and Grape Composition. *Am. J. Enol. Vitic.* **2006**, *57*, 397–407.

17. Brown, K.; Jackson, D.I.; Steans, G.F. Effects of Chlormequat, Girdling, and Tipping on Berry Set in Vitis Vinifera L. *Am. J. Enol. Vitic.* **1988**, *39*, 91–94.

18. Coombe, B. Fruit Set in Grape Vines: The Mechanism of the CCC Effect. *J. Hortic. Sci.* **1970**, *45*, 415–425.

19. Longbottom, M.L.; Dry, P.R.; Sedgley, M. A Research Note on the Occurrence of "Star" Flowers in Grapevines: Observations during the 2003–2004 Growing Season. *Aust. J. Grape Wine Res.* **2004**, *10*, 199–202.

20. De Bei, R.; Hook, J.; Fuentes, S.; Gilliham, M.; Tyerman, S.; Collins, C. Linking Canopy Architecture to Grape Quality using the LAI Canopy App. In Proceedings of the 19th International Meeting of Viticulture GIESCO, Montpellier, France, 31 May 2015; pp. 585–588.

21. Fuentes, S.; de Bei, R.; Pozo, C.; Tyerman, S. Development of a Smartphone Application to Characterise Temporal and Spatial Canopy Architecture and Leaf Area Index for Grapevines. *Wine Vitic. J.* **2012**, *27*, 56–60.

22. Diago, M.P.; Sanz-Garcia, A.; Millan, B.; Blasco, J.; Tardaguila, J. Assessment of Flower Number Per Inflorescence in Grapevine by Image Analysis Under Field Conditions. *J. Sci. Food Agric.* **2014**, *94*, 1981–1987.

23. IDC: Smartphone OS Market Share 2015, 2014, 2013, and 2012. Available online: http://www.idc.com/prodserv/smartphone-os-market-share.jsp (accessed on 13 August 2015).

24. Connolly, C.; Fliess, T. A study of efficiency and accuracy in the transformation from RGB to CIELAB color space. *IEEE Trans. Image Process.* **1997**, *6*, 1046–1047.

25. Lorenz, D.H.; Eichhorn, K.W.; Bleiholder, H.; Klose, R.; Meier, U.; Weber, E. Growth Stages of the Grapevine: Phenological Growth Stages of the Grapevine (Vitis Vinifera L. Ssp. Vinifera)? Codes and Descriptions According to the Extended BBCH Scale? *Aust. J. Grape Wine Res.* **1995**, *1*, 100–103.

26. Skene, K. A Comparison of Effects of Cycocel and Tipping on Fruit Set in *Vitis Vinifera* L. *Aust. J. Biol. Sci.* **1969**, *22*, 1305–1312.

68

27. Christensen, P. Timing of Zinc Foliar Sprays. I. Effects of Application Intervals Preceding and during the Bloom and Fruit-Set Stages. II. Effects of Day VS. Night Application. *Am. J. Enol. Vitic.* **1980**, *31*, 53–59.

28. Dunn, G.M.; Martin, S.R. The Current Status of Crop Forecasting in the Australian Wine Industry. In Proceedings of the ASVO Seminar Series: Grapegrowing at the Edge, Tanunda, Barossa Valley, South Australia, 10 July 2003; pp. 4–8.

29. Mobile Penetration in Spain & Digital Users. Available online: http://www.neomobile-blog.com/spain-2015-mobile-market-digital-user-habits/ (accessed on 13 August 2015).

30. Google Play. Available online: https://play.google.com/store/apps/details?id=com.ur.android.grapegenius (accessed on 13 August 2015).

3.1.3 Image based modelling for flower number assessment

Título de la publicación: Image analysis-based modelling for flower number estimation in grapevine

Autores: MILLAN, B., AQUINO, A., DIAGO, M.P., TARDAGUILA, J.

Publicado en: Journal of the Science of Food and Agriculture 97(3), 784-792 (2017) DOI: 10.1002/jsfa.7797

Resumen:

El número de flores por inflorescencia proporciona información que puede ser usada para la estimación de la cosecha. En trabajos previos de investigación, se ha conseguido desarrollar algoritmos basados en análisis de imagen que permiten estimar el número de flores por inflorescencia. Sin embargo, es necesario evaluar la dependencia de los modelos con respecto a la variedad para que esta herramienta pueda ser usada de forma fiable. Asimismo, en el presente trabajo también se ha cuantificado la capacidad predictiva del número de flores para la estimación de la producción, y la influencia de información adicional como la tasa de cuajado o el peso medio de baya.

Se capturaron imágenes de 11 variedades de *Vitis vinifera* L. en el viñedo, extrayendo el número de flores visibles por imagen de forma manual y automática (mediante un algoritmo de análisis de imagen). Los datos obtenidos se utilizaron para entrenar y evaluar modelos independientes de la variedad, lineales (de una variable y multivariable) y no lineales. La herramienta compuesta por el algoritmo de análisis de imagen y el modelo no lineal proporcionó el mejor resultado (RPD=8,32, RMSE=37,1) en la estimación del número de flores por inflorescencia. Con respecto a la estimación de la producción, el coeficiente de determinación (R^2) entre el número de flores y el peso final del racimo durante la cosecha fue de 0,79 utilizando el valor de la tasa de cuajado y llegando a 0,91 cuando se combinó con el peso medio de baya.

Este estudio demuestra que la estimación del número de flores por inflorescencia utilizando análisis de imagen es generalizable a diferentes

variedades de vid y puede proporcionar una estimación de la producción en fases muy tempranas de desarrollo.

Contribución del autor de la Tesis:

La aportación de Borja Millán incluye el diseño experimental, toma de datos en campo y generación de los algoritmos de análisis de imagen. También redactó el documento final.

The Publisher and copyright holder corresponds to Journal of the Science of Food and Agriculture. The online version of this journal is the following URL:

http://onlinelibrary.wiley.com/journal/10.1002/(ISSN)1097-0010

3.2   Yield estimation

There is a high level of demand from the wine industry for tools that can provide yield forecasting. The principal motivation is the economic benefit (Wolpert & Vilas, 1992; Martin et al., 2002; Dunn, 2010), but it will also help optimise wine production and enable the management of the vines to reach the desired quality and yield goals.

The first study of this section describes an algorithm for yield estimation from images manually captured on the field. This methodology provided a good performance (>90%) for the segmentation of different vine organs (clusters, wood, leaves and gaps) allowing precise yield estimation (R^2=0.73).

The segmentation process of images captured on the field is challenging, mainly because of the uncontrolled scene characteristics and the lack of uniformity in the colouration of the berry surface caused by the pruine (Diago et al., 2015). Also, it must be noted that not all the berries in a cluster are visible due to occlusions from other berries or vegetal material from the vine. To improve the results of yield estimation, the second article included in this section presents the application of Boolean models as a methodology that can overcome these problems (occlusions and segmentation errors). When Boolean model were applied on images captured automatically and on-the-go, the yield was precisely estimated (R^2=0.78) and with low error per vine (RMSE=200g).

3.2.1 Yield estimation from manually captured images

Título de la publicación: Grapevine yield and leaf area estimation using supervised classification methodology on RGB images taken under field conditions

Autores: DIAGO, M.P., CORREA, C., **MILLÁN, B.,** BARREIRO, P., VALERO, C., TARDAGUILA, J.

Publicado en: Sensors 12, 16988-17006 (2012) DOI: 10.3390/s121216988

Resumen:

Este trabajo tiene como objetivo la caracterización de la "canopy", estimación de la superficie foliar y producción por cepa mediante un algoritmo de clasificación supervisada basado en la distancia de Mahalanobis. El algoritmo propuesto analiza automáticamente conjuntos de imágenes, calculando el área (número de píxeles) correspondiente a siete clases (racimo, madera, porosidad y cuatro tipos de hoja en función de su edad). Cada una de las clases es inicializada por el usuario mediante la selección de un conjunto representativo de píxeles que se utilizan como semilla para la clasificación.

El algoritmo se ha evaluado utilizando 70 imágenes correspondientes a 10 vides (*Vitis vinifera* L. cv Tempranillo) capturadas en un viñedo comercial, situado en La Rioja. Las cepas fueron progresivamente deshojadas y aclareadas para aumentar la variabilidad de los datos. Los resultados de la segmentación mostraron un porcentaje de clasificación correcta del 92% para las hojas y del 98% para racimos, permitiendo la estimación precisa de la superficie foliar (R^2=0,81; $p<0,001$) y la producción (R^2=0,73; $p<0,002$).

La metodología propuesta se basa en un sistema de adquisición de imágenes simple y económico y proporciona información de gran interés para facilitar la toma de decisiones del viticultor en la gestión del viñedo.

Contribución del autor de la Tesis:

El autor de la presente Tesis doctoral, participó en todas las fases de este trabajo de investigación, incluyendo la implementación y ajuste de los algoritmos de análisis de imagen que permiten la estimación de la producción y de la superficie foliar. También participó en la redacción del documento final.

Article

Grapevine Yield and Leaf Area Estimation Using Supervised Classification Methodology on RGB Images Taken under Field Conditions

Maria-Paz Diago [1,*], **Christian Correa** [2], **Borja Millán** [1], **Pilar Barreiro** [2], **Constantino Valero** [2] **and Javier Tardaguila** [1]

[1] Instituto de Ciencias de la Vid y del Vino (CSIC, University of La Rioja, La Rioja Government) Madre de Dios, 51, 26006 Logroño, Spain; E-Mails: borja.millanp@unirioja.es (B.M.); javier.tardaguila@unirioja.es (J.T.)

[2] Department of Agricultural Engineering, ETSIA, Technical University of Madrid, Av. Complutense s/n Ciudad Universitaria, 28043 Madrid, Spain; E-Mails: ccorrea@udec.cl (C.C.); pilar.barreiro@upm.es (P.B.); constantino.valero@upm.es (C.V.)

* Author to whom correspondence should be addressed; E-Mail: mpaz.diago.santamaria@gmail.com; Tel.: +34-941-299-760; Fax: +34-941-199-721.

Abstract: The aim of this research was to implement a methodology through the generation of a supervised classifier based on the Mahalanobis distance to characterize the grapevine canopy and assess leaf area and yield using RGB images. The method automatically processes sets of images, and calculates the areas (number of pixels) corresponding to seven different classes (Grapes, Wood, Background, and four classes of Leaf, of increasing leaf age). Each one is initialized by the user, who selects a set of representative pixels for every class in order to induce the clustering around them. The proposed methodology was evaluated with 70 grapevine (*V. vinifera* L. cv. Tempranillo) images, acquired in a commercial vineyard located in La Rioja (Spain), after several defoliation and de-fruiting events on 10 vines, with a conventional RGB camera and no artificial illumination. The segmentation results showed a performance of 92% for leaves and 98% for clusters, and allowed to assess the grapevine's leaf area and yield with R^2 values of 0.81 ($p < 0.001$) and 0.73 ($p = 0.002$), respectively. This methodology, which operates with a simple image acquisition setup and guarantees the right number and kind of pixel classes, has shown to be suitable and robust enough to provide valuable information for vineyard management.

79

1. Introduction

The great economic, social and environmental importance of the viticulture and wine industry worldwide encourages the development and application of innovative technologies aimed at objective monitoring vineyards to improve grape and wine quality.

One of the historical main goals of the wine industry has been the accurate and objective estimation of the yield [1–3] and of the vineyard's winegrape quality potential. More specifically, *yield forecasting* has been identified in recent years as one of the more profitable topics for scientific research in viticulture [4] as it could lead to more efficiently managed vineyards producing wines of better quality [5]. So far, most of the methods employed for yield estimation are destructive, labour and time demanding [6], or very expensive [7]. Similarly, the assessment of a vineyard's winegrape quality potential has often been attempted by the use of vineyard score sheets [8–12] which required visual evaluation of several grapevine canopy variables, such as vigour, leaf status, exposed leaf area, canopy porosity and fruit exposure, all of them intrinsically related to final grape and wine composition and quality [13–19]. Consequently, there is a need for assessing the vineyard yield and winegrape quality potential by objective monitoring the grapevine canopy features, but customary methods for obtaining canopy measurements, such as the Point Quadrate [8] or LIDAR [20–22], though quantitative, are limited in their precision and practicality, either because they are time-consuming or expensive. Hence, new methods are required to assess grapevine canopy status, and image capturing and analysis may be an objective and potentially useful technique to replace time-consuming procedures and to provide useful information for more efficient grapevine canopy management.

In recent years several studies, based on image processing, have been conducted in order to assess features of the vineyard canopies, like in [23–25] for general purposes and also for specific applications like disease detection [26], smart spraying [27,28] and yield estimation [29]. These studies were carried out in order to quantify features such as leaves, vine shoots, trunks and grapes. However these investigations required sophisticated equipment and specialized software for analysis and interpretation. A simpler layout for image capturing and processing for the assessment of grapevine canopy features was described in the works of Dunn and Martin [1], who estimated the yield, and of Tardaguila *et al.* [30,31]. In these works digital image analysis techniques applied to sample data from a defoliation study revealed quantitative descriptions of canopy biomass distribution, fruit exposure, cluster compactness, and treatment efficacy, although the image processing was not completely automated.

Colour classification techniques in the Red Green and Blue (RGB) colour space can be divided into supervised and unsupervised [32]. In supervised methods, the number of classes is specified and the supervisor selects the prototype of these classes. Conversely, in unsupervised methods, the characteristics of the classes are unknown, and the classification algorithm ascribes membership in such a way that the elements in each class will exhibit similar characteristics and are more similar to each other, than with respect to elements of other classes. Supervised and unsupervised methods

80

have been used outdoors [33] and specifically for vineyard feature extraction aiming at vigour characterization [34]; grape clusters and foliage [27]; single grapes [35]; count 'fruit pixels' for yield estimation [1], or segregate grapes, leaves and shoots [36,37].

In unstructured environments, such as an agricultural field, conditions are variable, so robustness of unsupervised algorithms may be at risk [32]. Therefore supervised classification techniques are of special interest in this field, since a training set can be prepared by *a priori* establishing what features will correspond to the elements of a class [38], which, in turn, reduces uncertainty and leads to the possible solutions.

Our work aims to develop a fast, robust and inexpensive methodology for straightforward RGB image processing and interpretation, using images taken in the field, for grapevine canopy feature extraction that would enable accurate leaf area and yield estimation.

2. Experimental Section

To be able to correlate the estimated leaf area and yield data with real plant measurements, a detailed experimental setup for the acquisition of images was developed, based on successive defoliations and cluster thinning steps of individual vines.

2.1. Experimental Site

The experiments were conducted in 2010 in a commercial dry-farmed cv. Tempranillo (*Vitis vinifera* L.) vineyard, located in Casas Blancas, Cidamón (lat. 42°29'8.83" N; long. 2°50'22.57" W; 181 m asl, La Rioja, Spain). Tempranillo vines were grafted onto 41B rootstock and planted in 2005 following a between-row and within-row spacing of 2.70 m × 1.15 m respectively. The vines were spur-pruned (12 buds per vine) on a bilateral cordon and trained to a VSP trellis system. The trellis featured a supporting wire at 0.70 m, two wires at 1.00 m aboveground for protection against wind damage, and a pair of movable shoot-positioned wires at 1.45 m.

2.2. Defoliation, Cluster Thinning and Assessment of Removed Leaf Area and Fruit

In order to provide a good validation of the images' classification method, at harvest (30 September 2010), 10 vines were randomly chosen, and each of them was individually and successively defoliated and cluster thinned in several steps as shown in Table 1. After each step, the leaf area and/or fruit removed were also recorded. This way, a range of different conditions of leaf area and cluster exposure were created to provide a better validation of the image analysis methodology.

The whole canopy of each vine was successively defoliated: first by removing the first six main basal leaves (step 1), then other six (in total 12 leaves) main basal leaves (step 3), and then the remaining main leaves and laterals (complete defoliation, or step 5). The number of leaves removed at each step was recorded and measured using a leaf area meter (LI-3100C; Li-Cor, Lincoln, NE, USA). Similarly, the whole canopy of each vine was successively de-fruited by thinning some clusters: first by removing every third cluster (step 2), then every second remaining cluster (step 4) and then the remaining clusters (step 6). The number of clusters removed and their combined weight was recorded after each cluster thinning event.

Table 1. Description of the defoliation and de-fruiting steps during the session of image acquisition of each individual vine.

Image #	Canopy manipulation event	Image
I0	Initial stage of the vine (step 0)	
I1	Removal of the first 6 basal leaves per shoot (step 1)	
I2	Removal of one third of clusters (step 2)	
I3	Removal of additional 6 basal leaves per shoot (12 leaves removed in total) (step 3)	
I4	Removal of one third of clusters (step 4)	
I5	Removal of remaining main leaves and laterals (step 5)	
I6	Removal of all remaining clusters (step 6)	

2.3. Image Acquisition

Before any defoliation or cluster thinning, and after each canopy manipulation step, each vine (10 vines in total) was photographed with a conventional RGB camera (Pentax model K200D, Tokio, Japan) mounted on a tripod set normal to the canopy 2 m from row axis and 1.05 m aboveground. Note that, when the defoliation process was performed over highly dense canopies, the distance to the remnant foliage increased and consequently the objects size seemed to be reduced. In order to correct this problem, images were scaled to fit the images acquired at 2 m. In this way all images represented the same area. A white screen was placed behind the canopy to avoid confounding effects from background vegetation and no artificial illumination was employed. Images were captured at a resolution 3,504 × 2,336 and reduced to 800 × 600 in order to speed up processing time. For each individual vine a total number of seven images were taken (Table 1).

2.4. Image Processing (Clustering Algorithm)

Several measurements of similarity between groups in terms of multiple characteristics have been proposed in the literature [37], but the Mahalanobis distance has been found to be the most suitable in a majority of applications, and it is widely used for pattern recognition and data analysis [39]. It is now known that many standard distance measurements such as Kolmogorov's variational distance, the Hellinger distance, Rao's distance, *etc.* are increasing functions of Mahalanobis distance under assumptions of normality and homoscedasticity [40].

Mahalanobis measures the similarity between an unknown sample group and a known one; it takes into account the correlations of the data set, and it is scale-invariant. It also accounts for the fact that the variances in each direction are different as well as for the covariance between variables.

The Mahalanobis distance between two random vectors $(\vec{x}, \vec{y})$ with the same distribution, and covariance matrix S, can be defined as:

$$d(\vec{x}, \vec{y}) = \sqrt{(\vec{x} - \vec{y})^T S^{-1} (\vec{x} - \vec{y})} \tag{1}$$

The Mahalanobis colour distance standardizes the influence of the distribution of each feature considering the correlation between each pair of terms [41].

In the case of RGB colour images S is computed as:

$$S = \begin{bmatrix} \sigma_{RR} & \sigma_{RG} & \sigma_{RB} \\ \sigma_{GR} & \sigma_{GG} & \sigma_{GB} \\ \sigma_{BR} & \sigma_{BG} & \sigma_{BB} \end{bmatrix} \tag{2}$$

and the elements of S can be calculated as:

$$\sigma_{RG} = \sigma_{GR} = \frac{1}{n-1} \sum_{i=0}^{n} (R_i - \overline{R})(G_i - \overline{G}) \tag{3}$$

where R_i, G_i, B_i are the values of the ith match (I = 1,2,3,...n), and $\overline{R}, \overline{G}, \overline{B}$ are the mean color values for R, G, and B in the given image, respectively.

83

For our purposes $\vec{x}$ was a three dimensional vector (R, G, B), that represented pixels from the image to be processed and $\vec{y}$ was also, a three dimensional vector (R, G, B), that represented the reference pixels (reference group) for each class to be identified.

The effect of S was to scale the distance along each feature. For image processing purposes, each channel R, G, B was considered as a feature.

Figure 1, shows a random selection of 2,000 pixels in a typical grapevine image (RGB colour space). Note that, the variances in each direction (R, G, B) were different. This is the reason why it was necessary to implement a classifier that considered such differences, like Mahalanobis does. The region of constant Mahalanobis distance around the mean formed an ellipse in 2D space as in Figure 1(b).

Figure 1. (**a**) Random selection of 2,000 pixels in a typical grapevine image (image I0 in RGB colour space). (**b**) RG plane. Ellipses represent equidistant points. (**c**) RB plane. (**d**) GB plane.

(a)   (b)

(c)   (d)
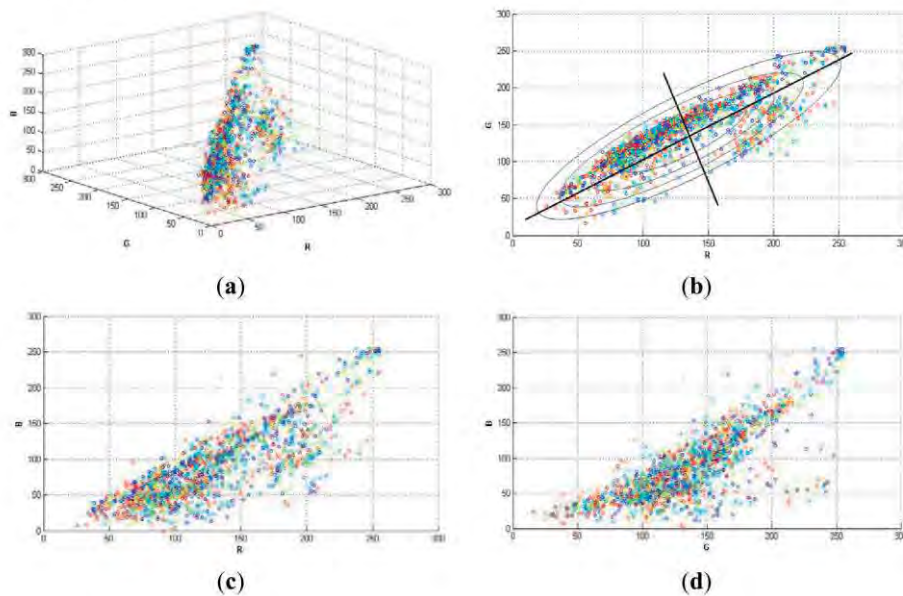
2.5. Software Implementation

In the proposed methodology of this work seven reference groups of pixels were selected in order to generate the classification, in which every group represented a relevant characteristic of the grapevine canopy. The seven classes identified were: Young leaves (two classes), Old leaves (two classes), Wood (including shoots and trunk), Grapes and Background (or canopy gaps). However, if any of these classes was not present (depending on the growing stage), or a new class appeared on the image, the number and/or the group labels could be modified.

In this way, each pixel group was manually selected from a set of 10 representative images. For every pixel reference group a set of 40 pixels was chosen. Once the reference pixels were selected, the

Mahalanobis distance was computed over a set of 70 images and its pixels were assigned to the class with the lowest distance. Of the total pool of 70 images (seven images per vine), images I0, I2 and I4 were used to train the model for the estimation of leaf area, as these images corresponded to the defoliation events. Similarly, I1, I3 and I5 were used to build the model for yield estimation.

In order to implement the classification algorithm and to provide graphical interface to the user, software based on Matlab 7.11 was developed. Figure 2 shows a software screenshot, at the moment when reference pixels are manually selected and depicted as a set of bars in the lower part of the image. These bars are displayed to bring visual feedback regarding the pixels selected as reference.

The number of pixels used as reference, as well the name and number of clusters can be modified by the users, in order to adjust the algorithm to different conditions, such as illumination changes or new characteristics that had not been previously observed, for example leaf colouration/discolouration produced by diseases.

Figure 2. Screenshot of the manual selection of reference pixels.

2.5.1. Feature Extraction Methodology Steps

The implemented methodology consisted on twelve steps which can be summarized as follows:

Step 1   Selection of representative images, containing as much variability (inside each class) as possible, and reading of reference images.

Step 2   Selection of 40 reference pixels for each class of interest.

Step 3   Reading from the directory containing the images to be processed.

Step 4   Processing of a section of the image (region of interest, ROI) or the whole image. Selection of the ROI if applicable.

Step 5   For each class, computation of the Mahalanobis distance between the reference pixels and the image/section to be analyzed.

Step 6   Assignation to class membership based on the rule that minimum distance from pixel to class reference pixels drives the allocation in a given class.

Step 7   Performance of morphological operations over the Grape class. Removal of small pixels groups and filling "holes" inside the Grape cluster by using erode and dilate morphological operations, respectively.

Step 8   Allocation of pixels to the Grape class only if they corresponded to the lower half of the image. e.g., If the image resolution was 800 × 600, the pixels to be considered as valid for the Grape class must be within the 400 to 800 position of the vertical axis.

Step 9   Computation of the number of pixels for each class.

Step 10   Saving the numerical results on a spreadsheet.

Step 11   Saving the class images in a directory.

Step 12   Displaying the class images on screen.

2.6. Algorithm Validation

A validation process for these specific grapevine canopy images was carried out. This validation was manually performed, selecting some ROIs on images that showed representative conditions of illumination and colours. Once the ROI was selected, the number of pixels for each class was manually counted by an expert, both on the original and the clustered image.

2.7. Correlations. Leaf Area and Yield Estimation

For leaf area and yield estimation, the set of images was divided into two groups: the training group, in which two thirds of data were used to generate the model, and the validation group, where the remaining one third of data was allocated for validation purposes. For the training group, linear correlations were run between the number of pixels of the Leaves and Grape classes in each image, and the actual leaf area and yield present in the vine at that time, respectively (SPSS v15.0, IBM, Armonk, NY, USA). Hence, these correlations were used to estimate leaf area and yield in the set of images of the validation group, and correlations between the estimated and observed (real) values for leaf area and yield were run, and the coefficients of determination (R^2) and root mean squared error (RMSE) were computed.

3. Results and Discussion

3.1. Algorithm Validation

Examples of the ROI (30 × 30 pixels) selected for the manual validation process of the algorithm are depicted on Figure 3. The manual validation showed a 98% of correct classification for the Grape class and a 92% for the Leaves (Young and Old leaves groups added). Most of the misclassifications in the Leaves' groups were due to younger shoots and laterals, which exhibited almost the same green colour than leaves.

As the Figure 4(a,b) and the manual validation process show, the classifiers performed very well without any image pre-treatment, such as improvement of contrast, brightness or colour adjustment. This is an important outcome, which makes the process simpler, compared to previous works where

images had to be cut, reoriented or strongly pre-processed [42], and especially interesting, given the fact that no artificial illumination was used for the image acquisition in the vineyard.

Figure 3. Manual validation of classification. (**a**) Original image, where 73.1% are Grape pixels. (**b**) Clustered image. Blue pixels correspond to the Grape class, and represented 72% of the image. (**c**) Original image, where 58% are Leaf's pixels. (**d**) Clustered image. Black pixels correspond to leaves, and represented 63% of the image.

(**a**)   (**b**)   (**c**)   (**d**)
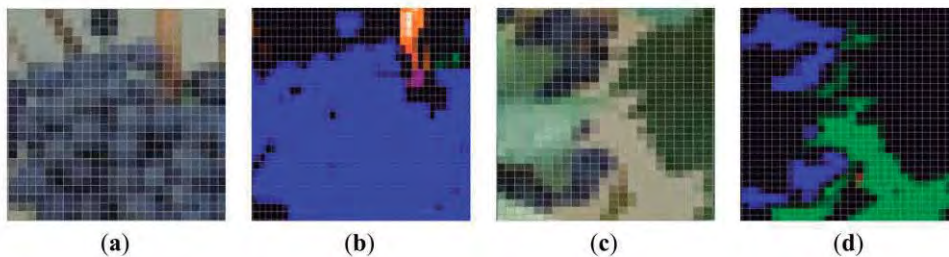
Figure 4. (**a**) Grapes class detail in the original image. (**b**) Detail of the identified grapes before the morphological operations.

(**a**)
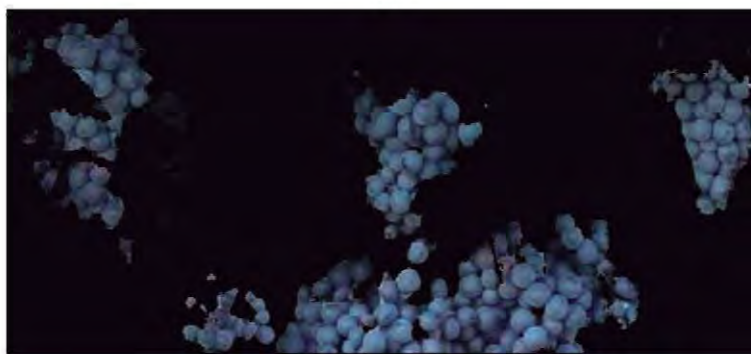
(**b**)

3.2. Classifier Performance

In order to illustrate the classifier's performance, three images that were representative of the presence of misclassification errors were selected for detailing all generated classes. These images corresponded to three different defoliation stages and are presented in Figures 5–7. Likewise, in Figure 5, a non-defoliated, non-thinned grapevine image at step 0 illustrating Grape pixels misclassification errors was chosen.

Figure 5. Classification example performed over a grapevine image of a non-defoliated, non-thinned vine (Image I0). (**a**) Original image. (**b**) Clustered image. (**c**) Vine wood. (**d**) Background. (**e**) Grape class, without morphological operations. (**f**) Grape class after morphological operations. (**g**) Zoomed area in part (**e**) showing small pixel groups misclassified. (**h**) Zoomed area in part (f) showing how the morphological operations removed the small pixel groups. (**i**) Old leaves grade 1. (**j**) Old leaves grade 2. (**k**) Young leaves grade 1. (**l**) Young leaves grade 2.

88

16998
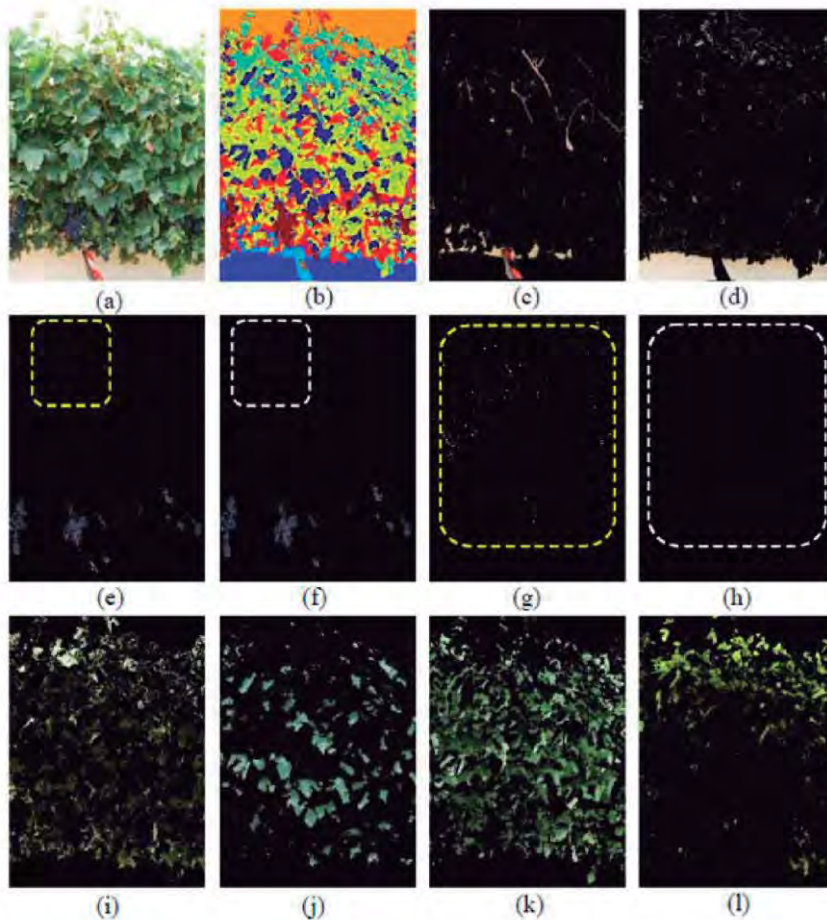
Then, two images showing other common misclassification errors such as atypical leaf colouration (Figure 6) or the influence of the sky (Figure 7) were selected.

Figure 6. Classification example, performed over a grapevine image after the first defoliation step (I1) to show the algorithm capability to separate between different kinds of leaves (**a**) Original image. (**b**) Clustered image. (**c**) Grape class, without morphological operations. (**d**) Wood. (**e**) Old leaves grade 1. (**f**) Old leaves grade 2. (**g**) Young leaves grade 1. (**h**) Young leaves grade 2.
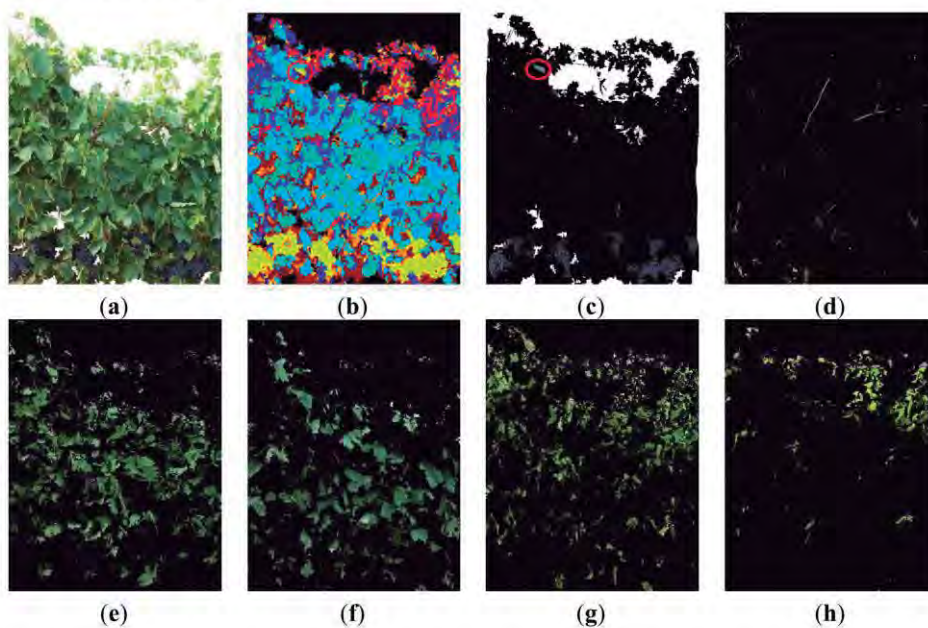
In Figure 5 seven classes were generated: Grapes, Wood (shoots and trunk), Background, and four different types of Leaves, which included Young leaves grade 1, Young leaves grade 2, Old leaves grade 1 and Old leaves grade 2, being the numbering of grades equivalent to increasing stages of leaves' maturity. The differentiation of several kinds of leaves (Figure 5(I–l)) has important implications if a visual assessment of the vine physiology performance is intended, as younger leaves are photosynthetically more active than older leaves [43] and reveal differences in the physiological behaviour of the plant, which may alert of the presence of abiotic stresses such as water or nutrient deficiencies. Grape class was wrongly estimated at a first stage (Figure 5(e)) due to two combined effects. First, the Grape regions also included small white bright pixels wrongly assigned to the Background class (Figure 5(d)), which actually corresponded to the waxy-white coating that is visible in grapes, and known as bloom, leading to underestimation of the Grape class. On the other hand, bluish pixels on the top of the image corresponding to some leaves' areas (Figure 5(e), and detail in part (g)) were misclassified into the Grape class, with its subsequent overestimation. These errors were drastically reduced when these small pixel groups were deleted by a set of morphological operations.

Specifically, erode and dilate consecutive operations over the Grape class were performed to eliminate these pixels as depicted on the Figure 5(f) (detailed in (h)).

When the first defoliation step was performed (image I1), more clusters were exposed, the lighting conditions over the grapes improved, and consequently, their detection rate increased (Figure 6(a,b)). In Figure 6b, the Grape class appears in yellow, Wood class in dark blue, and the four classes of leaves (Young leaves grade 1, Young leaves grade 2, Old leaves grade 1, Old leaves grade 2), are presented in blue, light blue, cyan and red, respectively. When compared with the four Leaf classes shown in Figure 5, leaves in Figure 6 (classes (e) (f) (g) and (h)) were similar, showing that the classification algorithm was robust at segregating several foliar maturity stages when lighting conditions changed and defoliation was conducted.

In this image (I1), the Grape class also showed a misclassification event, as in the left upper corner, enclosed in a red circle (Figure 6(b,c)) some leaves with a blue colouration induced by the spraying of a fungicide (copper sulphate) were confounded and considered as Grape pixels. In this case, the misclassification was not caused by a poor performance of the classification methodology, but by the hue similarity between the sprayed leaves and the Grape class. In this scenario, and to improve the global algorithm performance, pixels were classified as Grape pixels, only if they were located at the bottom half of the image. Also in the case of images with low variability of leaf types and adverse sunlight conditions, the algorithm showed adequate response and adaptability (Figure 7).

Figure 7. Classification example performed over a grapevine image after the third defoliation stage (Image I5). (**a**) Original image. (**b**) Clustered image. (**c**) Grape class. (**d**) Bright background. (**e**) Dark background. (**f**) Vine wood. (**g**) Young leaves. (**h**) Old leaves.
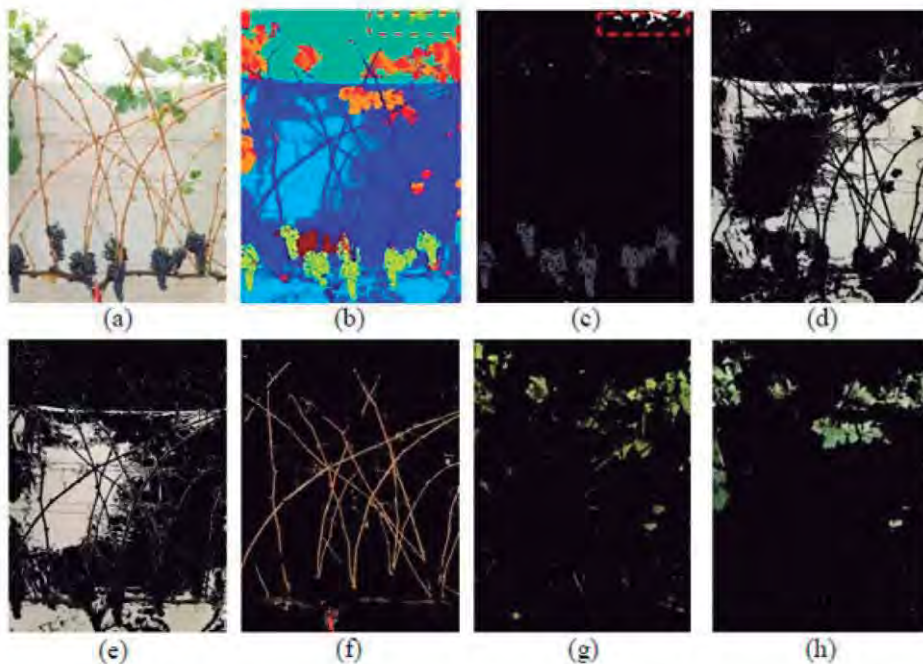
After the final defoliation stage, only the vine shoots and remaining clusters were visible on the grapevine canopy (image I5, Figure 7(a)). Under these conditions, and as the background could not cover the entire area, the sky could be partially distinguishable, and the sunlight penetrated into the image scene creating shadows and bright areas over the background. To overcome this situation, two different classes of background were selected, and identified as Dark and Bright Background classes (Figure 7(d,e)) and the four classes of leaves described and identified in previous steps, were reduced to only two clusters: Old and Young leaves (Figure 7(g,h)). The complete classification performance is shown in Figure 7(b).

Depicted on Figure 7(f), the Wood class included the vine trunk, shoots, and trellis wires. On the other hand, Figure 7(c) shows the Grape class, with preliminary misclassifications, enclosed in red in the upper part of the image, due to some pixels of blue colouration corresponding to the sky. This misclassification was also solved by considering as grape pixels only those located at the lower half of the image.

3.3. Grape Yield and Leaf Area Estimation

The correlation and validation curves for the estimation of leaf area and grape yield using the classification methodology and image analysis are shown in Figures 8 and 9, respectively.

Figure 8. (**a**) Correlation between the actual leaf area ($m^2 \cdot vine^{-1}$) of the grapevine canopy in the images of the training set, and the number of pixels corresponding to the Leaf class computed by the classification methodology and image analysis. (**b**) Comparison between the actual values of leaf area ($m^2 \cdot vine^{-1}$) of the grapevine canopy in the images of the validation set, and the predicted leaf area values calculated with the correlation equation in (a). Dotted line is 1:1 line.
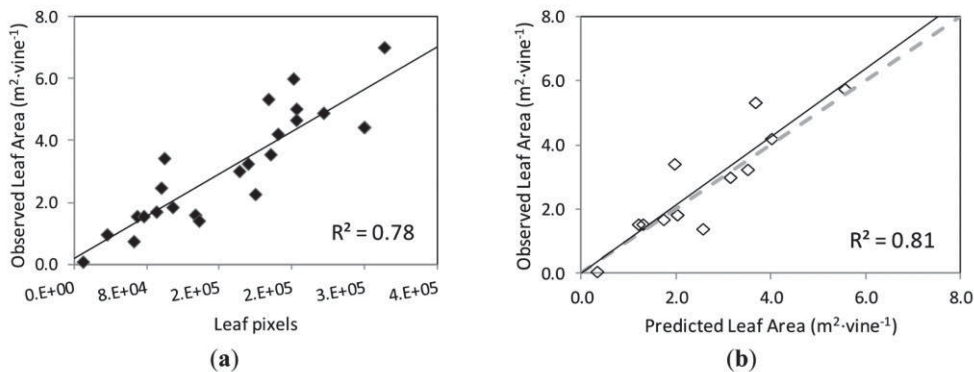
The actual leaf area on the grapevines' images and the number of pixels corresponding to the Leaf class were found to be strongly correlated, following a linear relationship ($y = 0.1712x + 0.1863$) with coefficient of determination $R^2 = 0.78$ at $p < 0.001$ (Figure 8(a)). When this function was used to predict the leaf area of another set of grapevine images (validation set), the correlation between the observed and predicted leaf areas was very close to the 1:1 line ($y = 1.0598x + 0.0117$) and the values of $R^2 = 0.81$ at $p < 0.001$ and RMSE $= 0.745$ m^2 (Figure 8(b)).

In dense and very dense canopies, grape clusters are typically covered with leaves, preventing them from being exposed to the sun and also visible to the human or machine vision. This fact, which occurred in the images of the initial non-defoliated, non-thinned grapevines (I0) and also in images corresponding to the first defoliation step (I1 and I2), seems to have impacted the performance of the yield prediction by the image analysis methodology, as the coefficient of determination values for yield estimation were smaller than those for leaf area prediction.

Similarly to leaf area, the prediction of the grape yield from the model established by image analysis was satisfactory, and covered a broad range of grape exposure and visibility conditions, generated by the successive defoliation and grape thinning steps. When grapes in the canopy are partially covered by the leaves during maturation, and at harvest (especially in moderate to high vigour vineyards and in vineyards where defoliation was not performed or was only mildly performed) this method seems to be more applicative for leaf area estimation than yield. However, basal defoliation is a canopy management practice, widely conducted worldwide, between fruit-set and veraison, on one or two sides of the canopy, which is aimed at improving the fruit exposure for grape quality [15,17,44–47] and health purposes [48]. Since the visibility of the clusters is certainly increased after basal defoliation, the accuracy of the yield estimation by the classification methodology and image analysis presented in this work would significantly increase, hence allowing a very accurate yield prediction.

A truthful estimation of the potential grape yield soon after veraison is very valuable information not only for logistical purposes at harvest (*i.e.*, labour needs, winemaking capacity at the winery…) but also for economic reasons, especially when a wine producer has to buy grapes from other grapegrowers and suppliers, as the total grape yield of a given region or appellation area is an important driving force of the final grape price in a given vintage.

4. Conclusions

The methodology for canopy feature extraction and image analysis described in the present work has proved to be a useful and reliable tool for leaf area and yield assessment in the vineyard. It seems, though, more applicative to leaf estimation as grape visibility may be limited across the ripening period and harvest in non-defoliated, moderate to high vigour canopies. The setup proposed is simple, inexpensive and non-destructive for image-acquisition as only a commercial RGB camera is needed. The processing methodology has shown to be highly adaptable and robust to changes in illumination and in the distance to the targeted grapevine, which are two critical factors in machine vision applications under field conditions.

The classification methodology allowed discriminating seven different classes, corresponding to seven types of canopy features in the grapevines' images, although only the Leaf and Grape classes were successfully calibrated and validated against real plant measurements. The classifier's performance for the identification of leaves and grapes was very high and their effectiveness exceeded the 90% in both cases.

An accurate estimation of the grapevine leaf area and yield during the growing season by a fast and non-destructive method, such as the one described in this work, may provide very valuable information for the grape and wine industry for canopy management decisions, as well as for logistical and economical purposes, and can be further implemented for on-board analysis.

Figure 9. (**a**) Correlation between the yield (kg) of the grapevines in the images of the training set, and the number of pixels corresponding to the Grape class, computed by the classification methodology and image analysis. (**b**) Comparison between the actual values of yield (g) of the grapevines in the images of the validation set, and the predicted yield values calculated with the correlation equation in (a). Dotted line represents the 1:1 line.

(**a**)   (**b**)
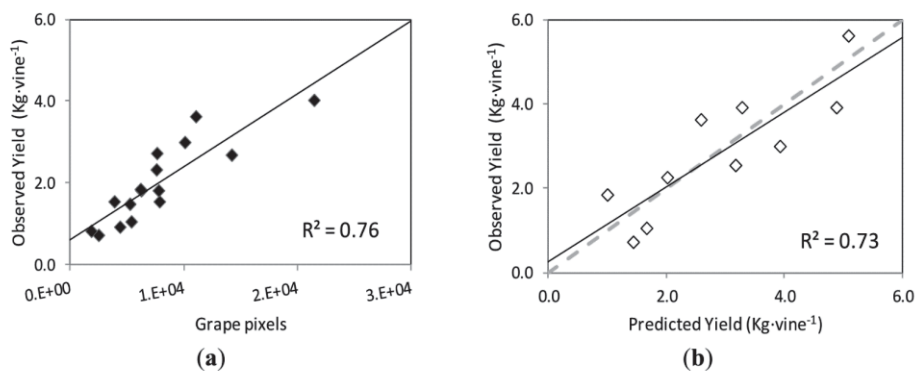
The differences in foliar density of the imaged vines, as interpreted as more or less number of leaf layers, may have impacted the estimation of the grapevine's leaf area by image analysis. In this way, in very dense canopies (with several superimposed layers of leaves) the initial defoliation steps (Images I1 and I3) might not have caused a significant "disappearance" of leaves from the image, as expected, so that the vine remained fully covered with leaves, and only until the defoliation stage 3 was reached, the observed grapevine canopy area was drastically reduced. In other words, for very dense canopies, the removal of leaves in the very early steps did not always mean lower estimated leaf area by image analysis.

The images used in the present work corresponded to grapevines of medium to very dense canopies, in general, which seems to be the least favourable scenario for the estimation of leaf area by image analysis. However, the prediction of the leaf area from the model established by image analysis was very satisfactory, and it should be expected to perform better for grapevines with less dense canopies, as it is the case of low to moderate vigour vineyards.

Furthermore, a reliable and accurate estimation of the grapevine leaf area at several timings during the growing season may be of great usefulness to the grapegrower to monitor the vegetative growth of the plant, and identify symptoms of several abiotic and biotic stresses, such as water stress and diseases pressure, respectively, in a dynamic way. Likewise, this information may also help the grapegrower in taking canopy management decisions to improve the balance between vegetative and reproductive growth.

Regarding grape yield estimation, the correlation between the actual yield on the grapevines' images and the number of pixels corresponding to the Grape class followed a linear relationship $(y = 0.1787x + 0.611)$ with coefficient of determination $R^2 = 0.78$ at $p < 0.001$ (Figure 9(a)).

When this curve was employed to predict the yield of the images of the validation set, the correlation between the observed and predicted yield values was also close to the 1:1 line $(y = 0.8907x + 0.253)$, with a $R^2 = 0.73$ at $p = 0.002$, and RMSE = 0.749 kg (Figure 9(b)).

References

1. Dunn, G.M.; Martin, S.R. Yield prediction from digital image analysis: A technique with potential for vineyard assessments prior to harvest. *Aust. J. Grape Wine Res.* **2004**, *10*, 196–198.

2. Clingeleffer, P.R.; Krstic, M. *Final Report for Project CSH 96/1. Crop Development, Crop Estimation and Crop Control to Secure Quality and Production of Major Wine Grape Varieties: A National Approach*; CSIRO and NRE: Victoria, Australia, 2001; p. 148.

3. Wolpert, J.A.; Vilas, E.P. Estimating vineyard yields: Introduction to a simple, two-step method. *Am. J. Enol. Vitic.* **1992**, *43*, 384–388.

4. Dunstone, R.J. *Final Report for Project DNR 02/02. Winegrape Crop Forecasting Module*; CWRDC: Adelaide, Australia, 2002; p. 39.

5. Dunn, G.M.; Martin, S.R. The current status of crop forecasting in the australian wine industry. In *ASVO Seminar Series: Grapegrowing at the Edge*; Tanunda, Australia, 2003; pp. 4–8.

6. Martin, S.; Dunstone, R.; Dunn, G. *How to Forecast Wine Grape Deliveries Using Grape Forecaster Excel Workbook Version 7*; GWRDC: Adelaide, Australia, 2003; p. 100.

7. Blom, P.E.; Tarara, J.M. Trellis tension monitoring improves yield estimation in vineyards. *HortScience* **2009**, *44*, 678–685.

8. Smart, R.; Robinson, M. *Sunlight into the Wine. A Handbook for Winegrape Canopy Management*; Winetitles: Adelaide, Australia, 1991; p. 88.

9. Bertamini, M.; Tardaguila, J.; Iacono, F. Valutazione dell'equilibrio vegeto-produttivo e microclimatico del vigneto per l'ottimizzazione delle tecniche colturali a verde: Aspetti teorici e pratici. *Rivista dell'Istituto Agrario San Michele all'Adige (Bolletino ISMA)* **1994**, *2*, 24–40.

10. Gray, J.D.; Gibson, R.J.; Coombe, B.G.; Giles, L.C.; Hancock, T.W. Assessment of winegrape value in the vineyard—A preliminary, commercial survey. *Aust. NZ Wine Ind. J.* **1994**, *9*, 253–261.

11. Carbonneau, A. La surface foliaire exposee potentielle. Guide pour sa mesure. *Prog. Agric. Vitic.* **1995**, *112*, 204–212.

12. Tardaguila, J.; Martines de Toda, F. Assessment of tempranillo grapes quality in the vineyard by vitur score-sheet. *J. Int. Sci. Vigne Vin* **2008**, *42*, 59–65.

13. Kliewer, W.M.; Lider, L.A. Influence of cluster exposure to sun on composition of thompson seedless fruit. *Am. J. Enol. Vitic.* **1968**, *19*, 175–184.

14. Kliewer, W.M. Effect of day temperature and light intensity on coloration of vitis vinifera l grapes. *J. Am. Soc. Hort. Sci.* **1970**, *95*, 693–697.

15. Crippen, D.D.; Morrison, J.C. The effects of sun exposure on the compositional development of cabernet sauvignon berries. *Am. J. Enol. Vitic.* **1986**, *37*, 235–242.

16. Crippen, D.D.; Morrison, J.C. The effects of sun exposure on the phenolic content of cabernet sauvignon berries during development. *Am. J. Enol. Vitic.* **1986**, *37*, 243–247.

94

17. Reynolds, A.G.; Pool, R.M.; Mattick, L.R. Influence of cluster exposure on fruit composition and wine quality of seyval blanc grapes. *Vitis* **1986**, *25*, 85–95.

18. Mabrouk, H.; Sinoquet, H. Indices of light microclimate and canopy structure of grapevines determined by 3D digitising and image analysis, and their relationship to grape quality. *Aust. J. Grape Wine Res.* **1998**, *4*, 2–13.

19. Smart, R.E. Principles of grapevine canopy microclimate manipulation with implications for yield and quality. A review. *Am. J. Enol. Vitic.* **1985**, *36*, 230–239.

20. Garrido, M.; Mendez, V.; Valero, C.; Correa, C.; Torre, A.; Barreiro, P. Online dose optimization applied on tree volume through a laser device. In *Proceedings of First International Conference on Robotics and Associated High-Technologies and Equipment for Agriculture*, Pisa, Italy, 19–21 September 2012; pp. 325–330.

21. Fleck, S.; van der Zande, D.; Schmidt, M.; Coppin, P. Reconstruction of tree structure from laser-scans and their use to predict physiological properties and processes in canopies. In *International Archives of Photogrammetry, Remote Sensing and Spatial Information Sciences*; Thies, M., Spiecker, B.K.H., Weinacker, H., Eds.; ISPRS: Freiburg, Germany, 2004; Volume 36, pp. 119–123.

22. Moorthy, I.; Miller, J.R.; Berni, J.A.J.; Zarco-Tejada, P.J.; Qingmou, L. Extracting tree crown properties from ground-based scanning laser data. In *Proceedings of IEEE International Geoscience and Remote Sensing Symposium*, Barcelona, Spain, 23–28 July 2007; pp. 2830–2832.

23. Dey, D.; Mummert, L.; Sukthankar, R. Classification of plant structures from uncalibrated image sequences. In *Proceedings of IEEE Workshop on Applications of Computer Vision (WACV)*, Breckenridge, CO, USA, 9–11 January 2012; pp. 329–336.

24. Correa, C.; Valero, C.; Barreiro, P.; Diago, M.P.; Tardaguila, J. Feature extraction on vineyard by gustafson kessel fcm and k-means. In *Proceedings of 16th IEEE Mediterranean Electrotechnical Conference*, Hammamet, Tunisia, 25–28 March 2012; pp. 481–484.

25. Correa Farias, C.; Valero Ubierna, C.; Barreiro Elorza, P. Characterization of vineyard's canopy through fuzzy clustering and svm over color images. In *Proceedings of the International Conference of Agricultural Engineering*, Valencia, Spain, 8–12 July 2012.

26. Meunkaewjinda, A.; Kumsawat, P.; Attakitmongcol, K.; Srikaew, A. Grape leaf disease detection from color imagery using hybrid intelligent system. In *Proceedings of 5th International Conference on Electrical Engineering/Electronics, Computer, Telecommunications and Information Technology*, Krabi, Thailand, 14–17 May 2008; pp. 513–516.

27. Berenstein, R.; Shahar, O.B.; Shapiro, A.; Edan, Y. Grape clusters and foliage detection algorithms for autonomous selective vineyard sprayer. *Intell. Serv. Robot.* **2010**, *3*, 233–243.

28. Braun, T.; Koch, H.; Strub, O.; Zolynski, G.; Berns, K. Improving pesticide spray application in vineyards by automated analysis of the foliage distribution pattern in the leaf wall. In *Proceedings of the 1st Commercial Vehicle Technology Symposium*, Kaiserslautern, Germany, 16–18 March 2010.

29. Nuske, S.; Achar, S.; Bates, T.; Narasimhan, S.; Singh, S. Yield estimation in vineyards by visual grape detection. In *Proceedings of IEEE/RSJ International Conference on Intelligent Robots and Systems (IROS)*, San Francisco, CA, USA, 25–30 September 2011; pp. 2352–2358.

95

30. Tardaguila, J.; de Toda, F.M.; Poni, S.; Diago, M.P. Impact of early leaf removal on yield and fruit and wine composition of vitis vinifera L. Graciano and carignan. *Am. J. Enol. Vitic.* **2010**, *61*, 372–381.

31. Tardaguila, J.; Herrero-Langreo, A.; Barreiro, P.; Valero, C.; Poni, S.; Diago, M.P. Using rgb image analysis to assess the impact of early defoliation on the fruit zone. In *Proceedings of 17th International Symposium GiESCO 2011*, Asti-Alba, Italy, 29 August–2 September 2011.

32. Kotsiantis, S.B. Supervised machine learning: A review of classification techniques. *Informatica* **2007**, *31*, 249–268.

33. Tian, L.F.; Slaughter, D.C. Environmentally adaptive segmentation algorithm for outdoor image segmentation. *Comput. Electron. Agric.* **1998**, *21*, 153–168.

34. Bjurström, H.; Svensson, J. Assessment of grapevine vigour using image processing. M.S. Thesis, Linköping University, Linköping, Sweden, 2002.

35. Chamelat, R.; Rosso, E.; Choksuriwong, A.; Rosenberger, C.; Laurent, H.; Bro, P. Use of zernike moments for grape detection with image processing. In *Proceedings of 32nd Annual Conference on IEEE Industrial Electronics*, Paris, France, 6–10 November 2006; pp. 3697–3702.

36. Correa, C.; Moya, A.; Baguena, E.; Herrero, A.; Diago, M.a.B. J.; Tardaguilla, J.; Valero, C.; Barreiro, P. Feature extraction of the vineyard canopies, using images acquired on-the-go (RGB and RGIR. In *Proceedings of VI Congreso Ibérico de AgroIngeniería*, Évora, Portugal, 5–7 September 2011.

37. Correa, C.; Valero, C.; Barreiro, P.; Diago, M.P.; Tardaguila, J. A comparison of fuzzy clustering algorithms applied to feature extraction on vineyard. In *Proceedings of the XIV Conference of the Spanish Association for Artificial Intelligence*, Tenerife, Spain, 7–11 November 2011.

38. González, D.P. Algoritmos de agrupamiento basados en densidad y validación de clusters. Ph.D. Thesis, Universitat Jaume I, Castellón, Spain, 2010.

39. Son, J.; Inoue, N.; Yamashtia, Y. Geometrically local isotropic independence and numerical analysis of the mahalanobis metric in vector space. *Patt. Recog. Lett.* **2010**, *31*, 709–716.

40. McLachlan, G.J. Mahalanobis distance. *Reson. J. Sci. Educ.* **1999**, *4*, 20–26.

41. Al-Otum, H.M. Morphological operators for color image processing based on mahalanobis distance measure. *Opt. Eng.* **2003**, *42*, 2595–2606.

42. Herrero-Langreo, A.; Barreiro, P.; Diago, M.P.; Baluja, J.; Ochagavia, H.; Tardaguila, J. Pixel classification through mahalanobis distance for identification of grapevine canopy elements on rgb images. In *Proceedings of the Conference* on *Spectral Imaging of the International Association for Spectral Imaging*, Dublin, Ireland, 18–19 November 2010; pp. 40–41.

43. Palliotti, A.; Cartechini, A.; Ferranti, F. Morpho-anatomical and physiological characteristics of primary and lateral shoot leaves of cabernet franc and trebbiano toscano grapevines under two irradiance regimes. *Am. J. Enol. Vitic.* **2000**, *51*, 122–130.

44. Percival, D.C.; Fisher, K.H.; Sullivan, J.A. Use of fruit zone leaf removal with vitis vinifera l. Cv. Riesling grapevines. Ii. Effect on fruit composition, yield, and occurrence of bunch rot (botrytis cinerea pers.:Fr.). *Am. J. Enol. Vitic.* **1994**, *45*, 133–140.

45. Reynolds, A.G.; Yerle, S.; Watson, B.; Price, S.F.; Wardle, D.A. Fruit environment and crop level effects on pinot noir. III. Composition and descriptive analysis of oregon and british columbia wines. *Am. J. Enol. Vitic.* **1996**, *47*, 329–339.

96

46. Bergqvist, J.; Dokoozlian, N.; Ebisuda, N. Sunlight exposure and temperature effects on berry growth and composition of cabernet sauvignon and grenache in the central san joaquin valley of california. *Am. J. Enol. Vitic.* **2001**, *52*, 1–7.

47. Kliewer, W.M.; Dokoozlian, N.K. Leaf area/crop weight ratios of grapevines: Influence on fruit composition and wine quality. *Am. J. Enol. Vitic.* **2005**, *56*, 170–181.

48. Bledsoe, A.M.; Kliewer, W.M.; Marois, J.J. Effects of timing and severity of leaf removal on yield and fruit composition of sauvignon blanc grapevines. *Am. J. Enol. Vitic.* **1988**, *39*, 49–54.

3.2.2 On-the-go grapevine yield estimation using image analysis and Boolean model

Título de la publicación: On-the-go grapevine yield estimation using image analysis and Boolean model

Autores: MILLAN, B., VELASCO-FORERO, S., AQUINO, A., TARDÁGUILA, J.

Publicado en: En proceso de revisión

Resumen:

En este trabajo se describe una metodología para la estimación de la producción de forma no invasiva utilizando análisis de imagen y modelos Booleanos.

El análisis de imagen se ha utilizado para la estimación de la producción de uva anteriormente, pero el efecto de los errores de segmentación y las oclusiones por parte de los racimos u otros órganos de la vid afectan a la precisión obtenida. Con el fin de mejorar la estimación de la producción, se propone el uso del modelo Booleano, como alternativa para la estimación del número de bayas mediante análisis de imagen.

Se han utilizado tres conjuntos de datos diferentes para evaluar la metodología propuesta: imágenes de racimo, imágenes de cepa e imágenes de cepa capturadas automáticamente y en movimiento utilizando un vehículo agrícola. La estimación del número de bayas por racimo se obtuvo con un error cuadrático medio (RMSE) de 20 y R^2=0,80, mientras que en el caso de las imágenes de cepa capturadas manualmente los resultados fueron RMSE=310g y R^2=0,81. Finalmente, las imágenes capturadas en movimiento permitieron la estimación de la cosecha con una precisión de R^2=0,78 y RMSE=610g para segmentos compuestos por tres cepas (error de 200g por cepa).

La robustez del método frente a las oclusiones y los errores en la segmentación lo hacen ideal para la estimación de la producción, mejorando los resultados obtenidos frente a una estimación basada únicamente en el área del racimo.

Contribución del autor de la Tesis:

La contribución de Borja Millán fue determinante para la generación del artículo, e incluye el diseño experimental, coordinación del trabajo, captura de datos en campo y generación de los algoritmos de análisis de imagen. Además, Borja Millán escribió el artículo y realizó el análisis de los resultados.

1 # On-the-go grapevine yield estimation using image analysis and
2 Boolean model
3

4 Borja Millan[a,b], Santiago Velasco-Forero[b], Arturo Aquino[a] and Javier Tardaguila[a*]

5 * Corresponding author. E-mail: javier.tardaguila@unirioja.es (J. Tardáguila).
6 [1]: Instituto de Ciencias de la Vid y del Vino (University of La Rioja, CSIC, Gobierno de La Rioja), Finca La Grajera, 26007,
7 Logroño, La Rioja, Spain
8 [2]: MINES ParisTech, PSL Research University, CMM - Center of Mathematical Morphology
9

10 ## Abstract

11 This paper describes a new methodology for non-invasive, objective and automated
12 assessment of yield in vineyards using image analysis and Boolean model. Image analysis, as an
13 inexpensive and non-invasive procedure, has been studied for this purpose, but the effect of
14 occlusions from the cluster or other organs of the vine have an impact that diminish the
15 quality of the results. To reduce the impact of the occlusions in the estimation the number of
16 berries was assessed using the Boolean model.
17 To evaluate the methodology, three different datasets were studied: cluster images, manually
18 acquired vine images and vine images captured on-the-go using a quad. The proposed
19 algorithm estimated the number of berries in cluster images with a root mean square error
20 ($RMSE$) of 20 and a coefficient of determination (R^2) of 0.80. Vine images manually taken were
21 also analysed, providing 310 grams of mean error and R^2=0.81. Finally, images captured using a
22 quad equipped with artificial light and automatic triggering of a digital camera were also
23 analysed. The estimation obtained applying Boolean model had 610 grams of mean error per
24 segment (three vines) and R^2=0.78. The reliability against occlusions and segmentation errors
25 of the Boolean model makes it ideal for vineyard yield estimation. Its application greatly
26 improved the results when compared to a simpler estimator based on the relationship
27 between cluster area and weight.
28
29 **Keywords:** computer vision; precision agriculture; precision viticulture; non-invasive sensing
30 technologies; *Vitis vinifera* L.
31

32 ## Nomenclature
33

2D	two dimensional
3D	three dimensional
ATV	all-terrain vehicle
CC	connected component
FN	false negative
FP	false positive
HSV	hue saturation value colour space
MPM	membership probability map
rad	radius
RGB	red green blue colour space
RMSE	root mean square error
ROI	region of interest
TP	true positive

34

1. Introduction

Sustainable viticulture requires continuous monitoring of the vineyard to assist the decision-making procedure and to optimize cultural practices like pruning, irrigation and disease management. The use of non-invasive proximal sensors reduces the time and labour resources, favouring objective data acquisition. Image analysis techniques allows for fast and reliable measurements, and recent studies have aimed its use in viticulture. Application examples include canopy status assessment (Maria Paz Diago, Krasnow, Bubola, Millan, & Tardaguila, 2016; Gatti et al., 2016) and more recently, pruning mass determination (Kicherer et al., 2016). As a non-invasive, reliable and low-cost technology, image analysis is also a candidate for its integration in fully automated systems for vineyard monitoring (Kicherer et al., 2015). These tools are key devices for the future viticulture, as they will reduce management costs and will allow the application of more sustainable practices.

Grapevine yield estimation is encouraged by its economical relevance (G.M Dunn, 2010; Martin et al., 2002; Wolpert & Vilas, 1992), and can help to optimize plant growth and to improve fruit quality (Gregory M Dunn & Martin, 2003). Early yield estimation can be generated from the flower number per inflorescence obtained using computer vision (Millan, Aquino, Diago, & Tardaguila, 2016). Estimations representing final yield variability can be acquired nearby to harvest time using cluster images (Nuske, Achar, Bates, Narasimhan, & Singh, 2011). To improve the image quality and ease the segmentation process, some authors captured the images under controlled conditions, in the laboratory or using a specially developed chamber (Maria P. Diago et al., 2015; Liu, Whitty, & Cossell, 2015). Due to the destructive, slow and labour demanding nature of this process, it is hard to scale it to increase the sample points. Another approach would be the manual acquisition of images on the field (Maria Paz Diago et al., 2012; Gregory M Dunn & Martin, 2004; Herrero-Huerta, González-Aguilera, Rodriguez-Gonzalvez, & Hernández-López, 2015), but although this method requires less workforce, a more automatized approach is desirable for a commercial application. Finally, modified agricultural vehicles can be used to automate the image capture of large datasets (Font et al., 2015; Nuske et al., 2014). This approach has to face the limitation introduced by the lack of supervision during the capturing process that greatly affects to image quality. The segmentation process of images captured on the field is challenging, because of the uncontrolled scenario characteristics and the lack of uniformity in the berry surface caused by the pruine (Maria P. Diago et al., 2015). Also, it must be noted that not all the berries in a cluster are visible due to occlusions from other berries or vegetal material from the vine. A method that has resistance to these problems (occlusions and segmentation errors) will greatly improve the prediction reliability.

The Boolean model and random set theory was developed by Georges Matheron (1975) and Jean Serra (1980). From an image processing viewpoint, the practical advantage of this model relies in its capabilities to estimate the number of particles present in an image, even when errors in the segmentation or occlusions are present. It has been mainly used for modelling material structure characteristics (Jeulin, 2000; Matheron, 1975; J. Serra, 1980), for estimating the spatial distribution of bacterial colonies in cheese (Jeanson et al., 2011) or the number of cells in a cluster (Jesús Angulo, 2010). However, to the best of our knowledge, it has not been used in agriculture for berry and yield estimation.

This study aims at grapevine yield assessment using image analysis and Boolean model. This solution was tested under three different scenarios: cluster images, manually acquired vine images and on-the-go captured vine images using a quad at commercial speed.

102

1

2. Material and Methods

2.1. Image acquisition

4

The experiments were conducted in September 2014 and 2015 in a commercial vineyard located in Falces (Latitude 42°27′45.96″, Longitude 1°48′13.42″, Altitude 325 m; Navarra, Spain). The vines were growing in a vertical shoot positioning system, with north-south row orientation at 2 x 1 m disposition. Five different grapevine (*vitis vinifera* L.) varieties were used. The choice of a multi-varietal experiment was made to increase the variability in yield components. The six first basal leaves of the selected vines were manually removed after berry-set.

Three different sets of images were captured:

- **Manually acquired cluster images:** 45 images of clusters from four different grapevine varieties (Cabernet Sauvignon, Garnacha, Syrah and Tempranillo) were captured in the field the 4th of September 2014 and harvested next day. The images were taken using a Nikon D5300 digital reflex camera (Nikon corp., Tokyo, Japan) equipped with a Sigma 50mm F2.8 macro (Sigma corp., Kanagawa, Japan). RGB images were captured with uncontrolled illumination using an orange cardboard as background, and saved at a resolution of 24 Mpx (6000 × 4000 pixels), 8 bits per channel.
- **Manually acquired vine images:** 45 images from four different grapevine varieties (Cabernet Sauvignon, Garnacha, Syrah and Touriga Nacional) were taken in the field at the same date as cluster images using a Nikon D5300 digital reflex camera equipped with a Nikon AF-S DX 10 NIKKOR 18-55mm f/3.5-5.6G VR lens. RGB images were captured with a tripod and under uncontrolled illumination using a white panel as background. The distance between the camera and the vine was not pre-established, but kept around 120 cm. The images were saved at a resolution of 24 Mpx (6000 × 4000 pixels), 8 bits per channel.
- **On-the-go acquired vine images:** 64 images from three different grapevine varieties (Cabernet Sauvignon, Syrah and Tempranillo) were captured at night time the 9th of September of 2015 using an ATV (Trail Boss 330, Polaris Industries, Minnesota, USA) at a speed around 7 Km h^{-1}. Clusters were harvested and weighted the next day. The vehicle was equipped with a Sony alpha 7-II digital mirrorless camera (Sony Corp., Tokyo, Japan). The camera had a Vario-Tessar FE 24-70 mm lens. RGB images were saved at a resolution of 24 Mpx (6000 x 3376 pixels), 8 bits per channel and manually combined to obtain 28 sections composed by three vines. A 900 LED Bestlight panel and two Travor spash IS-L8 LED lights were used for scene illumination. The ATV was fitted with an adjustable mechanical structure that allowed for different height and depth fixation to adapt to the vines configuration (Figure 1A). The structure also provided protection against branch impact and allowed the attachment of the illumination equipment. The camera was triggered by a custom-built controller based on Arduino MEGA (Arduino LLC, Italy). The controller generated the shooting signal based on the information received from an inductive sensor attached to the rear axle. This sensor produced 3 pulses per rear-axle revolution, thus allowing to obtain images with an approximate 40% of superposition rate.

1 **2.2. Boolean model for berry number estimation**
2

3 Boolean Random Closed Sets (Matheron, 1975) have been widely used for particle number
4 estimation in images (J. P. Serra, 1982). The main strength of this model is its robustness
5 against partly covered objects and errors in segmentation.

6 The model can be applied if the structure is Boolean (J. Serra, 1980), but not limited to this
7 case due to the Central Limit Theorem (Jesús Angulo, 2010). To estimate the number of objects
8 in a region Z, the following formulation can be used:

$$9 \qquad Number\ of\ objects = \ -\frac{a_z}{a'}\log q$$

10 where a_z is the area under study (ROI), a' is the mean area of the object and q is the ROI
11 porosity:

$$12 \qquad q = \frac{\#pixels\ of\ the\ ROI - \#pixels\ of\ the\ segmented\ area}{\#pixels\ of\ the\ ROI}$$

13

14 The Boolean model can be directly used for berry number estimation, but the ROI must be
15 defined so that the concentration of particles is similar on it. In the case of vine images,
16 particles (berries) concentration is limited to portions in the image (clusters), so a ROI not
17 corresponding to all the image area must be selected for proper porosity calculation. The ROI
18 was obtained by applying a morphological opening (Soille, 2004) (morphological erosion
19 followed by dilation) for all the segmented clusters using a circular kernel of the same radius of
20 the mean berry size.

21 To test the prediction capabilities of the Boolean model, four tests were conducted (each one
22 composed of 100 simulations). The tests were performed by using Matlab (R2010b,
23 Mathworks, Natick, MA, USA) to generate synthetic images containing randomly placed
24 particles. First, the test compared the error of the Boolean model for 50 randomly positioned
25 particles of a radius equal to 5 in an image composed by 100 x 100 pixels. Next, random
26 variation on the radius of each particle (up to 30%) was used to generate a new set of
27 simulations. The same tests were also performed for 500 particles in an identical area for fixed
28 and variable radius.

29 For comparison purposes, a naïve estimator was also defined as follows:

$$30 \qquad Number\ of\ objects = \frac{\#pixels\ segmented\ as\ cluster}{\#pixels\ corresponding\ to\ mean\ object\ area}$$

31 This estimator only takes into account the relationship between the area of the particles
32 (cluster/s) and the mean particle area (berry). This formulation is similar to other approaches
33 used in the bibliography (Maria Paz Diago et al., 2012; Gregory M Dunn & Martin, 2004).

34 **2.3. Image analysis algorithm for berry number estimation**
35

36 The three previously described sets of images (cluster, vine manual and vine on-the-go) were
37 analysed using similar approaches: first the clusters were segmented, then the Boolean model
38 was applied to estimate berry number.

104

1   The Boolean model used for berry number estimation only requires as inputs an average
2   radius of the particle (berry) and the area of the segmented regions, or more specifically for
3   this application, the segmented cluster (the procedure is described in section 2.3.1). To
4   determine the mean berry radius, different approaches were used depending on the type of
5   the images to be analysed:

6   • **Cluster images:** the berry radius was manually extracted (an operator selected two
7   points at the equatorial line of a berry). This process was repeated for every image
8   because of the radius variation depending on the distance between the camera and
9   the cluster.
10   • **Vine images:** an average radius was set (manually extracted in one image as in the
11   cluster dataset) and applied to all images from the same grapevine variety.

12   The algorithm for image analysis was implemented in MATLAB and processes batches of
13   images in a fully automated way. The segmentation process was based in the Mahalanobis
14   distance, afterwards transformed to a membership probability map and is described in
15   section 2.3.1. For the on-the-go images, an additional filtering step was applied to reduce
16   misclassification between the pixels corresponding to clusters and the metal wires used for
17   the vine support. The generation of the filter is described in section 2.3.2.

18

2.3.1. Cluster segmentation

20

21   For every pixel, the Mahalanobis distance (McLachlan, 1999) was calculated using a six
22   dimensions classifier based on the Red-Green-Blue colour model (RGB) and the Hue-
23   Saturation-Value (HSV) representation. HSV and RGB are different colour spaces, being RGB
24   closer to physical image acquisition and HSV having the advantage of separating the colour and
25   illumination information (*croma* and *luma*, respectively), thus making colour information
26   invariant to non-uniform illumination. Hue component of the HSV transformed image is
27   angular and defined from 0° to 360°. This represents a problem when an image is stored in an
28   8 bit-per-band matrix, as there no exists continuity between 0 and 255 (in contrast to 0° and
29   360° in the HSV representation). To fix this, the converted images were modified to place the
30   blue colour (close to the average cluster colour) in the centre of the interval (128), so the
31   Mahalanobis distance can be calculated without discontinuities for this class. Seeds were
32   manually selected to train the Mahalanobis distance classifier. After the distance was
33   calculated for every pixel, it was converted to an occurrence probability to obtain a
34   membership probability map (Jesus Angulo & Velasco-forero, 2010) (MPM) using the
35   Boltzmann distribution (McQuarrie, 1976). The Boltzmann distribution is a transformation that
36   gives the probability for a system to be in a certain state as a function of that state's energy
37   and temperature. For this application, the Mahalanobis distance is used as the energy of the
38   system. The formula that describes the probability for a given pixel in the coordinates *(x,y)* for
39   a class *i* is:

40
$$MPMcolour_{x,y,i} = \frac{e^{\left(-d_i(x,y)/kT\right)}}{\sum_{j=1}^{M} e^{\left(-d_j(x,y)/kT\right)}}$$

where $d_k(x,y)$ corresponds to the Mahalanobis distance of the pixel located at the *(x,y)* coordinates and its reference value for the class *i*. *kT* is a constant that in the original formulation of the Boltzmann distribution corresponds to the multiplication of the Boltzmann constant and the thermodynamic temperature; for this application, it was fixed to 10. The denominator guarantees that all the probabilities are normalized and the sum of the *M* class probabilities is equal to 1 for every pixel of the MPM.

2.3.2. Additional filters for cluster segmentation for on-the-go captured images

The *MPMcolour* can be combined with other MPMs generated using morphological data to aid in the segmentation process. Hence, three additional MPMs were defined to improve the cluster segmentation for the on-the-go images:

- **Cluster proximity MPM (*MPMcluster_proximity*):** As a pre-process, a pyramidal decomposition with step values similar to berry size (5 by 5 pixels) was conducted on the pixels that had the maximum likelihood to cluster class (from *MPMcolour*). Next, a Gaussian filter with a standard deviation set to 3 times the average grape radius was used to expand the cluster pertinence probabilities. By doing this, pixels in the neighbourhood of the previously filtered cluster candidates increase their possibility of pertinence to the cluster class. Also, isolated pixels that were not close to clusters will decrease its cluster class membership probabilities.
- **Shape-Angle MPM (*MPMcable*):** Due to the misclassifications between the cluster and cable class, and taking advantage of the well-defined shape characteristics of the cable, a filter was defined. As a first step, all the connected components (CCs) corresponding to the cable and cluster class (from *MPMcolour*) were extracted, and all the CCs whose area were lower than the size of the mean berry were eliminated, what is to say:

$$Area(CC_i) > r_{berry}^2 * \pi$$

  where $Area(CC_i)$ corresponds to the number of pixels of *ith* CC and r_{berry} is the mean berry radius.

  Then, the length and orientation of the major and minor axis for every remaining CC were determined. The shape relation was calculated as the division of the major by the minor axis length:

$$Shape\ relation = \frac{major\ axis\ length}{minor\ axis\ length}$$

  Combining these two descriptors, a new MPM was generated as follows:

$$MPMcable = (1 - Shape\ relation) * (1 - abs(Major\ axis\ orientation/90))$$

- **Linear occurrence zone (*MPMlinear_occurrence_zone*):** As the cables along the vines were usually placed at fixed heights, there were horizontal sections in the images were the probability of a pixel to belong to the cable class was higher. To determine these zones independently from the camera or cable position in the image, an automatic

detector was built. The CCs most likely to correspond to the cable class were used. For this purpose, all the CCs with an orientation between $\pm 30°$ and with a shape relation lower than 0.5 were chosen to generate a binary image ($Cable_b$). From this, an accumulator for each row based on the sum of the number of pixels selected as cable class were generated using the following expression:

$$Accumulator_y = \sum_{x=1}^{\substack{number\ of \\ columns}} Cable_b(x,y)$$

being $Cable_b(x,y) = \begin{cases} 1\ if\ I(x,y) \in Filtered\ CCcable \\ 0\ otherwise \end{cases}$

for every column x and row y in the image I.

This accumulator holds the number of pixels of the filtered cable candidates for each row; as an example, the accumulator of Figure 2A is showed in Figure 2B. The next step is to apply a Gaussian filtering, thus allowing to some flexibility in the angle of the cables, not limiting it to the horizontal case. The result of the smoothing is presented in Figure 2C. The final MPM of the Linear occurrence zone is obtained by expanding the smoothed accumulator to all the rows of the image. Figure 2D shows the MPM (in grayscale) along with the filtered CCs that were overprinted in red colour for illustration purposes.

The final MPM used to classify the pixels as clusters for the on-the-go images was obtained by the elementwise multiplication of the four previously calculated MPMs: *MPMcolour*, *MPMcluster_proximity*, *MPMcable* and *MPMlinear_occurrence_zone*.

2.4. Validation

To evaluate the developed algorithms, yield estimation has to be confronted with real data. Also, due to the especial characteristics of the on-the-go images, the segmentation was ranked before and after the filtering MPMs were applied.

The ground truth for every data set was obtained as follows:

- **Manually acquired cluster images**: All the photographed clusters were cut and introduced into pre-tagged plastic bags to allow their conservation during their transport to the laboratory. Then, they were destemmed and the berries were detached, counted and weighted. The number of berries per cluster and their weight was used to obtain the average berry weight.
- **Manually acquired vine images**: After the image capturing process, all the vines were harvested and the clusters were weighted together to obtain the final yield per vine.
- **On-the-go acquired vine images:** After image acquisition, the sections composed of three vines were harvested and the clusters weighted together to obtain the final yield per section.

1 To evaluate the segmentation process of the on-the-go images and the improvements of the
2 multi-MPM filtering, it is necessary to obtain a ground truth. An application allowing to
3 manually select the berry centres was built to generate a mask representing the area occupied
4 by the clusters in the image. An example of photograph automatically captured on-the-go is
5 showed in Figure3A, and the manually selected pixel classification for benchmarking this image
6 is showed in Figure 3B.

7 The mask generated using this application was used to obtain the following metrics:

8 • **True positive (*TP*):** a pixel classified as corresponding to a cluster that actually matches
9 a cluster pixel in the manually selected mask.
10 • **False positive (*FP*):** a pixel classified as corresponding to a cluster that does not match
11 a cluster pixel in the manually selected mask.
12 • **False negative (*FN*):** A pixel that was automatically classified as not corresponding to
13 cluster but actually corresponding to a cluster in the mask.

14 Finally, the *Recall* and *Precision* metrics were used for evaluating the quality of each analysed
15 image as follows:

$$Recall = \frac{TP}{TP + FN}$$

16

17 where Recall provides the percentage of actual cluster pixels detected.

$$Precision = \frac{TP}{TP + FP}$$

18

19 where Precision indicates the percentage of pixels correctly assessed.

20 ## 3. Results and discussion
21 ### 3.1. Evaluation of the occlusion robustness of the Boolean model
22

23 As described in section 2.2, four tests were performed to evaluate the occlusion robustness of
24 the Boolean model and to compare its results to those generated by the naïve estimator.
25 Figure 4A and B show the simulations corresponding to 50 particles of fixed / variable radii,
26 respectively. As it can be checked in Table 1, the error rates for both estimators were low and
27 similar, but with slight improvement for the case of the naïve estimator. For the third and
28 fourth experiments, the number of particles was increased 10 times, being particle occlusion
29 more likely to occur under these conditions (Figure 4C and D). The Boolean model estimates
30 the number of particles with an error rate similar to the low occlusion case. Contrary, the error
31 yielded by the naïve estimator rose to 25% for fixed and variable radii. These findings are
32 coincident to the ones obtained by Jesús Angulo (2010) for the number of cell clusters
33 estimation in fluorescence marked cell images, were the number of nuclei obtained by the
34 Boolean model is more robust than a simple ratio of surfaces (equivalent to the naïve
35 estimator). Some approaches had been studied for evaluate berry occlusions within a cluster.
36 Nuske *et al.* (2014) tested the relation between total berry count, visible berry count and 3D
37 models from 2D images, but the results showed no improvement on partially occluded berry
38 assessment. As showed in the simulations, the use of the Boolean model would improve the
39 berry number estimation robustness.

	50 particles		500 particles	
	rad = 5	rad=5±15%	rad=5	rad=5±15%
Naïve estimator*	1.7%	2.3%	24.9%	25.1%
Boolean model*	2.4%	2.7%	2.1%	2.1%

4

5 ## 3.2. Evaluation of the berry number per cluster estimation

6

7 An example image of a cluster, corresponding to the Cabernet Sauvignon variety, is showed in
8 Figure 5A. The uncontrolled conditions during the capturing process explains the excess of
9 illumination in the berries that are placed at the right side of the image, which received direct
10 sun illumination, in contrast to the rest of the cluster that had indirect lighting. Due to the
11 image characteristics, segmentation errors occurred affecting the area finally segmented
12 (Figure 5B). Results obtained after applying the estimation models (Boolean and naïve) are
13 showed in Table 2 and in Figure 6A. The naïve estimator failed to provide a good prediction,
14 with a global $RMSE$=60 (Table 2) vs $RMSE$=20.1 obtained using the Boolean model. It can be
15 understood by observing Figure 6A, as the naïve estimation slope was not close to 1 (was
16 0.25), that would correspond to a perfect estimation trend. This contrasted with the
17 estimation from the Boolean model, whose slope was 0.93, demonstrating its prediction
18 capabilities.

Grapevine variety	Manual counting		Naïve estimator			Boolean model		
	Mean berry number	Number of clusters	Mean berry number	RMSE	R^2	Mean berry number	RMSE	R^2
Cabernet Sauvignon	68.4	15	26.7	48.8	0.34*	79.1	14.8	0.86***
Grenache	53.8	12	18.2	37.5	0.72***	44.1	23.3	0.54**
Syrah	79.0	11	32.3	50.7	0.72***	92.5	21.2	0.69**
Tempranillo	141.4	7	43.9	107.6	0.81**	136.6	22.0	0.66*
Total	85.7	45	30.3	60.0	0.71***	88.1	20.1	0.80***

24

25 Table 2 shows that the results obtained using the naïve estimator were very variable upon the
26 grapevine variety. This was caused by the occlusions (more likely to occur in more compact
27 varieties) and errors in the segmentation. In the other hand, the results obtained with the

1   Boolean model were more homogenous, minimizing differences between varieties and
2   improving the results when all of them were examined together. This homogeneity suggests
3   that this method is more generalizable, although more extensive studies must be conducted to
4   prove this premise.

5   The results obtained are comparable to others in the bibliography. The outcomes obtained by
6   Diago *et al.* (2015) are similar (Table 3), but it must be noted that their methodology is not
7   applicable under field conditions. The procedure requires to collect the clusters and to take the
8   images in a chamber with controlled lighting and background. Apart from that, the algorithm is
9   more complex, requiring the segmentation of the image, edge detection, circle detection and
10   filtering. In the other hand, the presented method only requires the segmentation and mean
11   berry radius for the berry number estimation. Herrero-Huerta *et al.* (2015) developed a system
12   for berry number assessment from images taken in the field. This procedure relies on a 3D
13   structure reconstruction from at least 5 images with high overlapping (80-90%). Their findings
14   (Table 3) are very similar to the ones detailed in this publication, but without the need of
15   multiple image acquisitions per cluster. Finally, Liu *et al.* (2015) proposed a similar
16   methodology using 3D models extracted from images captured in a laboratory under
17   controlled conditions. They presented their results combining Cabernet Sauvignon and Syrah
18   clusters; these figures are also included in Table 3. Results are similar to those obtained by the
19   Boolean model, but without the constraint of taking the images in laboratory. It must be noted
20   that the experiments conducted under laboratory conditions are destructive, labour
21   demanding and thus hence not easy to expand the sampling rate for a commercial application.

22   *Table 3: Comparison of the measured coefficient of determination (R^2) for the estimation of berry number per cluster*
23   *using image analysis for different varieties in other published studies (under different capturing conditions) and in*
24   *this work using Boolean model.*

	Tempranillo	Grenache	Syrah	Cabernet Sauvignon	Cabernet Sauvignon and Syrah	Capturing conditions
Diago *et al.* (2015)	0.84	0.69	-	0.62	-	Laboratory
Herrero-Huerta *et al.* (2015)	0.78	-	-	-	-	Field
Liu *et al.* (2015)	-	-	-	-	0.85	Laboratory
The present work	0.66	0.54	0.69	0.86	0.79	Field

25

26

27   ### 3.3. Evaluation of the yield estimation from manually captured vine images
28

29   An example image of a vine of cv. Cabernet Sauvignon can be observed in Figure 7A. The image
30   segmentation was carried out using the described Mahalanobis classifier (section 2.3.1), the
31   result of the segmentation can be observed in Figure 7B. Even when the overall classification
32   quality was good, some errors were observed, especially with parts of the trunk being
33   classified as clusters. This greatly affected the performance of the naïve estimator (Table 4),
34   providing a *RMSE* of 777.2 g when all the varieties were studied together. Contrary, the
35   Boolean model offered more robustness against errors in the segmentation and occlusions.
36   Indeed, the *RMSE* for yield estimation was 310.2 g when all the varieties were studied as a
37   whole, and also, performance for each grapevine variety was higher for the Boolean model
38   than for the naïve estimator. R^2 values showed less difference between the two models.

110

1 However, looking at Figure 6B, it is clear that the naïve model did not offer a correct
2 estimation (the slope is far from 1), even when providing appropriate R^2 values.

3

4 *Table 4: Results obtained for the yield estimation per vine based on manually captured grapevine images using the*
5 *naïve estimator and the Boolean model. Manual harvest refers to the weight of all the clusters corresponding to*
6 *each vine. Asterisks represent statistical significance: *: P ≤ 0.05; **: P ≤ 0.01; ***: P ≤ 0.001.*

Grapevine variety	Manual harvest		Naïve estimator			Boolean model		
	Mean Yield (g)	Number of vines	Mean Yield (g)	R^2	RMSE (g)	Mean Yield (g)	R^2	RMSE (g)
Cabernet Sauvignon	1311	12	736	0.82***	661.0	1386	0.85***	214.2
Grenache	1750	12	938	0.87***	993.9	1816	0.89***	320.6
Syrah	1231	11	509	0.93***	673.8	966	0.88***	263.7
Touriga Nacional	1249	10	622	0.55*	713.7	1202	0.45*	421.9
Total	1431	45	728	0.82***	777.2	1389	0.81***	310.2

7

8 Dunn *et al.* (2004) analysed the prediction potential of the segmentation of Cabernet
9 Sauvignon grapevines. They obtained a R^2=0.85 for the relation of normalized cluster area on a
10 section of 1m by 1m. It should be pointed out that their measured R^2 did not correspond to the
11 validation of a model, but it was calculated on the calibration set. Nevertheless, this value is
12 similar to those obtained for the validation of the models presented in this study without the
13 need of a hanging frame, that was used to extract the ROI. Diago *et al.* (2012) used the number
14 of pixels segmented as cluster class to generate a linear model for yield estimation. The
15 prediction produced R^2=0.73 and *RMSE*=749 g. This approach is similar to the use of the naïve
16 model, and the obtained results are equivalent to the ones produced by this estimator, but
17 sensibly surpassed by the performance of the Boolean model (R^2=0.81 and RMSE= 310 g).

18

19 **3.4. Evaluation of the yield estimation from on-the-go captured vine images**
20

21 The images were captured using the modified ATV showed in Figure 1A. The setup allowed for
22 image capture at a speed of 7 Km h^{-1}, similar to other agricultural vehicles. The continuous
23 movement of the vehicle, the vibrations induced by the rough terrain and the explosion motor
24 did not produce motion blur in the images due to camera automatic stabilization and high
25 speed capturing configuration (Figure 1B). Errors were encountered in the classification
26 process, with cross interference between the cluster and the cable class (representing the
27 metal wire used for the conduction vines in the vertical shoot positioning system). To evaluate
28 the convenience of the multi MPM filtering approach (described in section 2.3.2), the
29 segmentation was quantified using manually classified images as ground truth. The differences
30 in the results when multiple MPMs were applied are not remarkable in terms of Recall, but are
31 notable for the Precision (Table 5). This demonstrated that false positives were correctly
32 eliminated during the filtering, with little loss of true positives. The relative low values of Recall
33 (Table 5) can be explained by the difficulty in pixel discrimination because of the lack of
34 uniformity in the illumination. Figure 3B shows the regions manually segmented as clusters. As

of berries (ellipsoid 3D model) and clusters (convex hull 3D model). The results showed that the proposed correction models did not improved the overall estimation. In contrast to this, the Boolean estimator, that also compensates for partially occluded berries, generated better results (R^2=0.78).

4. Conclusions

This work presented a new method for accurate, non-destructive and in field grapevine yield estimation by using computer vision. Yield information is very valuable for viticulturists and grapegrowers, allowing them to take decisions prior to harvest based on objective measurements. A novel use of Boolean models has been assessed over three different data sets: images of isolated clusters, manually captured images of grapevines and on-the-go captured images of grapevines using a modified ATV at night time.

The use of Boolean models allowed to overcome two of the major difficulties in visual yield estimation: this technique is robust against segmentation errors and partial occlusions, situations that are usual in the case of images taken under field conditions. It provided more precision, using not only a model that is simpler than other previous proposals, but also less complex image analysis techniques. The capacity to estimate the visible berry number and the partially hidden ones was confirmed by the comparison between the results obtained with the Boolean model and the naïve estimator.

The simplicity and precision of the Boolean model formulation makes it ideal for its application on grapevine yield estimation, allowing its implementation in a fully automated system. The images were captured at a commercial speed, comparable to other agricultural equipment used in vineyard management, establishing this procedure close to viable application. This methodology can also be used to generate maps that represents the spatial variability of the vineyards, allowing for grapevine zoning and thus an increase in quality.

5. Acknowledgements

1 it can be confirmed, these regions were hardly distinguishable even by manual evaluation. An
2 illumination improvement might enhance the segmentation process and thus Recall.

3 *Table 5: Benchmark of the segmentation of clusters in images taken automatically on-the-go with and without*
4 *applying filtering (cluster proximity, shape-angle and linear occurrence zone). The performance of the segmentation*
5 *was tested against manually segmented images.*

Grapevine variety	Without filtering		With filtering	
	Recall	*Precision*	*Recall*	*Precision*
Cabernet Sauvignon	0.54	0.73	0.56	0.82
Syrah	0.64	0.68	0.57	0.80
Tempranillo	0.58	0.69	0.55	0.73
Total	0.58	0.71	0.56	0.79

6

7   The problems during the segmentation clearly affected the performance of the naïve estimator
8   (Table 6), whose *RMSE*=2472 g resulted in a lack of its practical application, even when the
9   coefficient of determination was acceptable (R^2=0.71). This represents the same scenario as in
10 cluster and manually taken images: the naïve estimator did not compensate for the occlusions
11 and errors in the segmentation, and the prediction did not follow the slope accurately (Figure
12 6D). In the other hand, the Boolean model was capable to correctly estimate yield, offering
13 *RMSE*=610.1 g. It must be noted that the estimation refers to segments composed by three
14 vines, so this value represents an improvement if it is compared to the manually captured
15 images, that yielded a *RMSE*=374.2 g for one isolated vine.

16 *Table 6: Results obtained for the estimation of yield per segment (composed of three vines) based on images*
17 *captured with an "on-the-go" platform. This measures were obtained when using a naïve estimator and the Boolean*
18 *model on images segmented using a Mahalanobis distance classifier and a three step filtering process. Asterisks*
19 *represent statistical significance: *: P ≤ 0.05; **: P ≤ 0.01; ***: P ≤ 0.001.*

Grapevine variety	Manual harvest		Naïve estimator			Boolean model		
	Mean Yield (g)	Number of segments	Mean Yield (g)	R^2	RMSE (g)	Mean Yield (g)	R^2	RMSE (g)
Cabernet Sauvignon	3406	8	1321	0.64*	1863.7	3235	0.50*	574.5
Syrah	3322	10	1598	0.87***	2031.9	3115	0.86***	390.6
Tempranillo	5031	10	2175	0.59**	3194.1	4660	0.60**	790.8
Total	3920	28	1698	0.71***	2472.0	3670	0.78***	610.1

20

21 Similarly to this work, Font *et al.* (2015) used an ATV equipped with cameras and artificial
22 illumination to capture 25 cluster images (not the entire grapevine) at night time. Then, they
23 estimated cluster weight from its segmented area. The prediction had 16% of error when all
24 the varieties were analysed together. In comparison, the results obtained for the Boolean
25 model had 15.6% of error using images framing three vines instead of cluster images (the
26 mean cluster number per section was 47). In other recent article, Nuske *et al.* (2014) also used
27 an ATV with artificial lighting for image capturing of grapevines. The collected images were
28 analysed to identify visible berries to estimate yield. This setup allowed to asses yield with a
29 R^2=0.73 for the best datasheet, being this comparable to the results given by the naïve
30 estimator (R^2=0.71), which also bases its estimation in the visible berries. They also tried to
31 boost the yield estimation thru an evaluation of the self-occlusion of berries using 3D models

1 References

Angulo, J. (2010). Nucleus modelling and segmentation in cell clusters. In A. D. Fitt, J. Norbury, H. Ockendon, & E. Wilson (Eds.), *Progress in Industrial Mathematics at ECMI 2008* (1st ed., pp. 217–222). London: Springer-Verlag Berlin Heidelberg. http://doi.org/10.1007/978-3-642-12110-4_30

Angulo, J., & Velasco-forero, S. (2010). Semi-supervised hyperspectral image segmentation using regionalized stochastic watershed. In S. S. Shen & P. E. Lewis (Eds.), *Proc. SPIE 7695, Algorithms and Technologies for Multispectral, Hyperspectral, and Ultraspectral Imagery XVI* (Vol. 7695, p. 76951F–76951F–12). Orlando: SPIE. http://doi.org/10.1117/12.850187

Diago, M. P., Correa, C., Millán, B., Barreiro, P., Valero, C., & Tardaguila, J. (2012). Grapevine yield and leaf area estimation using supervised classification methodology on RGB images taken under field conditions. *Sensors*, *12*(12), 16988–17006. http://doi.org/10.3390/s121216988

Diago, M. P., Krasnow, M., Bubola, M., Millan, B., & Tardaguila, J. (2016). Assessment of vineyard canopy porosity using machine vision. *American Journal of Enology and Viticulture*, *67*(2), 229–238. http://doi.org/10.5344/ajev.2015.15037

Diago, M. P., Tardaguila, J., Aleixos, N., Millan, B., Prats-Montalban, J. M., Cubero, S., & Blasco, J. (2015). Assessment of cluster yield components by image analysis. *Journal of the Science of Food and Agriculture*, *95*(6), 1274–1282. http://doi.org/10.1002/jsfa.6819

Dunn, G. . (2010). *Yield Forecasting. Grape and Wine research and development corporation*.

Dunn, G. M., & Martin, S. R. (2003). The current status of crop forecasting in the australian wine industry. In *ASVO Seminar Series: Grapegrowing at the Edge* (pp. 4–8). Tanunda, Barossa Valley, South australia.

Dunn, G. M., & Martin, S. R. (2004). Yield prediction from digital image analysis: A technique with potential for vineyard assessments prior to harvest. *Australian Journal of Grape and Wine Research*, *10*(3), 196–198.

Font, D., Tresanchez, M., Martínez, D., Moreno, J., Clotet, E., & Palacín, J. (2015). Vineyard yield estimation based on the analysis of high resolution images obtained with artificial illumination at night. *Sensors*, *15*(4), 8284–8301. http://doi.org/10.3390/s150408284

Gatti, M., Dosso, P., Maurino, M., Merli, M., Bernizzoni, F., José Pirez, F., … Poni, S. (2016). MECS-VINE®: A new proximal sensor for segmented mapping of vigor and yield parameters on vineyard rows. *Sensors*, *16*(12), 2009. http://doi.org/10.3390/s16122009

Herrero-Huerta, M., González-Aguilera, D., Rodriguez-Gonzalvez, P., & Hernández-López, D. (2015). Vineyard yield estimation by automatic 3D bunch modelling in field conditions. *Computers and Electronics in Agriculture*, *110*, 17–26. http://doi.org/10.1016/j.compag.2014.10.003

Jeanson, S., Chadœuf, J., Madec, M. N., Aly, S., Floury, J., Brocklehurst, T. F., & Lortal, S. (2011). Spatial distribution of bacterial colonies in a model cheese. *Applied and Environmental Microbiology*, *77*(4), 1493–500. http://doi.org/10.1128/AEM.02233-10

Jeulin, D. (2000). Random texture models for material structures. *Statistics and Computing*, *10*(2), 121–132. http://doi.org/10.1023/A:1008942325749

Kicherer, A., Herzog, K., Pflanz, M., Wieland, M., Rüger, P., Kecke, S., … Töpfer, R. (2015). An

automated field phenotyping pipeline for application in grapevine research. *Sensors*, *15*(3), 4823–4836. http://doi.org/10.3390/s150304823

Kicherer, A., Klodt, M., Sharifzadeh, S., Cremers, D., Töpfer, R., & Herzog, K. (2016). Automatic image-based determination of pruning mass as a determinant for yield potential in grapevine management and breeding. *Australian Journal of Grape and Wine Research*. http://doi.org/10.1111/ajgw.12243

Liu, S., Whitty, M., & Cossell, S. (2015). A lightweight method for grape berry counting based on automated 3D bunch reconstruction from a single image. In *ICRA*, *International Conference on Robotics and Automation (IEEE), Workshop on Robotics in Agriculture* (p. 4).

Martin, S. R., Dunn, G. M., Hoogenraad, T., Krstic, M. P., Clingeleffer, P. R., & Ashcroft, W. J. (2002). Crop forecasting in cool climate vineyards. In Winetitles (Ed.), *Proceedings for the 5th International Symposium on Cool Climate Viticulture and enology*. Melbourne, Australia: Winetitles.

Matheron, G. (1975). *Random sets and integral geometry*. New York: Wiley.

McLachlan, G. J. (1999). Mahalanobis distance. *Resonance*, *4*(6), 20–26.

McQuarrie, D. A. (1976). *Statistical Mechanics*. University Science Books.

Millan, B., Aquino, A., Diago, M. P., & Tardaguila, J. (2016). Image analysis-based modelling for flower number estimation in grapevine. *Journal of the Science of Food and Agriculture*. http://doi.org/10.1002/jsfa.7797

Nuske, S., Achar, S., Bates, T., Narasimhan, S., & Singh, S. (2011). Yield estimation in vineyards by visual grape detection. *IEEE International Conference on Intelligent Robots and Systems*, 2352–2358. http://doi.org/10.1109/IROS.2011.6048830

Nuske, S., Wilshusen, K., Achar, S., Yoder, L., Narasimhan, S., & Singh, S. (2014). Automated visual yield estimation in vineyards. *Journal of Field Robotics*, *31*(5), 837–860. http://doi.org/10.1002/rob.21541

Serra, J. (1980). The Boolean model and random sets. *Computer Graphics and Image Processing*, *12*(2), 99–126. http://doi.org/10.1016/0146-664X(80)90006-4

Serra, J. P. (1982). *Image analysis and mathematical morphology*. Orlando: Academic Press.

Soille, P. (2004). *Morphological image analysis: principles and applications* (2nd ed.). Berlin, Heidelberg: Springer-Verlag. http://doi.org/10.1007/978-3-662-05088-0

Wolpert, J. A., & Vilas, E. P. (1992). Estimating vineyard yields: Introduction to a simple, two-step method. *American Journal of Enology and Viticulture*, *43*(4), 384–388.

1 # Figure captions
2

3 **Figure 1:** On-the-go capturing system. (A) Modified ATV with automatic camera triggering, LED
4 illumination and structure for easy position adjustment. (B) Example image of a vine captured
5 on-the-go.

6 **Figure 2:** Steps for the generation of the MPMlinear_occurrence_zone aimed for reduction of
7 misclassification between cluster and cable class during segmentation. (A) Objects segmented
8 as cable candidates from images taken automatically with an ATV. (B) Accumulator of the
9 number of pixels of cable candidates for each row. (C) Smoothed accumulator. (D) Membership
10 probability map (MPM) for cable occurrence based on the position of the cable (in grayscale)
11 with the original candidates over imposed in red.

12 **Figure 3:** Ground truth generation for segmentation performance benchmarking. (A) Example
13 image of a vine captured "on-the-go" of cv. Tempranillo. (B) Ground truth mask of the clusters.
14 The berries were manually selected using a Matlab custom built aplication.

15 **Figure 4:** Simulation example of a random distribution of particles in a 100x100 pixel area. (A)
16 50 particles of radius= 5, (B) 50 particles with a random variation in the radius of the particle up
17 to 30%, (C) 500 particles with radius=5 and (D) and 500 particles with a random variation in the
18 radius of the particle up to 30%. The images were synthetically generated using Matlab.

19 **Figure 5:** Segmentation of manually taken cluster images. (A) Example image of a cluster of cv.
20 Cabernet Sauvignon captured under field conditions with an orange cardboard as background.
21 (B) Segmented image of the cluster using the Mahalanobis distance on six dimensions (i.e., using
22 RGB and HSV representations).

23 **Figure 6:** Graphic representation of the estimation results for weight estimation using the naïve
24 estimator (red and squares) and the Boolean model (blue and stars) for: (A) berry number per
25 cluster (naïve y=0.25x+8.4; Boolean y=0.93x+8.1), (B) yield per vine using manually captured
26 images (naïve y=0.42x+133.0; Boolean y=0.86x+195.2) and (C) yield per section (composed by
27 3 vines) using images captured on-the-go without filtering (naïve y=0.35x+345.4; Boolean
28 y=0.89x+151.9) (C) and applyng filters for cable pixels (naïve y=0.30x+460.6; Boolean
29 y=0.80x+552.7) (D). Dashed line represents 1:1 and dotted lines corresponds to 95% prediction
30 intervals.

31 **Figure 7:** Cluster segmentation on manually captured vine images. (A) Image of a vine cv.
32 Cabernet Sauvignon captured under uncontrolled illumination conditions with a digital camera
33 fixed on a tripod and using a white panel as background and (B) segmentation result using the
34 Mahalanobis distance clasifier on six dimensions (i.e. using RGB and HSV representations).
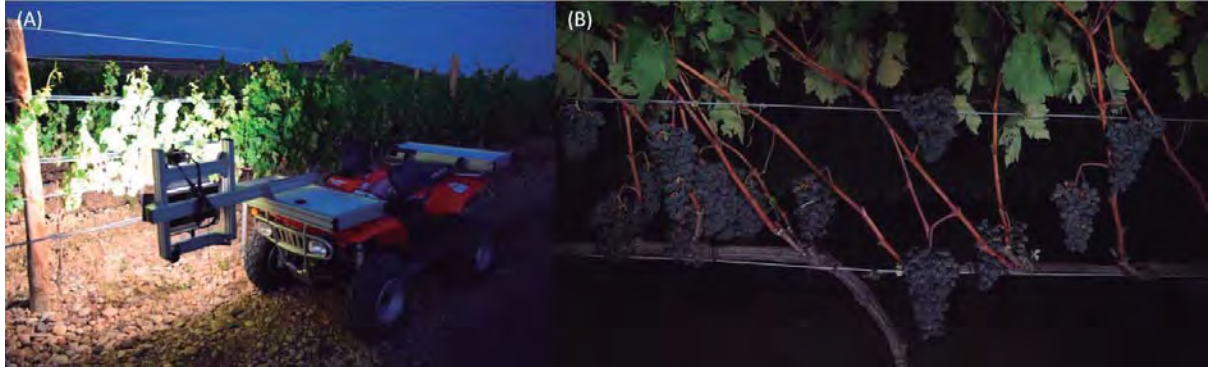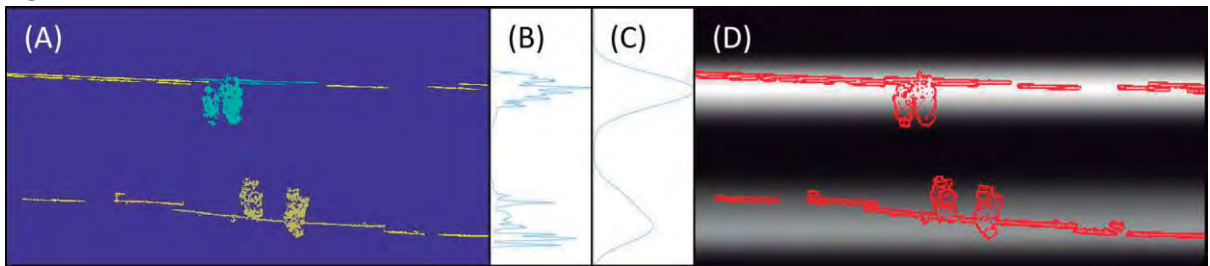
35

Figure 1

Figure 2

Figure 3

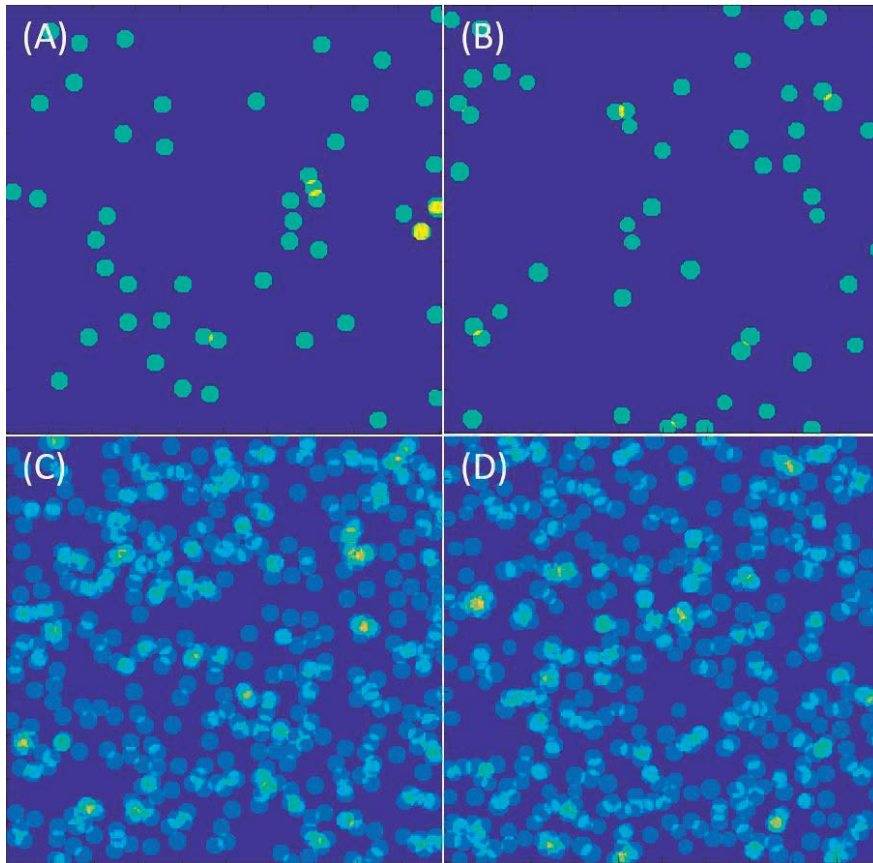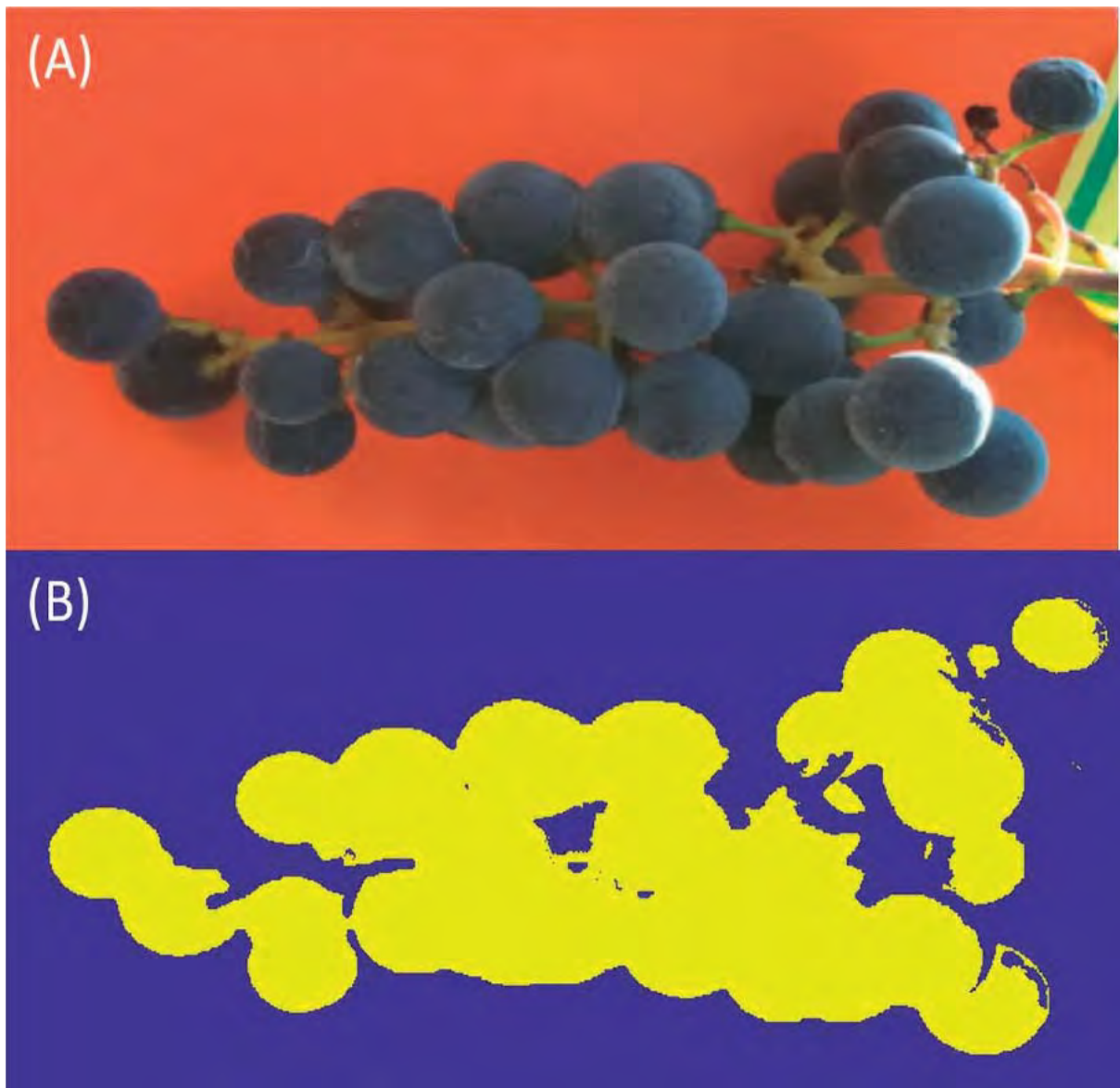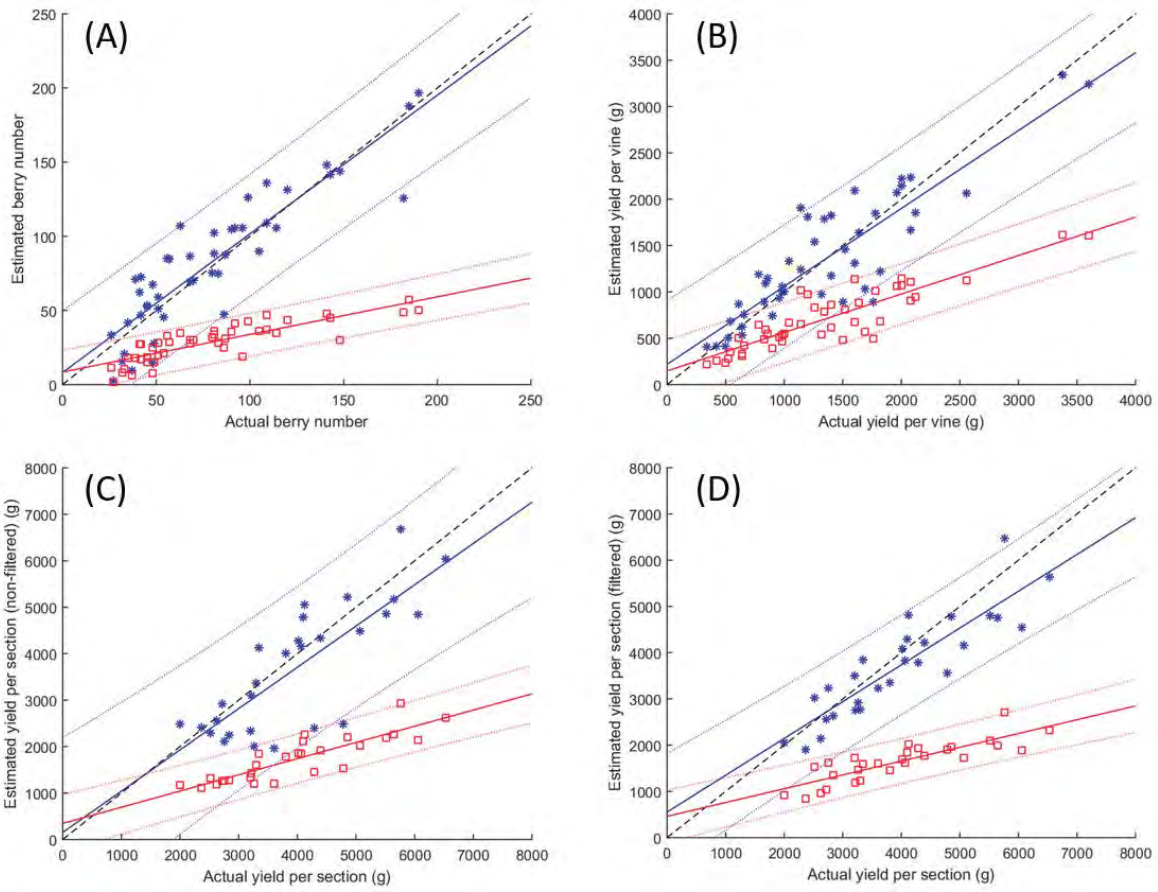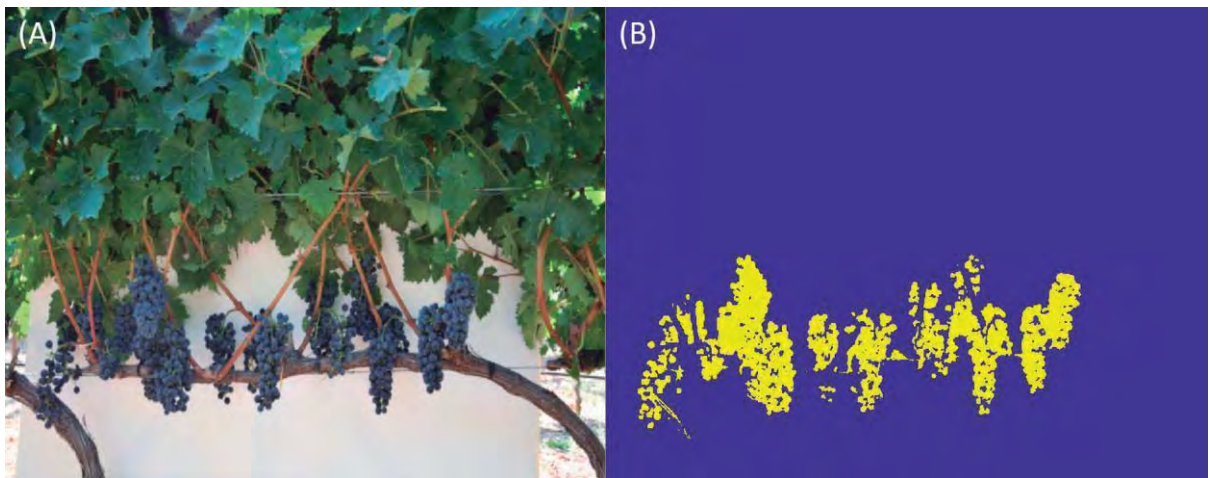Figure 4

Figure 5

Figure 6

Figure 7

3.3   Canopy status assessment

The management of the canopy affects grape quality, diseases incidence and yield. This is why canopy management is such an important part of vineyard management (Smart & Robinson, 1991).

Automated canopy assessment methodologies are key for precision viticulture, because the canopy management influences yield and quality intricately. The first study of this section describes an image analysis-based algorithm that can provide canopy porosity estimation with high precision (R^2>0.90) for gap assessment from images manually acquired.

The second study analysed images captured automatically and on-the-go providing high correlations when compared with the reference method for gap (R^2 >0.85); exposed leaves (R^2 >0.71); and exposed cluster (R^2=0.65) assessment. Moreover, the analysis of images captured on-the-go allows effortless massive sampling and map generation.

Finally, the third study focus on the assessment of pruning weight using computer vision algorithms. The proposed methodology is simple and provides a precise estimation (R^2>0.85) from images captured automatically on-the-go.

3.3.1 Assessment of vineyard canopy porosity from manually captured images

Título de la publicación: Assessment of vineyard canopy porosity using machine vision

Autores: DIAGO, M.P., KRASNOW, M., BUBOLA, M., **MILLAN, B.,** TARDAGUILA, J.

Resumen:

La porosidad de la "canopy" es un parámetro de gran interés vitícola, ya que favorece la exposición de los racimos y su aireación, facilitando la maduración, sanidad y calidad de la uva. El método estándar para la evaluación de la porosidad es el PQA (point quadrat analysis), pero es laborioso y lento, limitando su aplicabilidad en viñedos comerciales.

En el presente trabajo se expone una alternativa al PQA mediante análisis de imagen. Este método es objetivo, rápido, no invasivo y ha sido evaluado en viñedos de diferentes variedades y características localizados en Nueva Zelanda, Croacia y España. El coeficiente de determinación (R^2) entre el PQA y el análisis de imagen es superior a 0,90 ($p<0,05$) en cada uno de los experimentos, siendo el R^2 obtenido en la regresión global 0,93 ($p<0,05$). La hora del día y el lado de la "canopy" no fueron factores determinantes en la precisión del método.

La utilización de esta nueva herramienta permite evaluar el estado de la "canopy" y llevar a cabo las practicas vitícolas necesarias para la mejora de la calidad y sanidad de la uva.

Contribución del autor de la Tesis:

Borja Millán participó en el diseño experimental y su labor incluye la generación, testeo con datos de campo y ajuste de los algoritmos de análisis de imagen que permiten la estimación de la porosidad de la "canopy". También participó en la redacción del artículo.

The Publisher and copyright holder corresponds to American Journal of Enology and Viticulture. The online version of this journal is the following URL:

http://www.ajevonline.org/

3.3.2 Assessment and mapping of vineyard canopy porosity from on-the-go captured images

Título de la publicación: On-the-go assessment and mapping of vineyard canopy porosity, bunch and leaf exposure by image analysis

Autores: DIAGO, M.P., AQUINO, A., **MILLAN, B.,** TARDÁGUILA, J.

Publicado en: En proceso de revisión

Resumen:

La evaluación de la "canopy" es necesaria para una gestión correcta del viñedo. En este artículo se presenta un sistema de determinación de la porosidad de la "canopy" automático y no invasivo basado en análisis de imagen. La captura de imágenes se realizó de forma automatizada desde un vehículo en movimiento a 7 km/h, reduciendo de forma importante el esfuerzo necesario para la toma de datos.

Los resultados obtenidos se compararon con los generados por el método de referencia (PQA), obteniéndose altas correlaciones para el porcentaje de huecos (R^2 >0,85; p<0,001) y hojas expuestas (R^2 >0,71; p<0,001) por ambas caras de la "canopy" (defoliada y no defoliada), mientras que la exposición de racimos obtuvo una mejor relación para la cara expuesta (R^2=0,65; p<0,001).

Con los datos obtenidos con el algoritmo de análisis de imagen se pudieron generar mapas que representaban la variabilidad del estado de la "canopy". Estos mapas son de gran valor para el viticultor, ya que permiten delimitar zonas del viñedo con distintas necesidades y características. En el futuro, estos datos podrían combinarse con maquinaria automatizada para la defoliación o la aplicación de fito-sanitarios en función del vigor.

Contribución del autor de la Tesis:

Borja Millán participó en el diseño experimental y su labor incluye la captura de datos de campo, la generación y ajuste de los algoritmos de análisis de imagen que permiten la estimación de la porosidad de la "canopy". También participó en la redacción del artículo.

On-the-go assessment and mapping of vineyard canopy porosity, bunch and leaf exposure by image analysis

Journal:	Australian Journal of Grape and Wine Research
Manuscript ID	Draft
Manuscript Type:	Original Article
Date Submitted by the Author:	n/a
Complete List of Authors:	DIAGO SANTAMARIA, MARIA PAZ; Instituto de Ciencias de la Vid y del Vino (Universidad de La Rioja, CSIC, Gobierno de La Rioja) Aquino, Arturo; Instituto de Ciencias de la Vid y del Vino (Universidad de La Rioja, CSIC, Gobierno de La Rioja) Millan, Borja; Instituto de Ciencias de la Vid y del Vino (CSIC, Universidad de La Rioja, Gobierno de La Rioja) Logroño, La Rioja, Spain, Tardaguila, Javier; Instituto de Ciencias de la Vid y del Vino (Universidad de La Rioja, CSIC, Gobierno de La Rioja)
Keywords:	computer vision, canopy gaps, Point Quadrat Analysis, precision viticulture, grapevine

129

1 **On-the-go assessment and mapping of vineyard canopy**
2 **porosity, bunch and leaf exposure by image analysis**

3 Maria P. Diago, Arturo Aquino, Borja Millan, Javier Tardaguila*

4 Instituto de Ciencias de la Vid y del Vino (University of La Rioja, CSIC, Gobierno de La
5 Rioja). Finca La Grajera. Ctra. Burgos Km 6. 26007 Logroño (La Rioja) Spain.

6 *Corresponding author: Javier Tardáguila. E-mail: javier.tardaguila@unirioja.es;
7 Instituto de Ciencias de la Vid y del Vino (University of La Rioja, CSIC, Gobierno de La
8 Rioja). Finca La Grajera. Ctra. Burgos Km 6. 26007 Logroño (La Rioja) Spain. Phone: +34
9 941299741.

10

25 **Short running title:** On-the-go assessment and mapping of canopy status

26

27

28

29

30 **Abstract**

31 **Background and Aims:** The assessment of the canopy status can be used to drive informed

32 vineyard management decisions. A non-destructive, automated image-based system capable

33 of operating on-the-go was developed to determine the canopy porosity and the amount of

34 exposed leaves and bunches.

35 **Methods and Results:** A fully automated RGB imaging system, coupled to a GPS and controlled

36 artificial lighting was used to acquire on-the-go (7 Km/h) night time images of grapevine

37 canopy segments, on which the point quadrat analysis (PQA) was performed as reference

38 method. Strong correlations between the image analysis and PQA results for the percentage of

39 gaps (R^2>0.85; p<0.001) and exposed leaves (R^2>0.71; p<0.001) were obtained for both sides of

40 the canopy. For the amount of exposed bunches the best relationship was found on the

41 defoliated side (R^2=0.65; p<0.001). For both canopy faces, maps of the three canopy variables

42 were also built.

43 **Conclusion:** The developed imaging system, capable of operating fully automated on-the-go,

44 can provide reliable information on grapevine canopy status. The obtained information from a

45 whole vineyard can be mapped and used to delineate zones of homogeneous management in

46 the context of precision viticulture.

47 **Significance of the Study:** The computer vision developed system could be implemented in the

48 new generation of variable rate viticultural machinery to optimize the efficiency of several

49 tasks such as spraying or leaf removal.

50 **Keywords:** Computer vision, canopy gaps, Point Quadrat Analysis, precision viticulture,

51 grapevine.

52

Experimental section

53   **Introduction**

54   In viticulture, canopy features such as leaf area, canopy porosity and fruit exposure are key

55   factors that can be regulated by canopy management. In addition to achieving an adequate

56   balance between the grapevine vegetative and reproductive growth, canopy management

57   involves balancing the need for sunlight capture for photosynthesis but also gaps to allow

58   airflow through the canopy to reduce humidity and favour the production of healthy fruit.

59   Generally speaking, canopy management practices leading to improved leaf and bunch

60   exposure have been shown to result in better yield and wine quality (Smart and Robinson,

61   1991). The amount of exposed leaf area in the canopy is an important factor, as each layer of

62   leaves captures around 94% of the incident photosynthetically active radiation (PAR) (Smart

63   1987; Smart and Robinson, 1991). In this context the ideal grapevine canopy will have between

64   1-1.5 leaf layers (Smart and Robinson, 1991). Fruit sun exposure favours aroma/flavour

65   compound synthesis (Reynolds and Wardle 1989, Diago et al. 2010) as well as other secondary

66   metabolites, such as flavonols and anthocyanin pigments among other phenols (Diago et al.

67   2012a, Tardaguila et al. 2012). These phenolic compounds play a remarkable physiological role

68   as UV screening protectors, and are responsible of relevant sensory attributes of grape and

69   wine composition and quality, such as color and mouthfeel (Kennedy et al. 2006). However,

70   excessive fruit exposure, mainly in warm growing regions, can also lead to berry sunburn and a

71   diminishment of grape anthocyanins, hence berry color (Kliewer 1977, Mori et al. 2007).

72   As regards canopy porosity, the ideal grapevine canopy should have between 10 to 20 %

73   according to Palliotti and Silvestroni (2004) or between 20 to 40% gaps, as suggested by Smart

74   (1987) to ensure optimal sunlight capture and reduced shading. Canopy gaps are essential for

75   fruit health as airflow reduces the chance of crop losses to fungal disease (Austin et al. 2011).

76   On the other hand, the evaluation of the canopy elements and growth may be of interest not

77   only for canopy management purposes, but also to configure the differential dosages within

132

78 the context of recent variable rate application machinery, mostly focused on spraying (Gil et al.

79 2013; Grisso et al. 2013). A very recent work by Palleja and Landers (2017) stressed the need of

80 assessing the canopy characteristics in vineyards and fruit orchards to adjust operating

81 parameters of the spraying systems and focused on the calibration of a multiple ultrasound

82 sensor against PQA to determine the canopy density.

83 One of the most common ways of quantifiably assessing canopy porosity, leaf density and fruit

84 exposure is Point Quadrat Analysis (PQA), which was adapted for its application in grapevines

85 (Smart 1987) from the protocol described by Wilson (1958). This technique is based on the

86 insertion of a probe through the canopy of grapevines and subsequent counting the number

87 and sections of the vine the probe comes into contact with: leaves, bunches, canes, or gaps. In

88 addition to being subjective, PQA is labour and time intensive, and can potentially damage the

89 fruit, thus limiting its usefulness and adoption by the wine industry. Moreover, performing 10

90 insertions per vine in 20 vines can take around 1.5 h (Hill et al. 2011). This is a pitfall, which

91 restricts the number of vines that can be measured in a given time frame. In the last decade,

92 novel PQA metrics, capable of providing reliable quantitative description of canopy biomass

93 distribution and light environment have been developed (Meyers and Vanden Heuvel, 2008).

94 Computer vision is a non-invasive technology based on image analysis. In viticulture, the use of

95 computer vision outdoors from still photography with visible cameras has been used to

96 characterize aspects of the grapevine canopy (Tardaguila et al. 2010; Hill et al. 2011; Diago et

97 al. 2012a, 2016) and estimate parameters affecting the crop production (Aquino et al. 2017;

98 Dunn and Martin 2004; Nuske et al. 2014; Millán et al. 2017). However, most of these works

99 involved static, point to point, manual image acquisition, which, from an operational point of

100 view, is a constraint when a large number of grapevines have to be characterized.

101 In order to be efficient in responding through adequate canopy management to the canopy

102 status, an objective, fast and susceptible to be automated method to quantify the main canopy

Experimental section

103 features is needed. In Diago et al. (2016) an RGB imaging system to appraise the percent of

104 gaps or canopy porosity was developed and validated in different countries. Although the

105 results were remarkable, the manual mode of image acquisition and the use of a colour

106 background were identified as limiting factors for its practical implementation.

107 Next steps towards automation and on-the-go canopy status monitoring using computer vision

108 were given very recently. Gatti et al. (2016) installed a system equipped with matrix-based

109 optical RGB sensors in a conventional tractor to assess, on a stop and go mode, the leaf layer

110 number and fractions of canopy gaps and interior leaves at day time. Other authors have used

111 RGB imagery acquired at night time from an autonomous moving platform, at very low speed

112 (0.3 km/h) to reconstruct a textured 3D point cloud to quantify yield components (Rose et al.

113 2016). While the merit of these initiatives is very valuable, a non-invasive system capable of

114 on-the-go monitoring, at a commercial speed (3-7 km/h), the main canopy features, would be

115 desirable to provide information susceptible of being used in precision viticulture and variable

116 rate machinery.

117 The fully on-the-go approach at commercial speed has been addressed by several authors

118 using laser scanning (Llorens et al. 2010; Gil et al. 2013) and ultrasounds (Palleja et al. 2017) to

119 determine canopy density in grapevines and olive trees or to estimate the pruning weight in

120 vineyards (Tagarakis et al. 2013). However, having reliable information on several elements

121 (gaps, leaves, bunches) of the canopy status simultaneously is also aimed.

122 Therefore, the goal of this study was to develop a new, objective, non-invasive, automated

123 system to assess the exposed fruit and leaf area as well as the percent gaps of grapevine

124 canopies using images acquired on-the-go at commercial speed.

125

126 **Materials & Methods**

134

127 *Vineyard site and experimental layout*

128 The trials were carried out in a commercial Tempranillo (clone ISV-F-V6 planted on rootstock

129 SO4) vineyard located in Ábalos (lat. 42º34'44.1''N; long. 2º42'24.0''W; La Rioja, Spain). The

130 vines were planted in N-S orientation in 2006, dry-farmed, spur-pruned on a bilateral cordon

131 to retain eight spurs and two buds per spur and trained onto a vertical shoot positioned (VSP)

132 trellis system with 2.5 m row spacing and 0.8 m vine spacing. All plants were defoliated in its

133 east side after berry set.

134 For data acquisition, fifty consecutive segments comprising three adjacent vines each, (150

135 vines in total) were labelled and delimited. Each block constituted a unique segment in which

136 the three canopy features under evaluation (canopy porosity, % of exposed leaf area and % of

137 exposed bunches) were estimated using image analysis, and validated with the reference

138 measurements using Point Quadrat Analysis (PQA) (Smart and Robinson 1991).

139 *In-field image acquisition*

140 The images of the vine segments were acquired on-the-go, at 7 km/h, using a human-driven

141 sensor-equipped mobile platform specially developed for this purpose (Figure 1a). Specifically,

142 an all-terrain vehicle (ATV) (Trail Boss 330, Polaris Industries, Minnesota, USA) was modified to

143 incorporate the following elements (Figure 1):

144 • *RGB camera:* A Sony α7II RGB camera (Sony Corp., Tokyo, Japan) equipped with a Zeiss

145 24/70mm lens with optical stabilisation was selected for the purposes of this study.

146 This is a mirror-less camera mounting a CCD sensor, which provides high light

147 sensitivity and low noise generation. Furthermore, the camera also incorporates a 5-

148 axis sensor stabilisation system, and offers high shutter speed and quick image storage

149 (Figure 1b). These features allowed to capture and store on-the-go three images per

150 wheel-spin at around 7 km/h, producing high quality images despite the vibrations

151 caused by the quad's engine and the irregular ground's surface.

Experimental section

152   • *Artificial illumination system:* a white-light LED panel was incorporated to the platform

153   (Figure 1c) to enable the vineyard monitoring at night time.

154   • *Sensor supporting structure:* a modular and flexible structure was designed and built

155   with commercial aluminium profiles. The structure consisted on two fixed trays, one

156   upfront and one on the rear part, and an adjustable arm to be installed in the front

157   tray (Figure 1a). The arm was designed to mount the RGB camera and illumination

158   system and to make the combination adjustable to different vineyard heights (Figure

159   1b).

160   • *GPS receiver:* A Leica Zeno 10 Global Positioning System (Heerbrug, St. Gallen,

161   Switzerland) allowed to georeference the acquired images (Figure 1d).

162   • *Inductive sensor for camera triggering:* an inductive sensor was installed in the rear

163   axle. This sensor produced three activation pulses per wheel-spin for triggering the

164   camera (Figure 1e).

165   • *Custom-built electronic control system:* an electronic control system based on the

166   Arduino MEGA development board (Arduino LLC, Ivrea, Italy) was specially built to

167   manage the signals generated by the installed devices (GPS and inductive sensor), and

168   to trigger the camera using a galvanically isolated signal (Figure 1d). The system also

169   allows for data storage in an SD-card and for showing capture-status information in a

170   4.9" TFT screen.

171   Image acquisition was performed at night time using the artificial illumination system installed

172   in the multi sensor moving platform (Figure 2a). Likewise, the isolation (in the image) of the

173   vines under evaluation from those in the adjacent row was successfully achieved by means of

174   illumination and camera parametrization (Figure 2b). Otherwise, under natural sunlight

175   conditions, the whole scene was equally illuminated, producing images in which the vines

176   under study were hardly distinguishable from those at their back. The arm was adjusted for

136

177 the camera to be at around 1.5 meters from the canopy. The camera was set in manual mode,

178 configuring the aperture in f/4, shutter speed in 1/2500 seconds, ISO sensitivity in 5000 and

179 focus in manual mode.

180 *Image processing and analysis*

181 <u>*Image pre-processing*</u>

182 As it was described, three images per wheel-spin were acquired on-the-go with the multi

183 sensor moving platform. This frequency, along with the diameter of the wheel in the sensor-

184 equipped ATV and the distance of the camera to the canopy, ensured that vines of interest

185 were always captured. However, this also produced redundant information in images, since

186 two consecutive images always contained a repeated vine section (Figure 3a to 3c). To avoid

187 the analysis of redundant data, images were matched using the 'Auto Blend' tool provided by

188 Adobe Photoshop CC 2015 (Adobe Systems Incorporated; San José, California, USA) to this

189 effect. Thus, mosaic images were created, which were then piecewise analysed (Figure 3d).

190 <u>*Image processing*</u>

191 The mosaic images were piecewise analysed (hereafter, these pieces will be generically called

192 images for simplification) using a pixel-classification approach for producing a clustering

193 outcome. For that, an improved version of the clustering algorithm based on the Mahalanobis

194 distance (Mahalanobis, 1936) presented by Diago et al. (2012b) was developed.

195 First, the following five sets covering the expected objects in the images were defined: 'bunch',

196 'wood', 'leaf', 'gap' and 'post'. Then, the classifier was trained by manually selecting between

197 50 and 80 pixel samples per set, carefully covering as much variability as possible for every set.

198 Mathematically, a pixel p_i was defined by the following 6-dimensional vector:

$$p_i = (R_i, G_i, B_i, H_i, S_i, V_i)$$

137

199   R_i, G_i and B_i correspond to the pixel's Red, Green and Blue values according to the RGB colour

200   space, respectively. Furthermore, H_i, S_i and V_i stand for the pixel's Hue, Saturation and Value

201   in the HSV colour space, obtained by means of space conversion (Agoston 2005). These last

202   three values from the HSV colour space were not included in the original version of the

203   clustering algorithm by Diago et al. (2012b), so they were incorporated in this study.

204   Once the classifier was trained, images were analysed to obtain clustered outcomes. This is, for

205   a given image under analysis, every pixel was classified as 'bunch', 'wood', 'leaf', 'gap' or 'post'.

206   The assigned set for a pixel was that giving the minimum Mahalanobis distance (Mahalanobis,

207   1936) from the manually training sets to its vector. Finally, classified pixels were labelled in a

208   colour representative of the assigned set in the output image. Figure 4a show an example

209   image and 4b the resulting image produced by the classification algorithm.

210   *Image post-processing*

211   This last step consisted on improving the classification yielded by the algorithm by correcting

212   misclassified pixels.

213   As it can be checked in the clustered image shown in Figure 4b, the majority of

214   misclassifications referred to the 'bunch' class. On the one hand, there were many isolated

215   'bunch' pixels within canopy gaps. This was caused by the fact that in shadowed parts of the

216   bunches, the dark-red colour of grapes was much darker (almost black) in the images. On the

217   other hand, bunches presented holes mainly filled with 'leaf' pixels. This was due to the

218   epicuticular wax of berries tended to produce greenish tones. These two general classification

219   mistakes were corrected by post-processing clustered images using mathematical morphology.

220   Mathematical morphology is a nonlinear image processing technique aimed at extracting

221   objects of interest from the image (Serra 1982, Soille 2004). This was achieved by proving the

222   image with a known shape called structuring element (SE). The shape of the SE is usually

223   chosen using a-priori knowledge about the geometry of the target object in the image.

138

224 Let I be a clustered image as the one shown in Figure 4b. First, isolate 'bunch' pixels were

225 removed by applying a morphological erosion (Soille 2004) on this set using a small disk as SE:

$$I_e = \varepsilon_{SE}(I)$$

226 With this operation, all 'bunch' particles smaller than the SE are removed. Additionally, all

227 remaining 'bunch' objects in I_e were diminished according to the size of the SE. To recover the

228 original size and shape of these objects, a morphological reconstruction (Soille 2004) by

229 dilation on the 'bunch' set of I under I_e was performed:

$$I_R = R_I^\gamma(I_e)$$

230 Second, holes within bunches were filled employing the morphological fill-hole operator (Soille

231 2004). For this case, the application of this operator consisted on morphologically

232 reconstructing by erosion a border image of I_R, I_{R_B}, under I_R:

$$I_{def} = R_{I_R}^\varepsilon(I_{R_B})$$

233 where the border image was defined as:

$$I_{R_B}(p) \begin{cases} I_R(p), if\ p\ is\ a\ border\ pixel\ of\ I_R \\ t_{max}, otherwise \end{cases}$$

234 being t_{max} the maximum gray-level allowed (255 in this case, since images were of 8 bits per

235 channel).

236 The results of the application of the pre-processing described here can be visualized in Figure

237 4-(c).

238 *Image analysis*

239 As a first step all clustered images were cut to match the region of interest (ROI) comprising

240 the first 50 cm above the vine cordons (fruiting zone) defined during PQA measurements.

241 Then, the following indices obtained by image analysis were computed:

139

242 • Canopy porosity or percent of gaps (%): it was calculated as the number of 'gap' pixels

243 divided by the total number of pixels in the ROI, multiplied by 100.

244

$$Percent\ of\ gaps_{vine}(\%) = \frac{(\#Gap\ pixels)}{(\#ROI\ pixels)} * 100$$

245

246 • Percent of exposed bunches (%): it was calculated separately for each canopy side

247 (east and west) as the number of 'bunch' pixels divided by the total number of pixels in

248 the ROI, multiplied by 100. For the computation of the percent of exposed bunches (%)

249 of the whole vine segment the following equation was used:

250

$$Percent\ of\ exposed\ bunches_{vine}(\%) = \frac{(\#Bunch\ pixels_{east} + \#Bunch\ pixels_{west})}{(\#ROI\ pixels_{east} + \#ROI\ pixels_{west})} * 100$$

251

252 • Percentage of exposed leaves (%): it was calculated separately for each canopy side

253 (east and west) as the number of 'leaf' pixels divided by the total number of pixels in

254 the ROI image, multiplied by 100. For the computation of the percent of exposed

255 leaves (%) of the whole vine segment (similar to total exposed leaf area per vine

256 segment without taking into account the zenital top part of foliage), the following

257 equation was used:

258

$$Percent\ of\ exposed\ leaves_{vine}(\%) = \frac{(\#Leaf\ pixels_{east} + \#Leaf\ pixels_{west})}{(\#ROI\ pixels_{east} + \#ROI\ pixels_{west})} * 100$$

259

260 *Point Quadrat Analysis (PQA) reference measurements*

261 PQA was undertaken on the same day as the photographs were acquired following the

262 protocol described by Smart and Robinson (1991) on the first 50 cm above the cordon (fruiting

263   zone). A 5 mm diameter stainless steel probe was used for PQ insertions. For each segment of

264   three adjacent vines, 50 insertions through the canopy at approximately 15 cm horizontal

265   intervals at heights of 10 cm, 30 cm and 50 cm above the cane were performed. For each

266   insertion, the sequential contacts with the vine elements from one side of the canopy to the

267   other, using L (leaf), B (bunch) and G (gap) were recorded.

268   Two different approaches were used to compute the percent of external or exposed leaves

269   and exposed bunches from PQA insertions. The first approach aimed to mimic the 2D image

270   analysis. In this case, the percent of exposed leaves or bunches was computed separately for

271   each canopy side (east and west) as the ratio between the number of first L or B contacts,

272   divided by the total number of insertions, multiplied by 100. In total two indices, for the east

273   and west sides respectively, of the amount of exposed leaves$_{side}$ (%) were computed using the

274   equation below.

275

$$Amount\ of\ exposed\ leaves_{side}(\%) = \frac{\#L\ (only\ first\ contacts)}{\#\ Insertions} * 100$$

276

277   Similarly, two indices, amount of exposed bunches$_{east}$ (%) and amount of exposed bunches$_{west}$

278   (%) were calculated using the equation below.

279

$$Amount\ of\ exposed\ bunches_{side}(\%) = \frac{\#B\ (only\ first\ contacts)}{\#\ Insertions} * 100$$

280

281   The second approach intended to estimate the amount of exposed leaves or bunches of the

282   whole vine segment, and for this reason both sides of the canopy were considered. For this

283   second approach the amount of exposed leaves or bunches was calculated as the ratio of all

284   external (first and last contacts) L or B, divided by the total number of insertions multiplied by

285   two, respectively, then multiplied by 100.

286

$$Amount\ of\ exposed\ leaves_{vine}\ (\%) = \frac{\#L\ (first\ or\ last\ contacts)}{\#\ Insertions\ x\ 2} * 100$$

287

$$Amount\ of\ exposed\ bunches_{vine}\ (\%) = \frac{\#B\ (first\ or\ last\ contacts)}{\#\ Insertions\ x\ 2} * 100$$

288

289   The canopy porosity or percent gaps was calculated as the total number of gaps G by the

290   number of insertions, multiplied by 100, as described in the equation below.

$$Number\ of\ gaps\ (\%) = \frac{\#G}{\#\ Insertions} * 100$$

291

292   *Statistical analysis*

293   Linear regression analysis was performed on data obtained from image analysis and the PQA

294   method and the determination coefficients (R^2) were computed. Statistical *t*-tests were used

295   to assess whether the value of the slope coefficient for each regression was equal to 1 and the

296   intercept equal to 0. The 95% confidence intervals of the slope and intercept coefficients were

297   also calculated. All calculations and plots were carried out using Sigma Plot 12.0 (Systat

298   Software Inc., San Jose, California, USA).

299   *Mapping*

300   Once the image analysis and processing methodology was developed and validated against the

301   PQA method, it was applied in a practical use-case. Concretely, the multi sensor mobile

302   platform and the image analysis algorithm were used to assess the spatial variability of the

142

303 main canopy features of a Tempranillo (clone ISV-F-V6 planted on rootstock SO4) plot of

304 approximately 3.3 *ha* belonging to a commercial vineyard located in Ábalos (lat. 42º34'44.9''N;

305 long. 2º42'28.4''W; La Rioja, Spain). The vines were planted in NE-SW orientation in 2006, dry-

306 farmed, spur-pruned on a bilateral cordon to retain eight spurs and two buds per spur and

307 trained onto a VSP trellis system with 2.5 m row spacing and 0.8 m vine spacing. All plants

308 were defoliated in its east side at bunch closure.

309 The plot comprised 0.25ha approximately. Every other row was monitored, half on them on

310 the west side and the other half on the east side of the canopy with the same multi sensor

311 moving platform moving at 7 km/h. All the image acquisition parameters and conditions were

312 the same as described earlier in this study. Then, the images were analysed using the

313 developed clustering algorithm to characterize the plot in terms of canopy porosity, and

314 amount of exposed leaves and bunches. From this analysis, a set of georeferenced

315 measurements of the three parameters was obtained. This set was finally mapped using

316 ordinary kriging with ArcGIS 10.4 (ESRI, Redlands, CA, USA).

317

318 **Results**

319 A wide range of canopy porosity (expressed as percent of gaps) which spanned from

320 approximately zero to 60% (Figure 5) was sampled in the vineyard used for the calibration

321 between the image-derived canopy variables and those measured by PQA. For this variable,

322 strong correlations, with R^2 above 0.85 (p<0.001), were obtained for both sides of the canopy

323 (Figure 5a, 5b) and the two-side average (Figure 5c). Similarly, the correlation between the

324 percent of gaps determined by image analysis from the east and west sides of the canopy

325 (y=1.031x -2.832) yielded a R^2 = 0.932 (p<0.001) being the value of the slope significantly equal

326 to 1 (p=0.445) (Figure 6).

327   Regarding the amount of exposed bunches (Figure 7) their values ranged from zero to 50% in

328   the vineyard where the measurements were taken. The best correlation between the image-

329   derived data and those retrieved by PQA was found on the east side (defoliated side of the

330   canopy), with $R^2 = 0.651$ (p<0.001) (Figure 7a), while the relationships corresponding to the

331   west side of the canopy (Figure 7b) and to a whole vine basis (Figure 7c) showed lower R^2

332   values.

333   For the amount of exposed leaves, the values ranged from zero to 100 % (Figure 8). The

334   correlations between the image-analysis and PQA data (Figure 8a, 8b, 8c) yielded high R^2

335   values (above 0.71, p<0.001) and the strongest relationship was also obtained from data

336   acquired on the east side (R^2=0.851, p<0.001) (Figure 8a). Examples comparing the outputs

337   obtained from PQA and image-analysis (table aside) in a two different canopy segments are

338   illustrated in Figure 9.

339   While for the canopy porosity (Figure 5) and the amount of exposed leaves (Figure 8) the

340   ranges of the scale of the two correlated variables was comparable, for the amount of exposed

341   bunches the ranges for the PQA measurements (from 0 to 50%) and for the image-analysis

342   (between 0 and 15%) were substantially different. This was confirmed by the values of the

343   slopes and intercepts of the correlations summarized in Table 1. Table 1 shows the 95%

344   confidence intervals for the slope and intercept coefficients for all statistically significant

345   regressions (east and west sides and whole vine). The *t*-test and *p*-values of the statistical tests

346   to verify whether the slope coefficients were different from 1 and intercept coefficients were

347   different from 0 are also shown (Table 1). For any of the correlations, the slope and intercept

348   coefficients were statistically different (p<0.05) from 1 and 0, respectively. These results were

349   confirmed by the confidence intervals (Table 1), as the range covering the lower and upper

350   confidence threshold values did not include the value 1 for those correlations with slope

351   coefficient statistically different to 1, and the value 0 for those correlations with intercept

144

352 coefficient statistically different from 0. Visually speaking, the values of the intercepts can be

353 seen as an offset of approximately 10% of canopy gaps (Figure 5) and of approximately 30% of

354 exposed leaves (Figure 8). For the amount of exposed bunches, the offset or intercept values

355 were always below the 4% (Table 1, Figure 7).

356 Figure 10 displays the generated maps for canopy porosity, percentage of exposed bunches

357 and percentage of exposed leaves using the images acquired on-the-go from the east and west

358 sides of the grapevine canopies. Since the canopy porosity assessed from east and west sides

359 was found to be the same (Figure 6) a unique map involving the rows imaged on the two sides

360 was built (Figure 10a). As observed in Figure 10a, most of the grapevines had a canopy porosity

361 which ranged from 25 to 30 % gaps. Only a small area in the middle of the vineyard comprised

362 plants with smaller porosity values and three isolated areas on the boundaries of the plot

363 (north, south east and south west) exhibited a percent of gaps higher than 30 %. In terms of

364 the amount of exposed leaves (Figure 10b) and bunches (Figure 10c), the differences between

365 east and west maps were mostly quantitative, as similar variability patterns were found

366 between the two sides. In the case of the exposed leaves, lower values, which ranged from 45

367 % to 60% were observed in the map corresponding to the east side (defoliated), while higher

368 percentages of exposed leaves (from 55 above 65%) were recorded in the west side. In both

369 sides the lower values were found at the southwest edge of the plot while an area with larger

370 percentage of exposed leaves was identified in the east part of the vineyard. The opposite

371 pattern was observed for the amount of exposed bunches. Likewise, a larger amount of

372 exposed bunches was found in the map corresponding to the images captured on the east

373 side. However, the spatial pattern of bunch exposure always revealed increased values on the

374 west boundary of the vineyard, which tended to diminish towards the east direction of the

375 plot.

376

145

Experimental section

377 **Discussion**

378 The results obtained in the present work demonstrate the capability of the developed RGB

379 image-based system, operated on-the-go at commercial speed, to successfully determine the

380 canopy porosity and the amount of exposed leaves in the fruiting zone.

381 Using the developed image-analysis system on-the-go, the information on the main elements

382 of the canopy can be obtained separately from the two sides of the canopy or integrated in a

383 single value, representing the average status of the plant. This implies a significant advantage

384 over aerial remote sensing solutions, either manned (aircraft) or unmanned (satellite and

385 UAV), which provide zenithal views of the vineyard rows (usually covering between 30 to 50

386 cm widths). Moreover, the capability of separately monitoring the two canopy sides is of

387 special relevance when canopy management operations, such as leaf removal, are performed

388 only on one side. This is a common practice in many wine regions, where grapegrowers

389 defoliate the morning side to improve fruit exposure and aeration during the cooler hours of

390 the day along the ripening period (Dokoozlian, 2009). With the developed computer vision

391 system, a full, comprehensive picture of the canopy status and the required adjustments

392 required in each side can be visualized.

393 The developed on-the-go imaging system represents an improvement from previous works

394 (Hill et al. 2011; Diago et al. 2016; Fernández et al. 2013) in which robust and reliable image-

395 based methods were developed to quantify grapevine canopy elements. Likewise, in Hill et al.

396 (2011) and Diago et al. (2016) the image-derived outcome were validated against the standard

397 PQA but a colour background and manual image acquisition were required. A combined

398 approach involving the joint use of RGB and multispectral imagery to identify and quantify the

399 grapevine elements in unstructured natural environments without the use of any background

400 was proposed by Fernández et al. (2013), althoug image acquisition was still manual. A step

401 towards the on-the-go monitoring was given by Gatti et al. (2016). These authors acquired RGB

146

402   images on a stop-and-go mode using a conventional tractor (the tractor driver stopped and

403   triggered the sensor), and obtained significant correlations between an image-derived canopy

404   index value, which varied between 0 and 1000, and the fraction of canopy gaps and the leaf

405   layer number, as measured by PQA. Another recent approach was reported by Rose et al.

406   (2016) who acquired RGB images on-the-go at very low speed, less than 1 km/h, to estimate

407   yield parameters. In the present study all images were acquired fully automated, on-the-go,

408   without stopping, at a commercial speed of 7 km/h, as the inductive sensor installed in the

409   vehicle triggered the RGB camera at a given frequency of the wheel spin.

410   For the three evaluated variables of canopy growth the slope values of the obtained

411   correlations were significantly lower than 1. This fact was also reported by Diago et al. (2016)

412   who developed regression models of canopy porosity in different varieties and sites from

413   manually acquired RGB grapevine images. In the present work, while the correlations for

414   canopy porosity and exposed leaves were strong, the assessment of the amount of exposed

415   bunches was less satisfactory, mainly from the west side (not defoliated) and on a vine basis,

416   which integrated both canopy faces. This can be explained by the fact that the accuracy of the

417   PQA method is dependent on the size of the feature to be determined, and the total number

418   of insertions. In terms of the size of the feature in the canopy, the accuracy of the PQA was

419   smaller for those elements in the image in small proportion, like the bunches, and in very

420   dense canopies, the percent of gaps or canopy porosity also. To illustrate this fact, Figure 9

421   shows two examples of the RGB images of vine segments (west side) and the resulting image

422   classification, used to build the correlations. In Figure 9a a very small proportion of bunches

423   are visible and exposed, which were quantified as the 2.2% by image analysis, while the PQA

424   recorded 32%. Similarly, in Figure 9b, the amount of exposed bunches by image analysis was

425   6.7% while a 40% value was obtained from the PQA. Such discrepancies may arise from the

426   fact that in the PQA method the "record" of one insertion is "extrapolated" to an area of 100

427   cm^2 (if insertions are performed on a 10 x 10 cm grid, like in Gatti et al. (2016)) to 240 cm^2 (in

147

428 the present work) on average. The inconsistencies in the "extrapolation" of each insertion

429 record are larger for the minority elements, the bunches in Figure 9a and 9b. Since the visibility

430 of the bunches was lower in the undefoliated side (west side), the "extrapolation

431 inconsistencies" were magnified for this side of the canopy. As regards the number of

432 insertions, the larger this number, the most accurate are the PQA estimations, until a given

433 number of insertions, at which a plateau is reached. In the image analysis method, each pixel,

434 with a size much smaller than 1 cm^2 would correspond to an insertion. In other words, the

435 image analysis method can be seen as a high-resolution PQA which takes into account the gaps

436 and only the outer (exposed) layers of the canopy for the visibility of leaves and bunches.

437 The outcomes of this work have relevant practical implications for the wine industry, especially

438 when the results are expressed as maps, with the georeferenced positioning. In first place, the

439 capability of adopting different canopy management strategies or levels within a vineyard,

440 according to measured values of canopy porosity and leaf and bunch exposure is very valuable.

441 Should these canopy management practices be manually performed, the grapegrower may

442 adjust the intensity of for example, leaf or lateral removal to a desired value of canopy

443 porosity or bunch exposure, to promote air circulation and ensure optimal sunlight capture

444 and temperature. In the case of leaf removal, should defoliation be mechanically conducted, it

445 can also be more precisely accomplished using the new generation of leaf removers, such as

446 those based on leaf blowing in which the pressure of the compressors can be variably

447 adjusted, for instance according to different amounts of exposed leaves. Secondly, the built

448 maps could be used by the novel variable rate application machinery to implement more

449 precise and product-saving (fertilizer, fungicide, pesticide, etc...) applications. Examples of

450 variable dosage of pesticides in different crops (Dammer 2016; Maghsoudi et al. 2015;

451 Tackenberg et al. 2016) can be found using ultrasound and 3D sensors. In the case of

452 viticulture, the blooming of vineyard machinery with the variable rate technology (Llorens et

453 al. 2010; Gil et al. 2013; Palleja and Landers, 2017) pushes forward the need for automated

454   and accurate assessment of the grapevine canopy growth and development status, including

455   the quantification of the canopy porosity and amount of exposed leaves and bunches.

456   Oveall, a fully automated solution for on-the-go, georeferenced, image acquisition and

457   processing of grapevine canopy images, capable of providing information relative to the

458   canopy porosity and the amount of exposed leaves and bunches has been developed. Future

459   work will concentrate on adapting the image acquisition process to be performed at daytime

460   while avoiding the influence of adjacent rows, as the night capturing, though successful, may

461   be considered an operational limiting factor. Nevertheless, the existing system can be

462   mounted in any vineyard vehicle, from a conventional tractor, an ATV to even a robot for

463   vineyard monitoring (Rose et al. 2016; Tardaguila et al. 2016).

464

465   **Conclusions**

466   In modern and competitive viticulture, vineyard management decisions are aimed to be taken

467   by informed grapegrowers, who will certainly make their choices driven by measurements of

468   plants which are representative of their vineyards' variability. In this scenario, a non-

469   destructive, image-based system to be run on-the-go has been developed and tested to

470   provide useful information of the grapevine canopy growth. The knowledge of the canopy

471   development status can be used to adapt and improve the efficiency (at different levels,

472   qualitative, economic and environmental sides) of several canopy management and other

473   viticultural operations, such as spraying. The obtained information can be prepared as maps,

474   which may be used to drive vineyard management decisions benefiting from the arising

475   variable rate machinery, in the context of precision viticulture.

476

477   **References**

Experimental section

478 Agoston, M.K. (2005) Computer Graphics and Geometric Modeling: Implementation and

479 Algorithms. Springer, London, pp. 300-306.

480 Aquino, A., Diago, M.P., Millán, B. and Tardaguila, J. (2017) A new methodology for estimating

481 the grapevine Berry number per cluster using image analysis. Biosystems Engineering (in

482 press).

483 Austin, C.N., Gove, G.G., Meyers, J.M. and Wilcox W. F. (2011) Powdery mildew severity as a

484 function of canopy density: Associated impacts on sunlight penetration and spray coverage.

485 American Journal of Enology and Viticulture **62**, 23-31

486 Dammer, K.H. (2016) Real-time variable-rate herbicide application for weed control in carrots.

487 Weed Research **56**, 237-246.

488 Diago, M.P., Vilanova M. and Tardaguila, J. (2010) Effects of timing of manual and mechanical

489 early defoliation on the aroma of *Vitis vinifera* (L.) Tempranillo Wine. American Journal of

490 Enology and Viticulture **61,** 382-391.

491 Diago, M.P., Ayestarán, B., Guadalupe, Z., Poni, S. and Tardaguila, J.(2012a) Impact of pre-

492 bloom and fruit-set basal leaf removal on the flavonol and anthocyanin composition of

493 Tempranillo grapes. American Journal of Enology and Viticulture **63**, 367-376.

494 Diago, M.P., Correa, C., Millán, B., Barreiro, P., Valero, C. and Tardaguila, J. (2012b) Grapevine's

495 yield and leaf area estimation using supervised classification methodology on RGB images

496 taken under field conditions. Sensors **12**, 16988-17006.

497 Diago, M.P., Krasnow, M., Bubola, M., Millan, B. and J. Tardaguila. (2016) Assessment of

498 vineyard canopy porosity using machine vision. American Journal of Enology and Viticulture **67**,

499 229-238.

150

500 Dokoozlian, N. (2009) Integrated canopy management: A twenty-year evolution in California.

501 In *Recent Advances in Grapevine Canopy Management.* Nick Dokoozlian and James Wolpert,

502 editors. 16 July 2009. University of California, Davis (USA).

503 Dunn, G. & Martin, S. (2004). Yield prediction from digital image analysis: A technique with

504 potential for vineyard assessments prior to harvest. Australian Journal of Grape And Wine

505 Research **10**, 196–198.

506 Fernández, R., Montes, H., Salina, C., Sarria, J., and Armada, M. (2013) Combination of RGB and

507 multispectral imagery for discrimination of Cabernet Sauvignon grapevine elements. Sensors

508 **13**, 7838-7859.

509 Gatti, M., Dosso, P., Maurino, M., Merli, M.C., Benizzoni, F., Pirez, F.J., Platè, B., Bertuzzi, G.

510 and Poni, S. (2016) MECS-VINE®: A new proximal sensor for segmented mapping of vigor and

511 yield parameters on vineyard rows. Sensors **16**, 2009.

512 Gil, E., Llorens, J., Llop, J., Fàbregas, X., Escolà, A., Rosell-Polo, J.R. 2013. Variable rate sprayer.

513 Part 2-Vineyard prototype: Design, implementation and validation. Computers and Electronics

514 in Agriculture **95**, 136-150.

515 Grisso, R., Alley, M., Thomason, W., Holshouser, D. and Roberson, G.T. (2013) Precision

516 farming tools: Variable-rate application. Publication 442-505. College of Agriculture and Life

517 Sciences, Virginia Polytechnic Institute and State University. www.ext.vt.edu. (Virginia, USA).

518 Hill, G. N., Beresford, R.M., Wood, P.N., Kim, K.S. and Wright, P. J. (2011) Image-assisted gap

519 estimation, a simple method for measuring grapevine leaf canopy density. Crop Science **51**,

520 2801-2808.

521 Kennedy, J.A., Saucier, C. and Glories, Y. (2006) Grape and wine phenolics: history and

522 perspective. American Journal of Enology and Viticulture **57**, 239-248.

151

Experimental section

523   Kicherer, A., Herzog, K., Pflanz, M., Wieland, M., Ruger, P., Kecke, S., Kuhlmann, H. and Töpfer,

524   R. (2015). An automated field phenotyping pipeline for application in grapevine research.

525   Sensors **15**, 4823-4836

526   Kliewer, W.M. (1977) Effect of high temperatures during the bloom-set period on fruit-set,

527   ovule fertility, and berry growth of several grape cultivars. American Journal of Enology and

528   Viticulture **4**, 215–222

529   Llorens, J., Gil, E., Llop, J. and Escolà, A. (2010) Variable rate dosing in precision viticulture: Use

530   of electronic devices to improve application efficiency. Crop Protection **29**, 239-248.

531   Maghsoudi, H., Minaei, S., Ghobadian, B. and Masoudi, H. (2015) Ultrasonic sensing of

532   pistachio canopy for low-volume precision spraying. Computers and Electronics in Agriculture

533   **112**, 149-160.

534   Mahalanobis, P.C. (1936). On the generalised distance in statistics. In: Proc. Of the National

535   Institute of Science of India **12**, 49-55.

536   Meyers, J.M. and Vanden Heuvel, J. E. (2008) Enhancing the precision and spatial acuity of

537   point quadrat analyses via calibrated exposure mapping. American Journal of Enology and

538   Viticulture **59**, 425-431.

539   Millan, B., Aquino, A., Diago, M.P. and Tardaguila, J. (2017) Image analysis-based modelling for

540   flower number estimation in grapevine. Journal of the Science of Food and Agriculture **97**, 784-

541   792.

542   Mori, K., N. Goto-Yamamoto, K. Hashizume and M. Kitayama. (2007) Effect of high

543   temperature on anthocyanin composition and transcription of flavonoid hydroxylase genes in

544   'Pinot noir' grapes (*Vitis vinifera*). Journal of Horticultural Science and Biotechnology **82**, 199-

545   206

152

546   Nuske, S. T., Stephen Wilshusen, K., Achar, S., Yoder, L., Narasimhan, S. G. and Singh, S. (2014)

547   Automated Visual Yield Estimation in Vineyards. Journal of Field Robotics **31**, 837-860.

548   Palleja, T. and Landers, A. J. (2017) Real time canopy density validation using ultrasonic

549   envelope signals and point quadrat analysis. Computers and Electronics in Agriculture **134**, 43-

550   50.

551   Palliotti, A. and O. Silvestroni (2004) Ecofisiologia applicate alla vite. In: Viticoltura ed enologia

552   biologica. Eugenio Cozzolino (ed), pp. 41-88. Edagricole. Bologna, Italia.

553   Reynolds, A.G. and Wardle, D.A. (1989) Influence of fruit microclimate on monoterpene levels

554   of Gewürztraminer. American Journal of Enology and Viticulture **40**, 149-154.

555   Rose, J.C., Kicherer, A., Wieland, M., Klingbeil, L., Töpfer, R. and Kuhlmann. (2016) Towards

556   automated large-scale 3D phenotyping of vineyards under field conditions. Sensors **16**, 2136.

557   Serra, J. (1982). Image Analysis and Mathematical Morphology, vol I. Academic, London.

558   Soille, P. (2004). Morphological Image Analysis – Principles and Applications, 2nd. Ed. Springer-

559   Verlag, Belin.

560   Smart, R.E. (1987) Influence of light on composition and quality of grapes. Acta Horticulturae

561   **206**, 37-47.

562   Smart, R.E. and Robinson, M. (1991) Sunlight into the Wine: A Handbook for Winegrape

563   Canopy Management. Winetitles, Adelaide, 88 pp

564   Tackenberg, M., Volkmar, C. and Dammer, K.H. (2016) Sensor-based variable-rate fungicide

565   application in winter wheat. Pest Management Science **72**, 1888-1896.

566   Tardaguila, J., Martinez De Toda, F., Poni, S. and Diago, M.P. (2010) Impact of early leaf

567   removal on yield and fruit and wine composition of *Vitis vinifera* L. Graciano and

568 Carignan. Effects of timing of manual and mechanical early defoliation on the aroma of *Vitis*

569 *vinifera* (L.) Tempranillo wine. American Journal of Enology and Viticulture **61**, 372-381.

570 Tardaguila, J., Blanco, J.A., Poni, S. and Diago, M.P. (2012) Mechanical yield regulation in

571 winegrapes: Comparison of early defoliation and crop thinning. Australian Journal of Grape

572 and Wine Research **18**, 344-352.

573 Tardaguila, J., Rovira-Más, F., Blasco, J., Saiz-Rubio, V., Faenzi, E., Évain, S., Labails, S., Stoll, M.,

574 Scheidweiler, M., Millot, C. and Campos, E. (2016) VineRobot: A new Robot for vineyard

575 monitoring using non-invasive sensing technologies. Proceedings of the Ninth International

576 Cool Climate Wine Symposium. 26-28 May 2016. Brighton, England.

577 Wilson, J.W. (1958) Analysis of the spatial distribution of foliage by two-dimensional point

578 quadrats. New Phytologist **58**, 92-101.

579

580 **Figures' captions**

581 **Figure 1.** Illustration of the multi-sensor mobile platform developed for the on-the-go image

582 acquisition in the vineyard: (a) general view of the multi-sensor mobile platform; (b) RGB

583 camera installed in the platform by means of an ad-hoc designed structure; (c) LED

584 Illumination panel; (d) detail of the custom-built electronic control system and GPS receiver;

585 (e) inductive sensor installed in the rear axle for automatically triggering the camera

586 **Figure 2.** (a) On-the go Image acquisition with the multi-sensor mobile platform; (b) Image

587 acquired with artificial illumination in which, due to appropriate illumination and camera

588 parametrization, the vines under evaluation are discernible from the darkened background.

589 **Figure 3.** Image pre-processing illustration: (a), (b) and (c) show images automatically acquired

590 during a wheel-spin with the multi-sensor mobile platform. To identify overlapping areas

154

591　between the images, note that the red and white tape in them is exactly the same; (d)

592　resulting images after matching images (a), (b) and (c).

593　**Figure 4.** Result of the image processing and analysis: (a) close-up of a vine image; (b) result of

594　the analysis of image (a) in which pixels are represented in the colour associated to their

595　assigned class; (c) result of post-processing image (b) in which holes within bunches are filled

596　and isolate bunch pixels are removed.

597　**Figure 5.** Correlations between the percent of gaps or canopy porosity, assessed by image

598　analysis from images acquired using the multi-sensor platform on-the-go and the reference

599　values determined by PQA, from the (a) east side of the canopy (R^2=0.898); (b) west side of the

600　canopy (R^2=0.855); and (c) the whole vine, showing the average value from east and west sides

601　of the canopy (R^2=0.892). All determination coefficients (R^2) were significant at P<0.001. Solid

602　line represents the correlation line; dashed lines represent the prediction bands at 95%, and

603　dotted line refers to the 1:1 line. (n=50).

604　**Figure 6.** Correlation between the percent of gaps or canopy porosity, assessed by image

605　analysis from images acquired on east and west sides of the canopy, using the multi-sensor

606　platform on-the-go. Coefficient of determination R^2=0.937, at P<0.001. (n=50).

607　**Figure 7.** Correlations between the percent of exposed bunches, assessed by image analysis

608　from images acquired using the multi-sensor platform on-the-go and the reference values

609　determined by PQA, from the (a) east side of the canopy (R^2= R^2=0.651); (b) west side of the

610　canopy (R^2=0.283); and (c) the whole vine (R^2=0.373). All determination coefficients (R^2) were

611　significant at P<0.001. Solid line represents the correlation line; dashed lines represent the

612　prediction bands at 95%, and dotted line refers to the 1:1 line. (n=50).

613　**Figure 8.** Correlations between the percent of exposed leaves, assessed by image analysis from

614　images acquired using the multi-sensor platform on-the-go and the reference values

155

615   determined by PQA, from the (a) east side of the canopy (R^2=0.762); (b) west side of the

616   canopy (R^2=0.851); and (c) the whole vine (R^2=0.710). All determination coefficients (R^2) were

617   significant at $P<0.001$. Solid line represents the correlation line; dashed lines represent the

618   prediction bands at 95%, and dotted line refers to the 1:1 line. (n=50).

619   **Figure 9.** Comparison of the outputs obtained from PQA and image-analysis (table aside) in a

620   canopy segment (a) with very low percentage of exposed bunches, and (b) medium percentage

621   of exposed bunches.

622   **Figure 10.** Maps of the spatial variability of (a) canopy porosity or percent of gaps; (b) percent

623   of exposed bunches, and exposed (c) percent of exposed leaves (c). Images with the multi-

624   sensor platform were acquired on-the-go at 7 km/h from the east and west sides of the canopy

625   and analysed using the developed methodology.

626

Table 1. Slope coefficients of the regression models of the different canopy elements, estimated by image analysis versus point quadrat analysis (PQA) at the two sides of the canopy. The 95% confidence intervals for the slope coefficients are indicated in brackets. The t-test values and their corresponding p values for the null hypothesis of H_0: slope=1 and H_0: intercept=0 are presented.

Side/variable	Slope	t-test value[a]	p value	Intercept	t-test value[a]	p value
West side						
% of gaps	0.449 (0.396; 0.504)	-20.56	<0.0001	12.86 (11.37; 14.36)	17.34	<0.0001
% of exposed bunches	0.137 (0.074; 0.201)	-27.31	<0.0001	3.81 (2.49; 5.11)	5.84	<0.0001
% of exposed leaves	0.375 (0.305; 0.446)	-17.84	<0.0001	33.60 (29.22; 37.99)	15.41	<0.0001
East side						
% of gaps	0.492 (0.444; 0.540)	-21.17	<0.0001	9.80 (8.46; 11.14)	14.74	<0.0001
% of exposed bunches	0.186 (0.146; 0.225)	-41.55	<0.0001	1.27 (0.64; 1.88)	4.09	<0.0001
% of exposed leaves	0.534 (0.469; 0.599)	-14.47	<0.0001	28.83 (24.31; 33.34)	12.84	<0.0001
Vine						
% of gaps	0.471 (0.423; 0.519)	-22.41	<0.0001	11.33 (10.02; 12.65)	17.29	<0.0001
% of exposed bunches	0.127 (0.079; 0.175)	-36.67	0.0003	2.22 (1.07; 3.36)	3.90	<0.0001
% of exposed leaves	0.469 (0.393; 0.545)	-14.05	<0.0001	37.62 (33.74; 41.51)	19.47	<0.0001

[a]t-tests for the null hypothesis H_0: slope = 1 and H_0: intercept = 0 were only tested for those regressions with statistically significant slope coefficients (p<0.05).

Experimental section
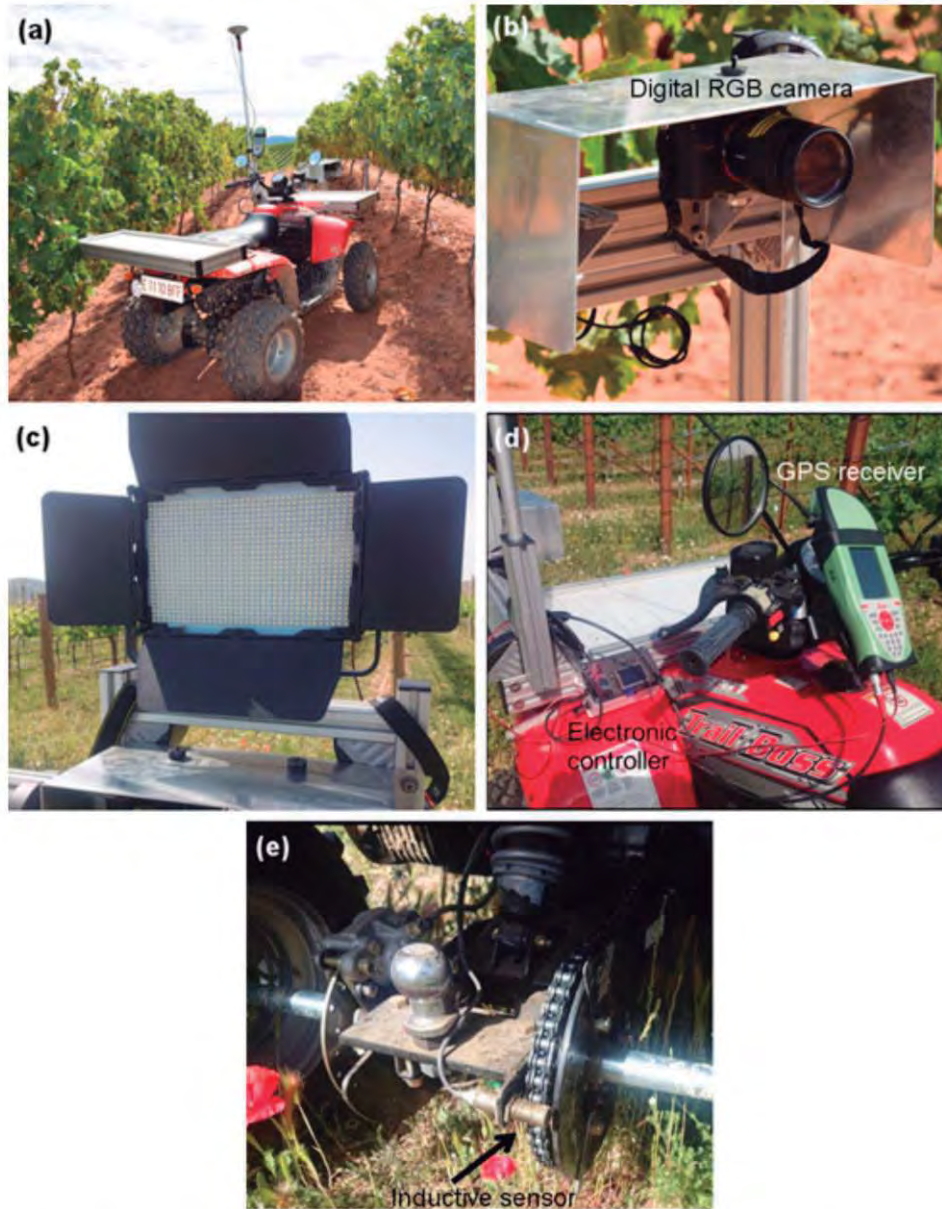
Figure 1. Illustration of the multi-sensor mobile platform developed for the on-the-go image acquisition in the vineyard: (a) general view of the multi-sensor mobile platform; (b) RGB camera installed in the platform by means of an ad-hoc designed structure; (c) LED Illumination panel; (d) detail of the custom-built electronic control system and GPS receiver; (e) inductive sensor installed in the rear axle for automatically triggering the camera

148x189mm (96 x 96 DPI)

Figure 2. (a) On-the go Image acquisition with the multi-sensor mobile platform; (b) Image acquired with artificial illumination in which, due to appropriate illumination and camera parametrization, the vines under evaluation are discernible from the darkened background.

212x76mm (96 x 96 DPI)

Experimental section

Figure 3. Image pre-processing illustration: (a), (b) and (c) show images automatically acquired during a wheel-spin with the multi-sensor mobile platform. To identify overlapping areas between the images, note that the red and white tape in them is exactly the same; (d) resulting images after matching images (a), (b) and (c).

197x131mm (96 x 96 DPI)

160
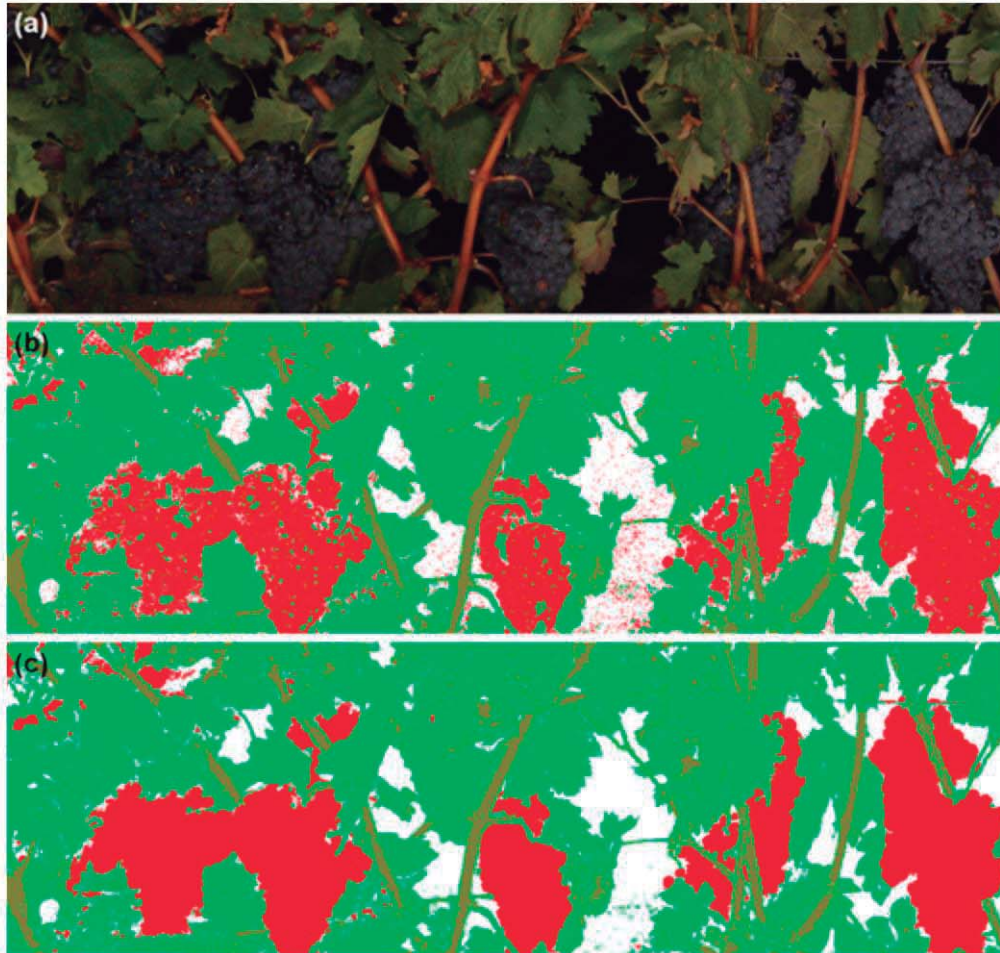
Figure 4. Result of the image processing and analysis: (a) close-up of a vine image; (b) result of the analysis of image (a) in which pixels are represented in the colour associated to their assigned class; (c) result of post-processing image (b) in which holes within bunches are filled and isolate bunch pixels are removed.

352x335mm (72 x 72 DPI)

161

Figure 5. Correlations between the percent of gaps or canopy porosity, assessed by image analysis from images acquired using the multi-sensor platform on-the-go and the reference values determined by PQA, from the (a) east side of the canopy (R^2=0.898); (b) west side of the canopy (R^2=0.855); and (c) the whole vine, showing the average value from east and west sides of the canopy (R^2=0.892). All determination coefficients (R^2) were significant at $P<0.001$. Solid line represents the correlation line; dashed lines represent the prediction bands at 95%, and dotted line refers to the 1:1 line. (n=50).

279x97mm (96 x 96 DPI)
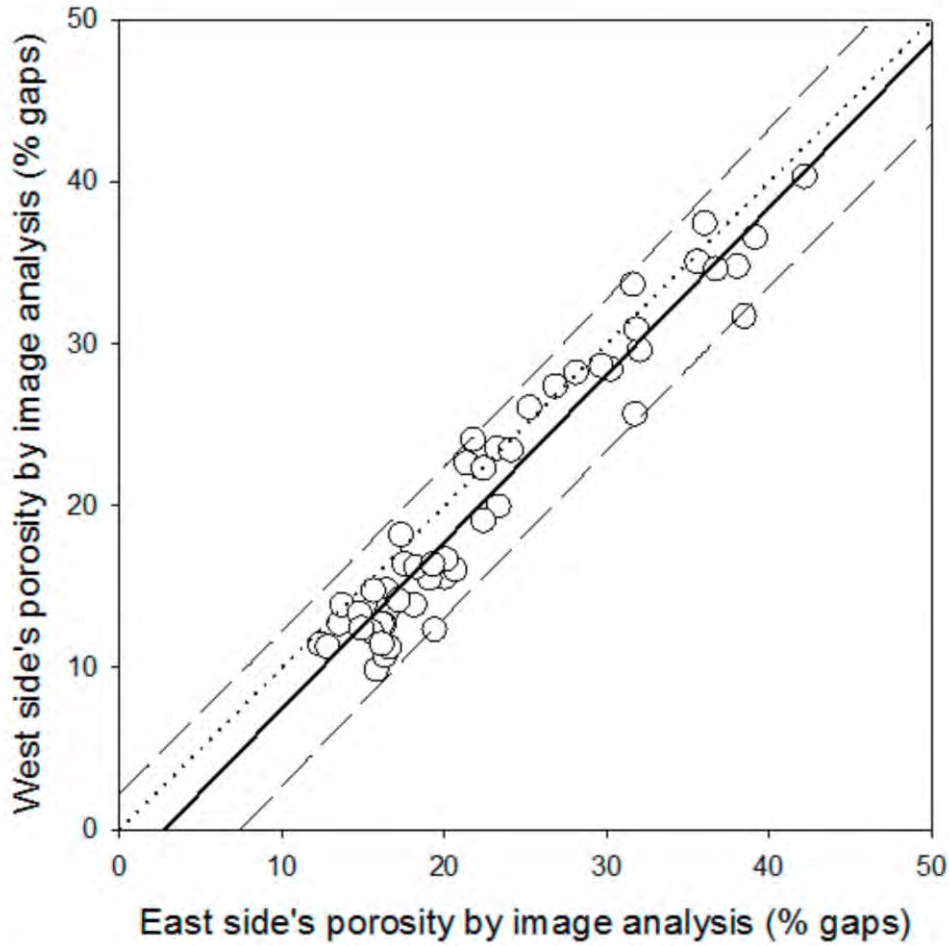
162

1
2
3
4
5
6
7
8
9
10
11
12
13
14
15
16
17
18
19
20
21
22
23
24
25
26
27
28
29
30
31
32
33
34
35
36
37
38
39
40
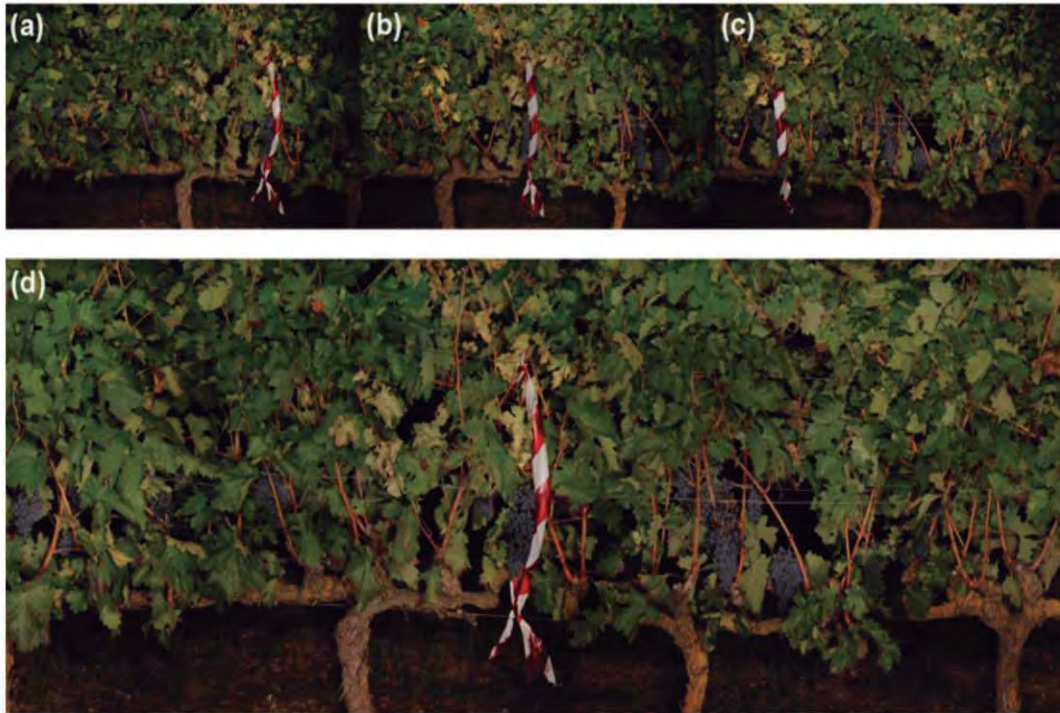41
42
43
44
45
46
47
48
49
50
51
52
53
54
55
56
57
58
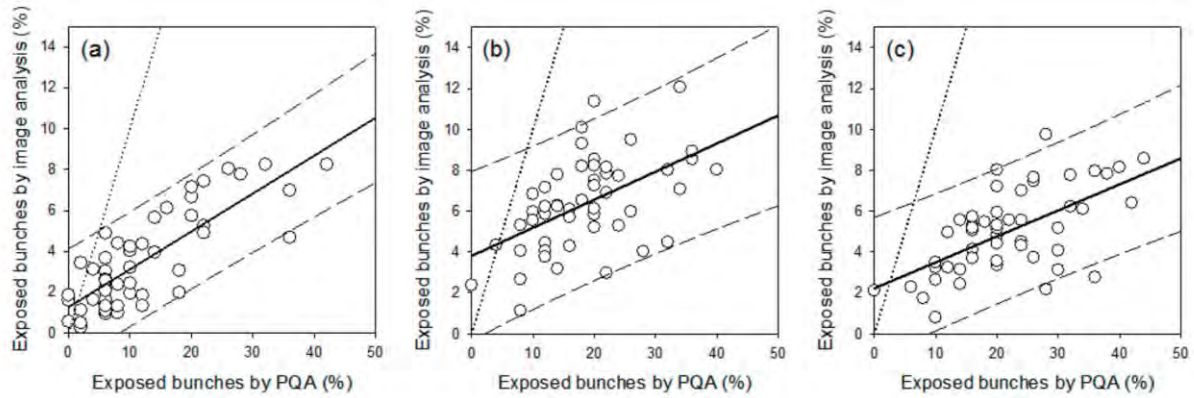
Figure 6. Correlation between the percent of gaps or canopy porosity, assessed by image analysis from images acquired on east and west sides of the canopy, using the multi-sensor platform on-the-go. Coefficient of determination $R^2=0.937$, at $P<0.001$. (n=50).

155x156mm (96 x 96 DPI)

Figure 7. Correlations between the percent of exposed bunches, assessed by image analysis from images acquired using the multi-sensor platform on-the-go and the reference values determined by PQA, from the (a) east side of the canopy (R^2= R^2=0.651); (b) west side of the canopy (R^2=0.283); and (c) the whole vine (R^2=0.373). All determination coefficients (R^2) were significant at $P<0.001$. Solid line represents the correlation line; dashed lines represent the prediction bands at 95%, and dotted line refers to the 1:1 line. (n=50).

281x97mm (96 x 96 DPI)
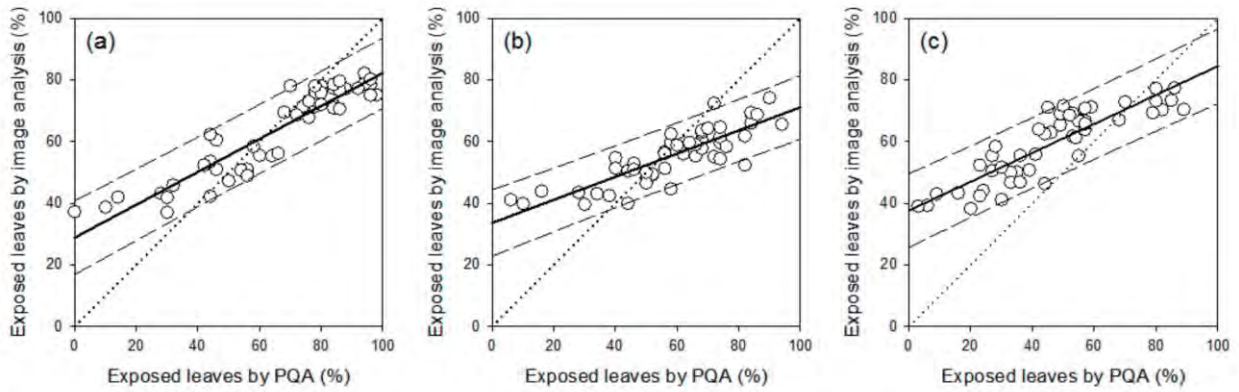
164

Figure 8. Correlations between the percent of exposed leaves, assessed by image analysis from images acquired using the multi-sensor platform on-the-go and the reference values determined by PQA, from the (a) east side of the canopy (R2=0.762); (b) west side of the canopy (R2=0.851); and (c) the whole vine (R2=0.710). All determination coefficients (R2) were significant at P<0.001. Solid line represents the correlation line; dashed lines represent the prediction bands at 95%, and dotted line refers to the 1:1 line. (n=50).

288x97mm (96 x 96 DPI)

Figure 9. Comparison of the outputs obtained from PQA and image-analysis (table aside) in a canopy segment (a) with very low percentage of exposed bunches, and (b) medium percentage of exposed bunches.

Segment	Method	Porosity (% gaps)	Exposed leaves (%)	Exposed bunches (%)
a	PQA	8	58	32
	Image analysis	19.4	59.7	4.5
b	PQA	20	40	40
	Image analysis	17.3	54.8	8.0

330x155mm (96 x 96 DPI)

166

a) West & East Sides

Canopy Porosity (%)
- <25.0
- 25.1 - 27.5
- 27.6 - 30.0
- 30.1 - 32.5
- >32.5

b)   West Side   East Side

Exposed Leaves (%)
- <50.0
- 50.1 - 55.0
- 55.1 - 60.0
- 60.1 - 65.0
- >65.0

c)   West Side   East Side

Exposed Bunches (%)
- <0.9
- 1 - 1.8
- 1.9 - 2.7
- 2.8 - 5.6
- 5.7 - 9

0 5 10   20   30
Meters   N
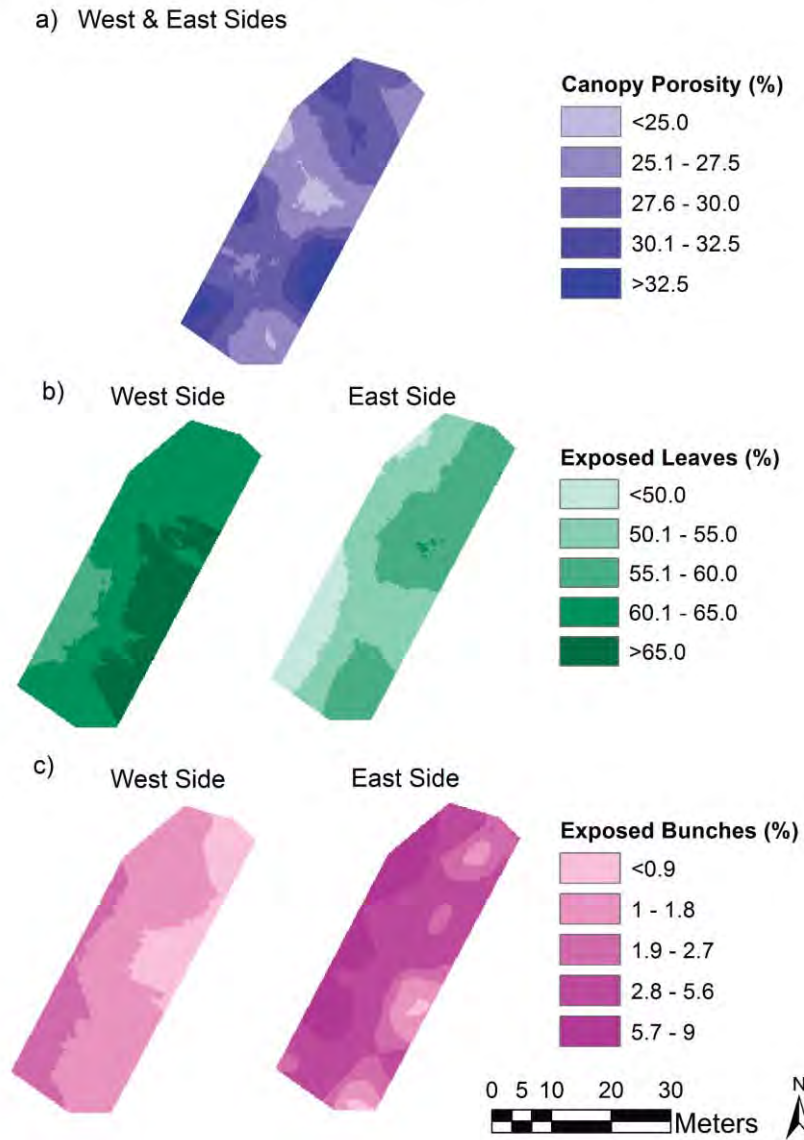
Figure 10. Maps of the spatial variability of (a) canopy porosity or percent of gaps; (b) percent of exposed bunches, and exposed (c) percent of exposed leaves (c). Images with the multi-sensor platform were acquired on-the-go at 7 km/h from the east and west sides of the canopy and analysed using the developed methodology.

290x410mm (300 x 300 DPI)

167

3.3.3 Assessment of vineyard pruning weight from on-the-go captured images

Título de la publicación: Development of an image-based method to appraise the grapevine pruning weight on-the-go

Autores: MILLAN, B., DIAGO, M.P., AQUINO, A., TARDÁGUILA, J.

Publicado en: En proceso de revisión

Resumen:

El peso de la madera de poda es un indicador del crecimiento vegetativo y el vigor. Tradicionalmente se ha determinado durante la poda, separando y pesando los sarmientos correspondientes a cada cepa, un proceso lento y que interrumpe el flujo de trabajo. En el siguiente artículo se presenta el uso de un algoritmo de análisis de imagen para la determinación del peso de madera de poda, como método automático, no invasivo y de bajo coste.

El estudio se ha realizado en un viñedo comercial en tres etapas: en la primera los sarmientos ya podados se colocaron encima de un fondo blanco para ser fotografiados en condiciones de luz semi-controladas; en la segunda, la captura se realizó de forma manual en el viñedo, utilizando un fondo de color blanco y con la cámara situada sobre un trípode; finalmente, se utilizó un "quad*"* modificado para la captura automática de imágenes a una velocidad de 7 km/h.

Las imágenes capturadas manualmente se analizaron y evaluaron mediante validación cruzada ("leave-one-out"), proporcionando una estimación con un coeficiente de determinación (R^2) de 0,91 (p<0,001), RMSE=87,7g y RPD ("ratio of performance to deviation") de 3,4. Las imágenes capturadas de forma automática generaron resultados similares, con un coeficiente de determinación (R^2) de 0,85 (p<0,001), RMSE=115,7g y RPD=2,6. Estos resultados demuestran que la estimación del peso de la madera de poda puede realizarse de manera rápida y no invasiva en el viñedo, proporcionando una herramienta de gran valor para el viticultor al permitir la evaluación del vigor y facilitar la generación de mapas.

Contribución del autor de la Tesis:

La contribución de Borja Millán fue determinante para la generación del artículo, e incluye el diseño experimental, coordinación del trabajo, captura de datos en campo y la generación de los algoritmos de análisis de imagen. Además, Borja Millán escribió el artículo y realizó el análisis de los resultados.

A new machine vision based method to assess the grapevine pruning weight on-the-go

Borja Millan, Maria P. Diago, Arturo Aquino and Javier Tardaguila*

Instituto de Ciencias de la Vid y del Vino (University of La Rioja, CSIC, Gobierno de La Rioja), 26006 Logroño, Spain.

*Corresponding author (javier.tardaguila@unirioja.es; tel: +34941299741; fax: +34941299722).

Short version of title: On-the-go Pruning Weight Assessment

1

28 **Abstract:**

29 Pruning weight is an indicator of vegetative growth and vigor. Traditionally, it is manually determined,

30 which is time-consuming and labor-demanding. The use of image analysis as a non-invasive and low-

31 cost method combined with automated and on-the-go image capturing for pruning weight estimation in a

32 commercial vineyard was evaluated in this study as a fast and reliable alternative. The on-the-go

33 methodology was developed in a three-step process: at first, the shoots were pruned, placed over a white

34 screen and photographed in semi-controlled conditions. Next step consisted on manual acquisition of

35 vine images in-the-field with a white background. Finally, a modified all-terrain vehicle (ATV)

36 equipped with a digital camera, automatic triggering, supplementary illumination and geo-referencing

37 system was used to take vine images on-the-go at 7 km hr^{-1} without controlled background. The model

38 was tested using the "leave-one-out cross-validation" method resulting in a determination coefficient

39 (R^2) equal to 0.91 (p<0.001), root-mean-square error (RMSE) equal to 87.7 g and ratio of performance

40 to deviation (RPD) equal to 3.4 for the manual in-field acquisition. On the other hand, the images

41 captured on-the-go provided a more applicable result with slight decrease in the precision as

42 demonstrated by R^2=0.85 (p<0.001), RMSE=115.7 g and RPD=2.6. The results showed that the

43 developed automated methodology based on the analysis of images acquired on-the-go was capable of

44 estimating the vine pruning weight in commercial vineyards. This may become a valuable tool for the

45 wine industry for rapid assessing and mapping of vine vigor and thus improve vineyard management.

46

47 **Key words:** computer vision; precision viticulture; non-invasive sensing technologies; vigor; *Vitis*

48 *vinifera* L.

49

50

2

172

51 **Introduction**

52 Precision viticulture, in contrast to traditional management techniques, favors more efficient crop

53 production, reducing waste and environmental impact (Cook et al. 1998, Bongiovanni and Lowenberg-

54 Deboer 2004). The term precision viticulture refers to the site-specific management of vineyards, or

55 more specifically to the concept of "applying the right treatment in the right place at the right time"

56 (Gebbers and Adamchuk 2010). To achieve this, accurate and precise evaluation of the status of the

57 vines is required to take informed decisions (Proffitt et al. 2006, Reynolds 2010). Generally speaking,

58 the implementation of precision agriculture becomes feasible with the development of advanced sensing

59 technologies in conjunction with procedures to link mapped variables to take appropriate farming

60 management actions (Dobrowski et al. 2003, Zarco-Tejada et al. 2014).

61

62 Proximal and remote sensors, as non-destructive tools have been widely applied in precision viticulture

63 (Matese and Di Gennaro 2015). Manually operated devices, like fluorescence sensors have been used for

64 nitrogen content evaluation (Rey-Caramés et al. 2016), while thermal (Pou et al. 2014) and spectral

65 reflectance sensors (De Bei et al. 2011) were used to estimate the plant water status. On the other hand,

66 vehicle mounted sensors greatly improved the commercial application and the sampling rate per

67 vineyard. On-the-go measurements were applied for water status characterization (Sepúlveda-Reyes et

68 al. 2016) or canopy and vegetative status evaluation (Diago et al. 2016b, Gatti et al. 2016, Palleja and

69 Landers 2017). Image analysis, as a non-invasive, fast and low-cost methodology has been utilized as a

70 proximal sensing tool, to measure several features of the grapevine. Some applications of manual image

71 acquisition include the estimation of the number of flowers per inflorescence (Millan et al. 2017) and the

72 assessment of the canopy architecture (Diago et al. 2016a). Alternatively, image sensors can be mounted

3

73   in agricultural vehicles for yield estimation (Nuske et al. 2011) and to assess the grapevine vegetative

74   status (Gatti et al. 2016).

75

76   Pruning weight is an important indicator used for the appraisal of biomass production, carbon storage

77   cycle, vigor and vine balance (Smart and Robinson 1991, Keller 2015). The ratio between the vine yield

78   and its pruning weight is defined as the vine balance (Smart and Robinson 1991). Manual pruning

79   weight assessment is a laborious and time-consuming process which interferes with the usual pruning

80   flow, because of the need to recollect the corresponding shoots and to weight them (Taylor and Bates

81   2012). Consequently, a rapid and precise method for pruning weight estimation is desirable.

82

83   Pruning weight has been estimated using different indirect and direct techniques, including remote and

84   proximal sensing. Indirect estimation has been used to assess the pruning weight from canopy

85   measurements. This approach was investigated by Grocholsky et al. (2011) to evaluate the canopy status

86   before harvest using a vehicle mounted Lidar scanner. Although precise, Lidar sensors were expensive

87   and delicate, hence, their commercial application was limited (Wolcott and Eustice 2014). Airborne

88   sensors have also been tested for indirect pruning weight estimation from canopy measurements

89   (Dobrowski et al. 2003). Airborne sensors can be used to monitor entire vineyards but at the cost of

90   using expensive technologies, weather constraints and costly revisiting operations if multi-temporal

91   measurements were required (Baluja et al. 2012). Another limitation of the utilization of aerial sensors

92   to monitor non-continuous crops from zenithal view (like vineyards), is the influence of the soil

93   reflectance in the calculation of indices (Stamatiadis et al. 2006). Conversely, proximal sensing using

94   ground sensors does not have this limitation, and can greatly reduce the cost of multi-temporal data

95   acquisition. Direct pruning wood measurements using a vehicle mounted Lidar was evaluated by

4

174

96   Tagarakis et al. (2013). These authors recorded the number of impacts with the canopy shoots detected

97   by the scanner to estimate the pruning weight. Image analysis was also proposed for this application, but

98   the lack of controlled background and illumination greatly hindered the segmentation of the shoots.

99   Botterill et al. (2013 and 2016) attempted to overcome these limitations by employing a wheeled

100   platform designed to completely cover the vines, equipped with controlled lighting. The problem of

101   uncontrolled lighting conditions and the interference from the vines in the background was also

102   addressed by Kicherer et al. (2016) with two different approaches: manual segmentation on vine images

103   using a white screen as background, and the use of a multi-camera system for depth reconstruction. The

104   development of a fully automated sensor will improve the commercial application of these manual

105   methodologies in viticultuure, that are time and labor demanding.

106

107   In the light of this, the aim of this study was to develop a fully automated image-based system, capable

108   to operate on-the-go at a commercial speed, to assess the pruning weight of grapevines under field

109   conditions.

110

111   **Materials and Methods**

112   Experimental layout

113   The trials were conducted at a commercial Tempranillo (Vitis vinifera L.) vineyard located in Logroño

114   (Latitude = 42.434853º, Longitude = 2.513719º, Altitude=477.64m asl; La Rioja, Spain) on December

115   2015 before winter pruning. The grapevines were trained to a vertically shoot-positioned (VSP) trellis

116   system, with Northwest-Southeast row orientation at 3.0×1.2 meters inter and intra row distances. The

117   vines were planted in 2010 and grafted on Richter 110 rootstock.

118   The methodology for pruning weight estimation was developed following three steps:

5

119   1.   Semi-indoor shoot images: the images were taken manually and statically without artificial

120   illumination, but under a roof to avoid direct sunlight. Ten shoots were pruned and placed one at

121   a time over a white screen laying on the floor. The first image included a single shoot.

122   Subsequent images were taken after addition of one shoot to the previous scene. By doing this,

123   ten images containing from one to ten shoots were obtained.

124   2.   In-field manually acquired vine images: 45 vines were manually and statically photographed in

125   the field, in an uncontrolled illumination scenario and using a white screen as background to

126   avoid the interference from grapevines in the adjacent rows.

127   3.   On-the-go captured vine images: 45 vines (the same as those photographed manually) were

128   automatically imaged on-the-go using a modified all-terrain vehicle (ATV) (Figure 1) equipped

129   with a camera and an automated triggering system. The images were georeferenced using a

130   global navigation satellite system (GNSS).

131

132   To increase the data range and test the methodology under different self-occlusion conditions, the vines

133   were chosen to cover the widest possible range of pruning weight. Towards this end, some vines of the

134   45 photographed were subjected to partial manual pruning to decrease their shoot number. The adjacent

135   vines within the row to the one under study were also manually pruned to prevent their canes to interfere

136   in the scene of the vine under analysis, and thus affecting to the precision of the ground truthing process.

137   After the image capturing process, for each vine the shoots were cut and weighted using a hanging scale

138   (Kern & Sohn GmbH, Balingen-Frommern, Germany) for its use as reference data.

139

140   <u>Image acquisition</u>

141   The manually acquired images (semi-indoor and in-field manually acquired vine images) were obtained

142   using a Nikon D5300 digital reflex camera (Nikon corp., Tokyo, Japan) equipped with a AF-S DX

6

176

143   NIKKOR 18-55mm f/3.5-5.6G VR. Images were taken at daytime using a white screen as background,

144   and saved at a resolution of 24 Mpx (6000 × 4000 pixels), in the RGB color space with eight bits per

145   channel. The camera was fixed to a tripod positioned at a distance of 3 m in the case of the semi-indoor

146   shoots, and around of 1.2 m in the case of vine images. No illumination was used apart from natural

147   sunlight. The camera was configured with a sensitivity of ISO 640, aperture of f/4.5 and the exposure

148   time was automatically selected.

149

150   The on-the-go captured vine images were acquired at night-time using an ATV (Trail Boss 330, Polaris

151   Industries, Minnesota, USA) moving at 7 km hr^{-1}. The vehicle was equipped with a Sony alpha 7-II

152   digital mirrorless camera (Sony Corp., Tokyo, Japan) mounted at 100 cm from the ground and 250 cm

153   from the canopy, with a Zeiss Vario-Tessar FE 24-70 mm lens with optical stabilization (Figure 1). The

154   images were saved at a resolution of 24 Mpx (6000 x 3376 pixels), in RGB color space with 8 bits per

155   channel. The camera has a high sensitivity CCD sensor capable to obtain high quality images at high

156   shooting speeds despite the vibrations generated by the uneven terrain and the ATV engine vibrations. A

157   900 LED Bestlight panel and two Travor spash IS-L8 LED lights were used for scene illumination. The

158   ATV was fitted with an adjustable mechanical structure (Figure 1), that could be fixed to different

159   heights and depths to adapt to the vines configuration. The structure also provided protection against

160   canopy impact and allowed the attachment of the illumination equipment. The camera was triggered by

161   a custom-built controller based on Arduino Mega (Arduino LLC, Ivrea, Italy). The controller generated

162   the shooting signal based on the information received from an inductive sensor attached to the rear axle,

163   which was activated three times per wheel revolution. A Leica Zeno 10 GNSS receiver (Heerbrug, St.

164   Gallen, Switzerland) was used to geo-position the images. The triggering signal along with the actual

7

165 position was processed by the controller, showed in a 4.3 inch tft screen for debugging purposes and

166 stored in an SD card.

167

168 <u>Image analysis algorithm</u>

169 The three previously described datasets were analyzed using an algorithm developed in Matlab (R2010b,

170 Mathworks, Natick, MA, USA). The procedure consisted of two steps:

171   1. Definition of the region of interest (ROI): The acquired images included not only the shoots of

172   the vine under consideration but other parts like the trunk, other vines or ground among others. A

173   ROI was manually selected by an operator using a custom developed Matlab application to

174   encompass only the region to be segmented.

175   2. Segmentation procedure: the images were first converted to grayscale by eliminating the hue and

176   saturation information while retaining the luminance. Then the Otsu's method (Otsu, 1979) was

177   applied over the histogram of pixel values to automatically establish a threshold (T_{otsu}) for each

178   grayscale image (I_G) thus separating the shoots from the background. For that, the Otsu's method

179   assumes that the image contains two types of pixels corresponding to different classes

180   (foreground and background) and that the intensity of these pixels distributes in a bimodal

181   histogram. Consequently, the threshold was calculated as the value maximizing their between-

182   class variance. As the manually acquired images were taken with a white background, the shoots

183   were segmented using the threshold as described:

184

185
$$I_S(x,y) = \begin{cases} 1 \ if \ I_{Gmanual}(x,y) \leq T_{otsu} \\ 0 \ if \ I_{Gmanual}(x,y) > T_{otsu} \end{cases}$$

186

187 where the pair of values (x,y) specified the position of a pixel in the image.

8

178

188   The on-the go images, which had a dark background because of the night-time capture, were

189   segmented as follows:

190

191
$$I_S(x,y) = \begin{cases} 1 \; if \; I_{G \; on-the-go}(x,y) > T_{otsu} \\ 0 \; if \; I_{G \; on-the-go} \leq T_{otsu} \end{cases}$$

192

193   After this procedure, I_S consisted on an image of the same dimensions as the original one but with only

194   two possible pixel values: one (represented as white in the images) for the shoots segmented inside the

195   ROI, and zero (represented as black in the images) for the remaining pixels. After this, the number of

196   pixels segmented as shoots was obtained from the image as follows:

197
$$Number \; of \; pruning \; wood \; pixels = \sum_{x=1}^{\substack{number \; of \\ columns}} \sum_{y=1}^{\substack{number \; of \\ rows}} I_S(x,y)$$

198

199   <u>Statistical analysis</u>

200   The data generated using the described image analysis algorithm and their relationship to the reference

201   values were analyzed using Sigma Plot 12.0 (Systat Software Inc., San José, CA, USA). The regression

202   lines, with their determination coefficient (R^2), 95% confidence intervals of the slope coefficients and p-

203   values were also calculated. Model validation was performed using Leave-one-out cross-validation

204   (LOOCV) in Weka 3.8.0 (University of Waikato, Hamilton, New Zealand). LOOCV separates the data

205   into two groups: n-1 samples are used for training and the remaining data point is used for validation.

206   The process is repeated for the n possible combinations of the training and validation sets, and the error

207   obtained for every model is averaged to generate the LOOCV error indices. The models were

9

208   benchmarked using the mean absolute error (*MAE*), root-mean-square error (*RMSE*) and the ratio of

209   performance to deviation (*RPD*) (Williams and Sobering 1996).

210

211   Mathematically *MAE* and *RMSE* are described as follows

212
$$MAE = \frac{1}{n}\sum_{i=1}^{n}|\widehat{Pw_i} - Pw_i|$$

213

214
$$RMSE = \sqrt{\frac{\sum_{i=1}^{n}(\widehat{Pw_i} - Pw_i)^2}{n}}$$

215   where $\widehat{Pw_i}$ and Pw_i are the predicted and actual pruning weight values for the *ith* vine respectively.

216   Additionally, *RPD* is defined as

217
$$RPD = \frac{\sigma^t}{RMSE}$$

218   being σ^t the standard deviation of the actual pruning weight values.

219

220   *MAE* is the average of the absolute errors in the prediction of the model, when *RMSE* offers an absolute

221   value of the prediction error. Since neither *MAE* nor *RMSE* take into account the distribution of the data,

222   its sparsity and range of values, they might not be completely descriptive on their own. Therefore, *RPD*

223   was also introduced (Williams and Sobering 1996). As stated in the literature (Nicolaï et al. 2007), a

224   model with a *RPD* value between 2 and 2.5 has a coarse quantitative prediction, a value between 2.5 and

225   3 is associated to models with good prediction accuracy and values equal to or greater than 3 indicate

226   that the model has excellent prediction accuracy.

227

228   **Results**

10

229 Semi-indoor manually acquired shoot images

230 The weight, size and shape of the shoots were heterogeneous with great weight variability. Single shoots

231 varied in weight from 110 to 310 g, while the average weight value of the ten-shoot population was190

232 g with coefficient of variation of 32%. The shoots were randomly placed over the white background, and

233 their shape (curve in some instances) and the presence of laterals generated a "3D structure", with some

234 shoots being closer to the camera than others (Figure 2A). The ROI selected for the analysis comprised

235 all the image area (Figure 2A, where ROI boundaries are represented in red). The result of the

236 segmentation is showed in Figure 2B, where white pixels correspond to wood and the background is

237 represented in black.

238

239 The relationship obtained for the pruning weight of the shoots present in each image against the number

240 of pixels segmented as corresponding to the pruning wood (equivalent to the area of the shoots in a 2D

241 representation) was very strong ($R^2 \approx 1$ with $p<0.001$) as it can be seen in Figure 3.

242

243 In-field manually acquired vine images

244 Figure 4 shows an image of a vine captured manually in the field. The ROI was selected to include all

245 the shoot laterals of the vine while avoiding the trunk. After that, the images were segmented, and the

246 results can be observed in Figure 4B, where the pixels corresponding to the shoots are shown in white

247 and the background in black. The regression plot for the number of pixels segmented as wood and the

248 pruning weight yielded a $R^2 = 0.92$ (Figure 5). The model was externally validated using LOOCV (Table

249 1) resulting in $R^2=0.91$, root mean square error (RMSE) of 87.7g and RPD=3.4.

250

251 On-the-go acquired vine images

11

252   The ROI for the on-the-go acquired vine images was selected similarly to the manually acquired images

253   (Figure 6A). It must be noted that, in contrast to the other two datasets, which used a white screen as

254   background, no background was used in this case. In this dataset, the differentiation of the vines under

255   evaluation from those in the adjacent row was successfully achieved by means of illumination and

256   camera parametrization. The results of the segmentation of the images can be observed in Figure 6B

257   where the pixels segmented as pruning wood are shown in white and the rest in black. The regression

258   plot for the number of pixels segmented as shoots and the pruning weight are displayed in Figure 7,

259   along with the 95% confidence interval. This correlation yielded a R^2=0.87. The LOOCV for external

260   validation of the linear model (Table 1) resulted in R^2=0.85, RMSE of 115.7g. and RPD=2.6.

261

Discussion

262

263   The results obtained in the present study confirm the capability of the presented method for pruning

264   weight estimation from in-field captured vine images. The possibility to work on-the-go at commercial

265   speed greatly improves the applicability of this new method for grapevine pruning weight estimation as

266   indicator of vegetative growth and vigor.

267

268   The semi-indoor shoot images were taken with the aim of simulating the outdoor capturing conditions,

269   but at the same time, reducing the influence of external objects (such as metal wires, parts of trunk,

270   posts, etc.) in the segmentation process. The results yielded a very strong correlation between the

271   number of pruning wood pixels and the shoots' weight. Based on this outcome, the next step was to test

272   the image-analysis algorithm with the in-field manually acquired vine images. In this dataset, the

273   illumination was less homogeneous, generating variations in the background (white screen) and

274   foreground (shoots and other objects). The presence of the metal wires and posts from the VSP trellis

12

182

275   system, which also had lignified tendrils from previous seasons, the trunk of the vine, and other objects

276   influenced the relationship between the segmented area corresponding to the wood class and the pruning

277   weight. The determination coefficient for these images was slightly lower than for the semi-indoor

278   images, but proved excellent prediction capabilities as demonstrated by its RPD. Comparing to other

279   studies, Kicherer et al. (2016) also estimated the pruning weight from a depth map obtained with a

280   manually operated image-based dispositive composed by three cameras. This setup provided a

281   determination coefficient of R^2=0.44 when the images were automatically evaluated. They also tested a

282   manual image analysis based on color information which required the use of a white background to

283   avoid the influence of the vines behind resulting in R^2=0.84 and RMSE=120g.

284

285   The lack of a controlled background and the motion during the capture for the on-the-go dataset was a

286   challenge in the image capturing process. The captured images were not blurry and the influence of the

287   background was greatly limited due to the correct calibration of the illumination, which obscured the

288   vines that were not in the foreground. The results obtained for this dataset exhibited a strong correlation

289   also for the LOOCV model testing. These outcomes were similar to the ones obtained for the in-field

290   manually acquired images despite of the harder capturing conditions, and also agreed with those

291   obtained in previous works (Kicherer et al. 2016) for manual and automated analysis. It is worth

292   highlighting that the images in the present study were taken on-the-go without any control of the

293   background. Furthermore, the model for the on-the-go approach was robust as demonstrated by its RPD

294   which corresponded to "good prediction accuracy" (Nicolaï et al. 2007).

295

296   Our results showed that the new computer vision based method is rapid and reliable. Moreover, laser

297   based sensors have also been tested for pruning weight estimation with similar performances. Tagarakis

13

183

298 et al. (2013) conducted an experiment consisting on winter shoot scanning using a laser sensor, while

299 Grocholsky et al. (2011) measured the canopy shape and volume using a laser sensor during the pre-

300 harvest period, obtaining an indirect estimation of the pruning weight. A similar approach with airborne

301 multispectral imaging sensors were also used to provide indirect correlations between spectral

302 reflectance indices such as NDVI and PCD with the pruning weight (Baluja et al. 2012). It must be

303 noted that these indirect measurements did not directly quantify the vine wood, but used the size of the

304 canopy to assess pruning weight. Moreover, these estimations are subjected to variations from season to

305 season and to other factors that affect the canopy and do not reflect as variations in the pruning wood.

306 Also, the remote measurements obtained using spectral sensors mounted in unmanned aerial vehicles

307 may suffer from the inability to distinguish between canopy and vegetation situated in the intra row

308 space (Gatti et al. 2016). All these pitfalls were overcome by this new developed image analysis method,

309 once the influence of the adjacent rows and other lighting issues are solved.

310

311 An image-based methodology for grapevine pruning weight estimation has been developed, presented

312 and validated with images acquired under different illumination (semi-indoor and outdoor), and capture

313 (manual static capture vs automated on-the-go acquisition) conditions. For the on-the-go mode, images

314 were taken at commercial speed (7 km hr^{-1}), confirming that the described methodology is adaptable to

315 other agriculture vehicles like tractors. Moreover, the flexibility of the system makes it also adaptable to

316 be installed in agricultural robots (Diago et al. 2016c, Rose et al. 2016), allowing continuous and

317 effortless vineyard monitoring. The obtained results proof that the developed methodology is robust and

318 reliable. The possibility to assess the pruning weight from geo-referenced images enables for the

319 mapping of large vineyards in a precise and effortless way. These maps can be used to adapt the pruning

320   severity, or the number of spurs per cordon among other cultural practices applied to grapevines to

321   optimize the vine balance.

322

Conclusion

323

324   A new methodology based on image analysis was developed and validated for grapevine pruning weight

325   estimation under different illumination and image acquisition conditions, from manual static capture to

326   automated on-the-go imaging. Our results proved that the grapevine pruning weight can be accurately

327   estimated from images captured directly under field conditions.

328

329   The possibility of automated and on-the-go image acquisition greatly increases the commercial

330   application of the developed machine-vision methodology. Moreover, image geo-referencing enables the

331   generation of pruning weight maps that will represent the grapevine vigor spatial variability within the

332   vineyard. The inexpensive, non-destructive, and time-saving presented procedure will support informed

333   decisions of viticultural operations to improve yield and grape quality.

334

335

15

336 **Literature Cited**

337 Baluja, J., Diago, M.P., Goovaerts, P., and Tardaguila, J. 2012. Assessment of the spatial variability of

338 anthocyanins in grapes using a fluorescence sensor: relationships with vine vigour and yield. Precis

339 Agric. 13:457–472.

340 Bei, R. De, Cozzolino, D., Sullivan, W., Cynkar, W., Fuentes, S., Dambergs, R., Pech, J., and Tyerman,

341 S.D. 2011. Non-destructive measurement of grapevine water potential using near infrared spectroscopy.

342 Aust J Grape Wine Res. 17:62–71.

343 Bongiovanni, R., and Lowenberg-Deboer, J. 2004. Precision agriculture and sustainability. Precis Agric.

344 5:359–387.

345 Botterill, T., Green, R., and Mills, S. 2013. Finding a vine's structure by bottom-up parsing of cane

346 edges. In: 2013 28th International Conference on Image and Vision Computing New Zealand (IVCNZ

347 2013). IEEE. pp. 112–117.

348 Botterill, T., Paulin, S., Green, R., Williams, S., Lin, J., Saxton, V., Mills, S., Chen, X., and Corbett-

349 Davies, S. 2016. A Robot System for Pruning Grape Vines. J F Robot.

350 Cook, S.E., Bramley, R.G. V., Cook, S.E., and Bramley, R.G. V. 1998. Precision agriculture —

351 opportunities, benefits and pitfalls of site-specific crop management in Australia. Aust J Exp Agric.

352 38:753.

353 Diago, M.P., Krasnow, M., Bubola, M., Millan, B., and Tardaguila, J. 2016a. Assessment of vineyard

354 canopy porosity using machine vision. Am J Enol Vitic. 67:229–238.

355 Diago, M.P., Rey-Carames, C., Moigne, M. Le, Fadaili, E.M., Tardaguila, J., and Cerovic, Z.G. 2016b.

356 Calibration of non-invasive fluorescence-based sensors for the manual and on-the-go assessment of

357 grapevine vegetative status in the field. Aust J Grape Wine Res. 22:438–449.

358 Diago, M.P., Rovira-Mas, F., Blasco, J., Saiz-Rubio, V., Faenzi, E., Sébastien Évain, Labails, S., Stoll,

16

186

359 M., Scheidweiler, M., Millot, C., et al. 2016c. Vinerobot: on-the-go vineyard monitoring with non-

360 invasive sensors. In: International Cool Climate Wine Symposium. Brighton.

361 Dobrowski, S.Z., Ustin, S.L., and Wolpert, J.A. 2003. Grapevine dormant pruning weight prediction

362 using remotely sensed data. Aust J Grape Wine Res. 9:177–182.

363 Gatti, M., Dosso, P., Maurino, M., Merli, M., Bernizzoni, F., José Pirez, F., Platè, B., Bertuzzi, G., and

364 Poni, S. 2016. MECS-VINE®: A new proximal sensor for segmented mapping of vigor and yield

365 parameters on vineyard rows. Sensors. 16:2009.

366 Gebbers, R., and Adamchuk, V.I. 2010. Precision agriculture and food security. Science. 327:828–831.

367 Grocholsky, B., Nuske, S., Aasted, M., and Bates, T. 2011. A camera and laser system for automatic

368 vine balance assessment. 2011 ASABE Annu Int Meet. 7004:1111651.

369 Keller, M. 2015. The science of grapevines: anatomy and physiology. Academic Press, San Diego,

370 California.

371 Kicherer, A., Klodt, M., Sharifzadeh, S., Cremers, D., Töpfer, R., and Herzog, K. 2017. Automatic

372 image-based determination of pruning mass as a determinant for yield potential in grapevine

373 management and breeding. Aust J Grape Wine Res. 23:120–124.

374 Matese, A., and Gennaro, S.F. Di. 2015. Technology in precision viticulture: a state of the art review. Int

375 J Wine Res. Volume 7:69.

376 Millan, B., Aquino, A., Diago, M.P.M.P., and Tardaguila, J. 2017. Image analysis-based modelling for

377 flower number estimation in grapevine. J Sci Food Agric. 97:784–792.

378 Nicolaï, B.M., Beullens, K., Bobelyn, E., Peirs, A., Saeys, W., Theron, K.I., and Lammertyn, J. 2007.

379 Nondestructive measurement of fruit and vegetable quality by means of NIR spectroscopy: A review.

380 Postharvest Biol Technol. 46:99–118.

381 Nuske, S., Achar, S., and Gupta, K. 2011. Visual yield estimation in vineyards: experiments with

17

405   Tagarakis, A., Liakos, V., Chatzinikos, T., Koundouras, S., Fountas, S., and Gemtos, T. 2013. Using

406   laser scanner to map pruning wood in vineyards. In: J. V Stafford, ed. Precision Agriculture '13.

407   Wageningen: Wageningen Academic Publishers. pp. 633–639.

408   Taylor, J.A., and Bates, T.R. 2012. Sampling and estimating average pruning weights in concord grapes.

409   Am J Enol Vitic. 63:559–563.

410   Williams, P.C., and Sobering, D. 1996. How do we do it: A brief summary of the methods we use in

411   developing near infrared calibrations. In: A.M.C. Daves, and P.C. Williams, eds. Near Infrared

412   Spectroscopy: The Future Waves. Chichester, UK: NIR Publications. pp. 185–188.

413   Wolcott, R.W., and Eustice, R.M. 2014. Visual localization within lidar maps for automated urban

414   driving. In: Intelligent Robots and Systems (IROS 2014), 2014 IEEE/RSJ International Conference on.

415   IEEE. pp. 176–183.

416   Zarco-Tejada, P.J., Hubbard, N., and Loudjani, P. 2014. Precision agriculture: an opportunity for EU

417   farmers - Potential support with the CAP 2014 - 2020.

418

19

382   different varietals and calibration procedures. Technical Report CMU-RI-TR-11-39. Pittsburgh.

383   Otsu, N. 1979. A threshold selection method from gray-level histograms. Syst Man Cybern IEEE Trans.

384   9:62–66.

385   Palleja, T., and Landers, A.J. 2017. Real time canopy density validation using ultrasonic envelope

386   signals and point quadrat analysis. Comput Electron Agric. 134:43–50.

387   Pou, A., Diago, M.P., Medrano, H., Baluja, J., and Tardaguila, J. 2014. Validation of thermal indices for

388   water status identification in grapevine. Agric Water Manag. 134:60–72.

389   Proffitt, T., Bramley, R., Lamb, D., and Winter, E. 2006. Precision viticulture : a new era in vineyard

390   management and wine production. Ashford South Australia: Winetitles.

391   Rey-Caramés, C., Tardaguila, J., Sanz-Garcia, A., Chica-Olmo, M., and Diago, M.P. 2016. Quantifying

392   spatio-temporal variation of leaf chlorophyll and nitrogen contents in vineyards. Biosyst Eng. 150:201–

393   213.

394   Reynolds, A.G. 2010. Managing Wine Quality. Cambridge, Woodhead Publishing.

395   Rose, C.J., Kicherer, A., Wieland, M., Klingbeil, L., Töpfer, R., and Kuhlmann, H. 2016. Towards

396   automated large-scale 3D phenotyping of vineyards under field conditions. Sensors. 16:2136.

397   Sepúlveda-Reyes, D., Ingram, B., Bardeen, M., Zúñiga, M., Ortega-Farías, S., and Poblete-Echeverría,

398   C. 2016. Selecting canopy zones and thresholding approaches to assess grapevine water status by using

399   aerial and ground-based thermal imaging. Remote Sens. 8:822.

400   Smart, R., and Robinson, M. 1991. Sunlight into wine; A handbook for winegrape canopy management.

401   Adelaide: Winetitles.

402   Stamatiadis, S., Taskos, D., Tsadilas, C., Christofides, C., Tsadila, E., and Schepers, J.S. 2006. Relation

403   of ground-sensor canopy reflectance to biomass production and grape color in two merlot vineyards. Am

404   J Enol Vitic. 57:415–422.

18

419 **Tables**

420 **Table 1** Leave one out cross validation (LOOCV) model analysis for the pruning weight estimation from
421 grapevine images taken manually and on-the-go under field conditions. Manually acquired images were taken
422 using a white screen as background while on-the-go images were captured during night-time to avoid interference
423 from vines in background rows.

	Number of measurements	Correlation coefficient (R^2)	MAE[a] (g)	RMSE[b] (g)
In-field manually acquired vine images	45	0.913	61.7	87.7
On-the-go acquired vine images	45	0.849	80.4	115.7

424 [a]: mean absolute error

425 [b]: root-mean-square error

426
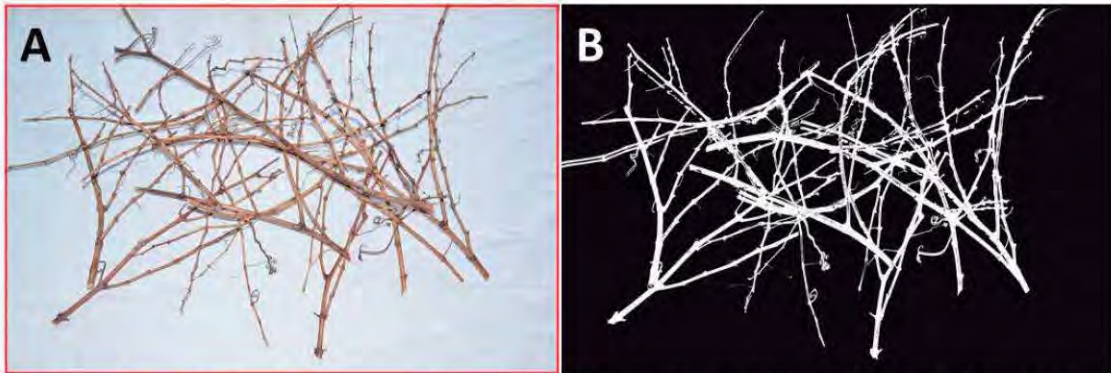
427   **Figures**

428

429   **Figure 1** Modified all-terrain vehicle equipped with a digital camera, automatic triggering system, illumination on
430   an adjustable structure and GNSS receiver for geo-referencing used for the on-the-go image acquisition to
431   estimate pruning weight.
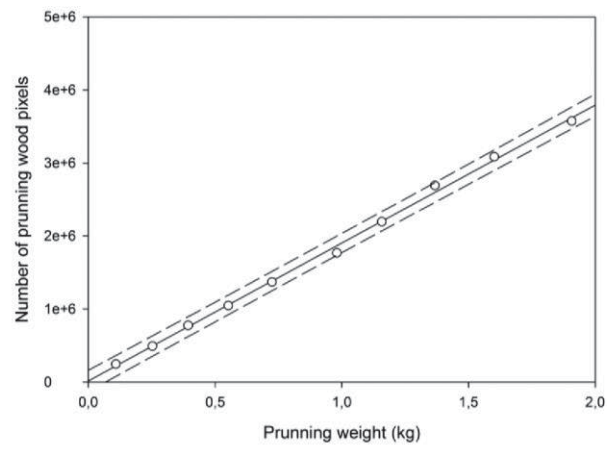
432

21

433

434
435 **Figure 2** (A) Example of semi-indoor manually acquired shoot images with the boundaries of the ROI used for
436 analysis in red. The images were captured with indirect and uncontrolled lighting using a white screen as
437 background. (B) Segmented image of the shoots using image analysis with the wood pixels represented in white
438 and background in black.

192

439
440 **Figure 3** Relationship between pruning wood weight and the number of pixels segmented as pruning wood on
441 semi-indoor manually acquired vine images. Ten images were analyzed corresponding to one up to ten shoots per
442 image. Solid line represents linear regression y=2E+06x − 15267 (R^2=0.998***). Dashed lines correspond to 95%
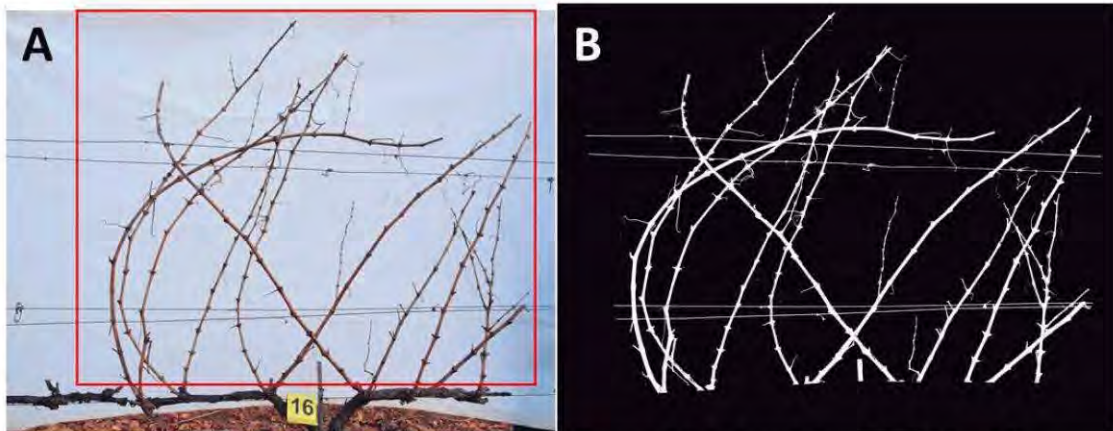443 confidence interval.

444

445
446 **Figure 4** (A) Example of the in-field manually acquired vine images with the boundaries of the ROI used for
447 analysis in red. The images were captured using a white screen as background. (B) Segmented image of the
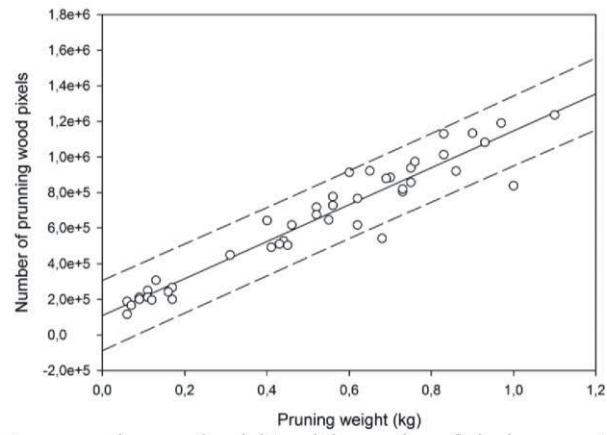448 pruning wood using image analysis with the wood pixels represented in white and background in black.

449
450 **Figure 5** Relationship between pruning wood weight and the number of pixels segmented as pruning wood for
451 manually acquired vine images. The images of 45 grapevines were captured in-field with uncontrolled light
452 conditions using a white screen as background. Solid line corresponds to the linear regression y=1E+06x +
453 109048 (R^2=0.919***). Dashed lines represent 95% confidence interval.

454

25
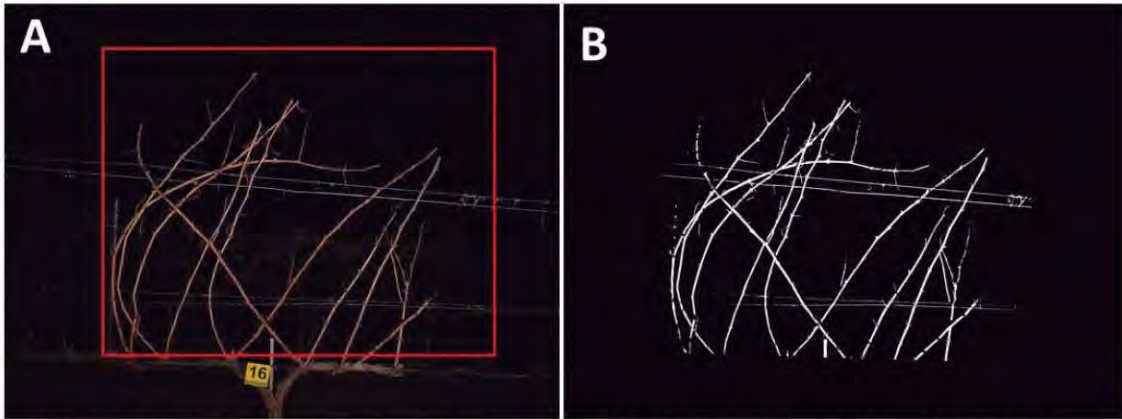
455
456 **Figure 6** (A) Example of the on-the-go acquired vine images with the boundaries of the ROI used for analysis in
457 red. (B) Segmented image of the pruning wood using image analysis. A modified ATV (all-terrain-vehicle) was
458 used for the automated capturing process of 45 grapevines at a speed around 7 km hr^{-1}.

459

460
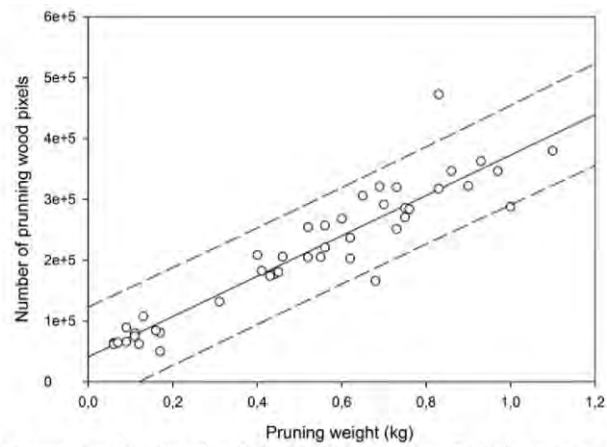461 **Figure 7** Relationship between pruning wood weight and the number of pixels segmented as pruning wood on
462 images captured in-field and on-the-go. A modified ATV (all-terrain-vehicle) was used for the automated
463 capturing process on 45 vines. Solid line corresponds to the linear regression y=331792x + 41011 (R^2=0.871***).
464 Dashed lines represents 95% confidence interval.

465

4 Conclusions

This PhD Thesis has established the usefulness of computer vision to assess vineyard status in the scope of precision viticulture.

The research presented here in provided the following main findings:

4.1 Assessment of flower number per inflorescence

1. The analysis of digital images captured under field conditions provides a useful estimation of the number of flowers per inflorescence at early stages of flowering.
2. The development of an innovative smartphone Android application, called vitisFlower is a powerful tool for easy and automatic flowering assessment in the vineyard.
3. The flower number per inflorescence estimation using image analysis and a non-linear model was generally applied to different grapevine varieties.

4.2 Yield components estimation

4. Image analysis methodology has proved to be a useful and reliable tool for yield assessment in the vineyard. The proposed setup for manual image acquisition is simple, inexpensive and non-destructive requiring only a commercial RGB camera.
5. Yield assessment can be performed by computer vision using images captured automatically on-the-go at a speed comparable to other agricultural equipment.
6. The use of Boolean models allowed overcoming two of the major difficulties in visual yield estimation: this technique is robust against segmentation errors and partial occlusions, situations that are normal in the case of cluster images taken under natural field conditions.

4.3   Canopy status assessment

7. The grapevine canopy status including cluster exposure, canopy porosity and exposed leaves within a vineyard was successfully assessed using manually captured images.
8. Canopy status assessment can be obtained from images captured on-the-go, reducing the effort necessary to carry out dense vineyard sampling.
9. The grapevine pruning weight can be accurately estimated using image analysis. The methodology was developed and validated under different illumination and image acquisition conditions ranging from manual static capture to automated on-the-go imaging.

4.4   On-the-go vineyard assessment and mapping

10. The development of an autonomous capture platform including a system for automatic camera triggering, geo-positioning information capturing from GNSS receiver and illumination system greatly reduces the man power necessary for infield image acquisition.
11. All the viticultural parameters determined by image analysis were geo-referenced, allowing map generation. These maps can be used to delineate zones of homogeneous management in the context of precision viticulture.

4.5   Global conclusion

Computer vision has been found to be a promising alternative to the traditional methods for vineyard monitoring. Flower number assessment, yield estimation and canopy status are key viticultural parameters. This information can be used by the vineyard manager in the scope of precision viticulture to reduce costs and environmental impacts, and increase fruit quality.

5 References

Adamchuk, V., Hummel, J., Morgan, M. & Upadhyaya, S. (2004). On-the-go soil sensors for precision agriculture. Computers and Electronics in Agriculture. 44 (1). pp. 71–91.

Aquino, A., Diago, M.P., Millán, B. & Tardáguila, J. (2017). A new methodology for estimating the grapevine-berry number per cluster using image analysis. Biosystems Engineering. 156. pp. 80–95.

Aquino, A., Millan, B., Gaston, D., Diago, M.-P. & Tardaguila, J. (2015a). vitisFlower®: Development and testing of a novel Android-smartphone application for assessing the number of grapevine flowers per inflorescence using artificial vision techniques. Sensors. 15 (9). p.p. 21204.

Aquino, A., Millan, B., Gutiérrez, S. & Tardáguila, J. (2015b). Grapevine flower estimation by applying artificial vision techniques on images with uncontrolled scene and multi-model analysis. Computers and Electronics in Agriculture. 119. pp. 92–104.

Arnó, J. (2005). Viticultura de precisió a Raimat (Lleida) experiències durant el període 2002-2004. ACE: revista d'enologia. 22 (73). pp. 12–17.

Arnó, J., Bordes, X., Ribes-Dasi, M., Blanco, R., Rosell, J.R. & Esteve, J. (2005). Obtaining grape yield maps and analysis of within-field variability in Raimat (Spain). In: J. V. Stafford (ed.). Precision Agriculture'05. Proceedings of the Fifth European Conference on Precision Agriculture. 2005, Wageningen, The Netherlands: Wageningen Academic Publishers, pp. 899–906.

Arnó, J., Martínez Casasnovas, J.A., Ribes Dasi, M. & Rosell, J.R. (2009). Review. Precision viticulture. Research topics, challenges and opportunities in site-specific vineyard management. Spanish Journal of Agricultural Research. 7 (4). pp. 779–790.

Ballard, D.H. & Brown, C.M. (1982). Computer vision. New Jersey: Prentice-Hall.

Baluja, J., Diago, M.P., Balda, P., Zorer, R., Meggio, F., Morales, F. & Tardaguila, J. (2012). Assessment of vineyard water status variability by thermal and multispectral imagery using an unmanned aerial vehicle (UAV). Irrigation Science. 30 (6). pp. 511–522.

Bansal, R., Lee, W.S. & Satish, S. (2013). Green citrus detection using fast Fourier transform (FFT) leakage. Precision Agriculture. 14 (1). pp. 59–70.

De Bei, R., Hook, J., Fuentes, S., Gilliham, M., Tyerman, S. & Collins, C. (2015). Linking canopy architecture to grape quality using the LAI canopy app. In: In proceeding of the 19th International Meeting of Viticulture GIESCO. 2015, Montpellier, pp. 585–588.

Bellvert, J., Zarco-Tejada, P.J., Girona, J. & Fereres, E. (2014). Mapping crop water stress index in a Pinot-noir vineyard: Comparing ground measurements with thermal remote sensing imagery from an unmanned aerial vehicle. Precision Agriculture. 15 (4).

Berenstein, R., Shahar, O. Ben, Shapiro, A. & Edan, Y. (2010). Grape clusters and foliage detection algorithms for autonomous selective vineyard sprayer. Intelligent Service Robotics. 3 (4). pp. 233–243.

Boso, S., Santiago, J.L. & Martínez, M.C. (2004). Resistance of eight different clones of the grape cultivar Albariño to Plasmopara viticola. Plant Disease. 88 (7). pp. 741–744.

Botterill, T., Paulin, S., Green, R., Williams, S., Lin, J., Saxton, V., Mills, S., Chen, X. & Corbett-Davies, S. (2016). A Robot System for Pruning Grape Vines. Journal of Field Robotics.

Bramley, R.G.V. (2001). Progress in the development of precision viticulture - variation in yield, quality and soil properties in contrasting Australian vineyards. In: L. D. Currie & P. Loganathan (eds.). Precision tools for improving land management. Palmerston North, New Zealand: Fertilizer and Lime Rese- arch Centre, Massey University, pp. 25–43.

Bramley, R.G.V. & Lamb, D.W. (2003). Making sense of vineyard variability in Australia. In: R. Ortega & A. Esser (eds.). Proceedings of an international symposium held as part of the IX C ongreso Latinoamericano de Viticultura y Enologia. 2003, Santiago, Chila: Centro de Agricultura de Precisión, Pontificia Universidad Católica de Chile, pp. 35–54.

Bramley, R.G.V. & Proffitt, A.P.B. (1999). Managing variability in viticultural production. Australian and New Zealand Grapegrower and Winemaker. 427. pp. 11–16.

Bramley, R.G.V., Proffitt, A.P.B., Corner, R.J. & Evans, T.D. (2000). Variation in grape yield and soil depth in two contrasting Australian vineyards. In:

Australian and New Zealand Second Joint Soils Conference. 2000, Lincoln, New Zealand, pp. 3–8.

Braun, T., Koch, H., Strub, O., Zolynski, G. & Berns, K. (2010). Improving pesticide spray application in vineyards by automated analysis of the foliage distribution pattern in the leaf wall. In: 1st Commercial Vehicle Technology Symposium. 2010, Kaiserslautern, Germany.

Cerovic, Z.G., Masdoumier, G., Ghozlen, N. Ben & Latouche, G. (2012). A new optical leaf-clip meter for simultaneous non-destructive assessment of leaf chlorophyll and epidermal flavonoids. Physiologia Plantarum. 146 (3). pp. 251–260.

Chaivivatrakul, S., Moonrinta, J. & Dailey, M.N. (2010). Towards automated crop yield estimation: Detection and 3D reconstruction of pineapples in video sequences. In: Fifth International Conference on Computer Vision Theory and Applications. 2010, Angers, France: INSTICC Press, pp. 180–183.

Chamelat, R., Rosso, E., Choksuriwong, A., Rosenberger, C., Laurent, H. & Bro, P. (2006). Grape detection by image processing. In: IECON 2006 - 32nd Annual Conference on IEEE Industrial Electronics. November 2006, Paris, France: IEEE, pp. 3697–3702.

Cipolla, R., Battiato, S. & Farinella, G. (2014). Registration and Recognition in Images and Videos.

Clingeleffer, P. (2001). Crop development, crop estimation and crop control to secure quality and production of major wine grape varieties: a national approach.

Cook, S.E. & Bramley, R.G. V (1998). Precision agriculture - opportunities, benefits and pitfalls of site-specific crop management in Australia. Australian Journal of Experimental Agriculture. 38 (7). pp. 753–763.

Costa, J.M., Grant, O.M. & Chaves, M.M. (2010). Use of thermal imaging in viticulture: current application and future prospects. In: S. Delrot, H. Medrano, E. Or, L. Bavaresco, & S. Grando (eds.). Methodologies and Results in Grapevine Research. Dordrecht: Springer Netherlands, pp. 135–150.

Cubero, S., Diago, M.P., Blasco, J., Tardáguila, J., Millán, B. & Aleixos, N. (2014). A new method for pedicel/peduncle detection and size assessment

of grapevine berries and other fruits by image analysis. Biosystems Engineering. 117. pp. 62–72.

Cubero, S., Diago, M.P., Blasco, J., Tardaguila, J., Prats-montalbán, J.M., Ibáñez, J., Tello, J. & Aleixos, N. (2015). A new method for assessment of bunch compactness using automated image analysis. Australian Journal of Grape and Wine Research. 21 (1). pp. 101–109.

Diago, M., Ayestarán, B., Guadalupe, Z., Garrido, Á. & Tardaguila, J. (2012a). Phenolic composition of Tempranillo wines following early defoliation of the vines. Journal of the science of food and agriculture. 92 (4). pp. 925–934.

Diago, M., Correa, C., Millán, B., Barreiro, P., Valero, C. & Tardaguila, J. (2012b). Grapevine yield and leaf area estimation using supervised classification methodology on RGB images taken under field conditions. Sensors. 12 (12). pp. 16988–17006.

Diago, M., Rey-Carames, C., Le Moigne, M., Fadaili, E.M., Tardaguila, J. & Cerovic, Z.G. (2016a). Calibration of non-invasive fluorescence-based sensors for the manual and on-the-go assessment of grapevine vegetative status in the field. Australian Journal of Grape and Wine Research. 22 (3). pp. 438–449.

Diago, M., Rovira-Mas, F., Blasco, J., Saiz-Rubio, V., Faenzi, E., Sébastien Évain, Labails, S., Stoll, M., Scheidweiler, M., Millot, C., Campos-Gomez, E. & Tardauila, J. (2016b). Vinerobot: on-the-go vineyard monitoring with non-invasive sensors. In: International Cool Climate Wine Symposium. 2016, Brighton.

Diago, M.P., Krasnow, M., Bubola, M., Millan, B. & Tardaguila, J. (2016c). Assessment of vineyard canopy porosity using machine vision. American Journal of Enology and Viticulture. 67 (2). pp. 229–238.

Diago, M.P., Sanz-Garcia, A., Millan, B., Blasco, J. & Tardaguila, J. (2014). Assessment of flower number per inflorescence in grapevine by image analysis under field conditions. Journal of the Science of Food and Agriculture. 94 (10). pp. 1981–1987.

Diago, M.P., Tardaguila, J., Aleixos, N., Millan, B., Prats-Montalban, J.M., Cubero, S. & Blasco, J. (2015). Assessment of cluster yield components by

image analysis. Journal of the Science of Food and Agriculture. 95 (6). pp. 1274–1282.

Dressler, N., Gundermann, S., Keese, S., Aulbur, W., Zhang, J., Amichi, S., Marinoni, A., Nagashima, S., Cherkin, E., Weber, C. & Höft, M. (2015). Business opportunities in precision farming. Munich, Germany.

Dunn, G.. (2010). Yield Forecasting.

Dunn, G.M. & Martin, S.R. (2004). Yield prediction from digital image analysis: A technique with potential for vineyard assessments prior to harvest. Australian Journal of Grape and Wine Research. 10 (3). pp. 196–198.

Erickson, B. & Widmar, D.A. (2015). 2015 Precision agricultural services dealership survey results. West Lafayette, Indiana, USA. Available from: http://agribusiness.purdue.edu/files/resources/2015-crop-life-purdue-precision-dealer-survey.pdf [Accessed: 22 April 2017].

Eurostat (2017). Structure of vineyards in 2015. Available from: http://ec.europa.eu/eurostat/documents/2995521/7964277/5-04042017-BP-EN.pdf/149e5e9a-4ae6-466b-baec-0273fe0c08a4

Fernandes, A.M., Melo-Pinto, P., Millan, B., Tardáguila, J. & Diago, M.P. (2014). Automatic discrimination of grapevine (Vitis vinifera L.) clones using leaf hyperspectral imaging and partial least squares. The Journal of Agricultural Science. 153 (3). pp. 1–11.

Fernández-Novales, J., Gutiérrez, S., Tardaguila, J., Millan, B. & Diago, M.P. (2017). In-field assessment of grapevine water status using a portable NIR spectrophotometer. In: J. Marsal & J. Girona (eds.). Acta Horticulturae. 25 January 2017, Lleida, Spain: International Society for Horticultural Science (ISHS), Leuven, Belgium, pp. 167–172.

Ferreira, V., Cheynier, V., Sarni-Manchado, P., Kennedy, J.A., Zoecklein, B.W., Fugelsang, K.C., Gump, B.H., Cozzolino, D., Dambergs, R.G., Osborne, J.P., Lesschaeve, I., Noble, A.C., Arvanitoyannis, I.S., van Leeuwen, C., Young, P.R., Vivier, M., Bramley, R.G.V., Scott, E.S., Dambergs, R.G., Stummer, B.E., Battilani, P., Silva, A., Christmann, M. & Freund, M. (2010). Contributor contact details. In: Managing Wine Quality. pp. xi–xiv.

Flexas, J., Briantais, J.-M., Cerovic, Z., Medrano, H. & Moya, I. (2000). Steady-State and Maximum Chlorophyll Fluorescence Responses to Water

Stress in Grapevine Leaves: A New Remote Sensing System. Remote Sensing of Environment. 73 (3). pp. 283–297.

Font, D., Pallejà, T., Tresanchez, M., Teixidó, M., Martinez, D., Moreno, J. & Palacín, J. (2014). Counting red grapes in vineyards by detecting specular spherical reflection peaks in RGB images obtained at night with artificial illumination. Computers and Electronics in Agriculture. 108. pp. 105–111.

Font, D., Tresanchez, M., Martínez, D., Moreno, J., Clotet, E. & Palacín, J. (2015). Vineyard yield estimation based on the analysis of high resolution images obtained with artificial illumination at night. Sensors. 15 (4). pp. 8284–8301.

Fuentes, S., De Bei, R., Pozo, C. & Tyerman, S. (2012a). Development of a smartphone application to characterise temporal and spatial canopy architecture and leaf area index for grapevines. Wine and viticulture journal. (6). pp. 56–60.

Fuentes, S., De Bei, R., Pozo, C., Tyerman, S. & Campus, W. (2012b). Development of a smartphone application to Less Bugs. (V). pp. 56–60.

Fuentes, S., De Bei, R. & Tyerman, S.D. (2013). Using smartphones and tablet PCs for canopy architecture assessment to upscale physiological parameters: LAICanopy© App. In: IX International Symposium on Grapevine Phisiology and Biotechnology. 2013, La Serena, Chile, p. 120.

Gatti, M., Dosso, P., Maurino, M., Merli, M., Bernizzoni, F., José Pirez, F., Platè, B., Bertuzzi, G. & Poni, S. (2016). MECS-VINE®: A new proximal sensor for segmented mapping of vigor and yield parameters on vineyard rows. Sensors. 16 (12). p. 2009.

Ghozlen, N. Ben, Cerovic, Z.G., Germain, C., Toutain, S. & Latouche, G. (2010). Non-destructive optical monitoring of grape maturation by proximal sensing. Sensors. 10 (11). pp. 10040–10068.

Griffin, T.W., Lowenberg-Deboer, J., Lambert, D.M., Peone, J., Payne, T., Daberkow, S.G. & Griffin, T.W. (2004). Adoption, profitability, and making better use of precision farming data. West Lafayette, Indiana, USA. Available from: http://ageconsearch.tind.io//bitstream/28615/1/sp04-06.pdf [Accessed: 22 April 2017].

Grocholsky, B., Nuske, S., Aasted, M. & Bates, T. (2011). A camera and laser system for automatic vine balance assessment. 2011 ASABE Annual International Meeting. 7004 (11). Paper number 1111651.

Hall, A., Lamb, D.W., Holzapfel, B.P. & Louis, J.P. (2011). Within-season temporal variation in correlations between vineyard canopy and winegrape composition and yield. Precision Agriculture. 12 (1). pp. 103–117.

Herrero-Huerta, M., González-Aguilera, D., Rodriguez-Gonzalvez, P. & Hernández-López, D. (2015). Vineyard yield estimation by automatic 3D bunch modelling in field conditions. Computers and Electronics in Agriculture. 110. pp. 17–26.

Herzog, K., Roscher, R., Wieland, M., Kicherer, A., Läbe, T., Förstner, W., Kuhlmann, H., Töpfer, R., Labe, T., Forstner, W., Kuhlmann, H. & Töpfer, R. (2014). Initial steps for high-throughput phenotyping in vineyards. Vitis - Journal of Grapevine Research. 53 (1). pp. 1–8.

Huang, T.S. (1996). Computer Vision: evolution and promise. Available from: http://cds.cern.ch/record/400313/files/p21.pdf [Accessed: 3 June 2017].

Ivorra, E., Sánchez, A.J., Camarasa, J.G., Diago, M.P. & Tardaguila, J. (2015). Assessment of grape cluster yield components based on 3D descriptors using stereo vision. Food Control. 50. pp. 273–282.

Jones, H.G. (1999). Use of infrared thermometry for estimation of stomatal conductance as a possible aid to irrigation scheduling. Agricultural and Forest Meteorology. 95 (3). pp. 139–149.

Jones, H.G. & Vaughan, R.A. (2010). Remote sensing of vegetation: principles, techniques, and applications. Oxford, UK: Oxford University Press

Kanizsa, G. (1997). Grammatica del vedere: saggi su percezione e gestalt. Bologna: Il mulino.

Keller, M. (2015). Phenology and Growth Cycle. In: M. Keller (ed.). The Science of Grapevines. Anatomy and Physiology. San Diego, USA: Academic Press, pp. 59–99.

Kicherer, A., Herzog, K., Pflanz, M., Wieland, M., Rüger, P., Kecke, S., Kuhlmann, H. & Töpfer, R. (2015a). An automated field phenotyping pipeline for application in grapevine research. Sensors. 15 (3). pp. 4823–4836.

Kicherer, A., Klodt, M., Sharifzadeh, S., Cremers, D., Töpfer, R. & Herzog, K. (2017). Automatic image-based determination of pruning mass as a determinant for yield potential in grapevine management and breeding. Australian Journal of Grape and Wine Research. 23 (1). pp. 120–124.

Kicherer, A., Roscher, R., Herzog, K., Šimon, S., Förstner, W. & Töpfer, R. (2015b). BAT (Berry Analysis Tool): A high-throughput image interpretation tool to acquire the number, diameter, and volume of grapevine berries. VITIS - Journal of Grapevine Research. 52 (3). p. 129.

Klodt, M., Herzog, K., Töpfer, R. & Cremers, D. (2015). Field phenotyping of grapevine growth using dense stereo reconstruction. BMC Bioinformatics. 16 (1). p. 143.

Kole, D.K., Ghosh, A. & Mitra, S. (2014). Detection of Downy Mildew disease present in the grape leaves based on fuzzy set theory. In: M. D. Kumar Kundu, D. Prasad Mohapatra, A. Konar, & A. Chakraborty (eds.). Advanced Computing and Informatics. 2014, Kolkata, India: Springer, Cham, pp. 377–384.

Lee, W.S., Slaughter, D.C. & Giles, D.K. (1996). Development of a machine vision system for weed control using precision chemical application. In: International Conference on agricultural machinery engineering. 1996, pp. 802–811.

Li, L., Zhang, Q. & Huang, D. (2014). A review of imaging techniques for plant phenotyping. Sensors. 14 (11). pp. 20078–20111

Liu, S., Cossell, S., Tang, J., Dunn, G. & Whitty, M. (2017). A computer vision system for early stage grape yield estimation based on shoot detection. Computers and Electronics in Agriculture. 137. pp. 88–101.

Liu, S. & Whitty, M. (2015). Automatic grape bunch detection in vineyards with an SVM classifier. Journal of Applied Logic.

Liu, S., Whitty, M. & Cossell, S. (2015). A lightweight method for grape berry counting based on automated 3D bunch reconstruction from a single

image. In: ICRA, International Conference on Robotics and Automation (IEEE), Workshop on Robotics in Agriculture. 2015, p. 4.

Mack, J., Lenz, C., Teutrine, J. & Steinhage, V. (2017). High-precision 3D detection and reconstruction of grapes from laser range data for efficient phenotyping based on supervised learning. Computers and Electronics in Agriculture. 135. pp. 300–311

Marciniak, M., Reynolds, A.G., Brown, R., Jollineau, M. & Kotsaki, E. (2017). Applications of geospatial technologies to understand terroir effects in an Ontario Riesling vineyard. American Journal of Enology and Viticulture. 68 (2).

Marr, D. (1982). Vision: a computational investigation into the human representation and processing of visual information. J. Wilson & P. Monsour (eds.). New York: W. H. Freeman and Company.

Martin, S., Dunstone, R., Dunn, G., Stephen, M., Rebecca, D. & Gregory, D. (2003). How to forecast wine grape deliveries.

Martin, S.R., Dunn, G.M., Hoogenraad, T., Krstic, M.P., Clingeleffer, P.R. & Ashcroft, W.J. (2002). Crop forecasting in cool climate vineyards. In: Winetitles (ed.). Proceedings for the 5th International Symposium on Cool Climate Viticulture and enology. 2002, Melbourne, Australia: Winetitles.

Matese, A. & Di Gennaro, S.F. (2015). Technology in precision viticulture: a state of the art review. International Journal of Wine Research. Volume 7. p. 69.

Matese, A., Di Gennaro, S.F., Zaldei, A., Genesio, L. & Vaccari, F.P. (2009). A wireless sensor network for precision viticulture: The NAV system. Computers and Electronics in Agriculture. 69 (1). pp. 51–58.

Matese, A., Toscano, P., Di Gennaro, S., Genesio, L., Vaccari, F., Primicerio, J., Belli, C., Zaldei, A., Bianconi, R. & Gioli, B. (2015). Intercomparison of UAV, aircraft and satellite remote sensing platforms for precision viticulture. Remote Sensing. 7 (3). pp. 2971–2990.

Meunkaewjinda, A., Kumsawat, P., Attakitmongcol, K. & Srikaew, A. (2008). Grape leaf disease detection from color imagery using hybrid intelligent system. In: 5th International Conference on Electrical Engineering/Electronics, Computer, Telecommunications and Information Technology. May 2008, Krabi, Thailand: IEEE, pp. 513–516.

Millan, B., Aquino, A., Diago, M.P. & Tardaguila, J. (2017). Image analysis-based modelling for flower number estimation in grapevine. Journal of the Science of Food and Agriculture. 97 (3). pp. 784–792.

Montero, F.., Meliá, J., Brasa, A., Segarra, D., Cuesta, A. & Lanjeri, S. (1999). Assessment of vine development according to available water resources by using remote sensing in La Mancha, Spain. Agricultural Water Management. 40 (2). pp. 363–375.

Nuske, S., Achar, S., Bates, T., Narasimhan, S. & Singh, S. (2011a). Yield estimation in vineyards by visual grape detection. IEEE International Conference on Intelligent Robots and Systems. pp. 2352–2358.

Nuske, S., Achar, S. & Gupta, K. (2011b). Visual yield estimation in vineyards: experiments with different varietals and calibration procedures. Technical Report CMU-RI-TR-11-39. Pittsburgh.

Nuske, S., Wilshusen, K., Achar, S., Yoder, L., Narasimhan, S. & Singh, S. (2014). Automated visual yield estimation in vineyards. Journal of Field Robotics. 31 (5). pp. 837–860.

Ogawa, Y., Kondo, N., Monta, M. & Shibusawa, S. (2006). Spraying Robot for Grape Production. In: S. Yuta, H. Asama, E. Prassler, T. Tsubouchi, & S. Thrun (eds.). Field and Service Robotics. Berlin/Heidelberg: Springer-Verlag, pp. 539–548.

Ojeda, H., Carrillo, N., Deis, L., Tisseyre, B., Heywang, M. & Carbonneau, A. (2005). Precision viticulture and water status II: Quantitative and qualitative performance of different within field zones, defined from water potential mapping. In: XIV International GESCO Viticulture Congress. 2005, Geisenheim, Germany: Groupe d'Etude des Systemes de COnduite de la vigne (GESCO), pp. 741–748.

Oliver, M.A. (2010). Geostatistical Applications for Precision Agriculture. M. A. Oliver (ed.). Dordrecht: Springer Netherlands.

Palleja, T. & Landers, A.J. (2017). Real time canopy density validation using ultrasonic envelope signals and point quadrat analysis. Computers and Electronics in Agriculture. 134. pp. 43–50.

Palliotti, A., Gatti, M. & Poni, S. (2011). Early leaf removal to improve vineyard efficiency: gas exchange, source-to-sink balance, and reserve

storage responses. American Journal of Enology and Viticulture. 62 (2). pp. 219–228.

Papert, S.A. (1966). The summer vision project. Massachusetts. Available from: http://hdl.handle.net/1721.1/6125 [Accessed: 4 June 2017].

Paulus, I., De Busscher, R. & Schrevens, E. (1997). Use of image analysis to investigate human quality classification of apples. Journal of Agricultural Engineering Research. 68 (4). pp. 341–353.

Peressotti, E., Duchêne, E., Merdinoglu, D. & Mestre, P. (2011). A semi-automatic non-destructive method to quantify grapevine downy mildew sporulation. Journal of Microbiological Methods. 84 (2). pp. 265–271.

Pérez, D.S., Bromberg, F. & Diaz, C.A. (2017). Image classification for detection of winter grapevine buds in natural conditions using scale-invariant features transform, bag of features and support vector machines. Computers and Electronics in Agriculture. 135. pp. 81–95.

Poblete-Echeverría, C., Olmedo, G., Ingram, B. & Bardeen, M. (2017). Detection and segmentation of vine canopy in ultra-high spatial resolution RGB imagery obtained from unmanned aerial vehicle (UAV): a case study in a commercial vineyard. Remote Sensing. 9 (3). p. 268.

Pou, A., Diago, M.P., Medrano, H., Baluja, J. & Tardaguila, J. (2014). Validation of thermal indices for water status identification in grapevine. Agricultural Water Management. 134. pp. 60–72.

Proffitt, T., Bramley, R., Lamb, D. & Winter, E. (2006). Precision viticulture: a new era in vineyard management and wine production. S. Ashford (ed.). Ashford South Australia: Winetitles.

Qureshi, W.S., Payne, A., Walsh, K.B., Linker, R., Cohen, O. & Dailey, M.N. (2017). Machine vision for counting fruit on mango tree canopies. Precision Agriculture. 18 (2). pp. 224–244.

Rangel, B.M.S., Fernandez, M.A.A., Murillo, J.C., Ortega, J.C.P. & Arreguin, J.M.R. (2016). KNN-based image segmentation for grapevine potassium deficiency diagnosis. In: 2016 International Conference on Electronics, Communications and Computers (CONIELECOMP). February 2016, IEEE, pp. 48–53.

Rey-Caramés, C., Tardaguila, J., Sanz-Garcia, A., Chica-Olmo, M. & Diago, M.P. (2016). Quantifying spatio-temporal variation of leaf chlorophyll and nitrogen contents in vineyards. Biosystems Engineering. 150. pp. 201–213.

Reynolds, A.G. (2010). Managing Wine Quality. A. G. Reynolds (ed.). Cambridge: Woodhead Publishing.

Robinson, J. & Harding, J. (2015). The Oxford companion to wine. 4th Ed. J. Harding & R. E. Smart (eds.). Oxford, UK: Oxford University Press.

Roscher, R., Herzog, K., Kunkel, A., Kicherer, A., Töpfer, R. & Förstner, W. (2014). Automated image analysis framework for high-throughput determination of grapevine berry sizes using conditional random fields. Computers and Electronics in Agriculture. 100. pp. 148–158.

Rossi, R., Pollice, A., Diago, M.-P.P., Oliveira, M., Millan, B., Bitella, G., Amato, M. & Tardaguila, J. (2013). Using an automatic resistivity profiler soil sensor on-the-go in precision viticulture. Sensors. 13 (1). pp. 1121–1136.

Schillaci G, Pennisi A, Franco F & Longo D (2012). Detecting tomato crops in greenhouses using a vision based method. In: International Conference on Safety Health and Welfare in Agriculture and in Agro-food Systems. 2012, Ragusa, Italy, pp. 20–26.

Schrijver, R. (2016). Precision agriculture and the future of farming in Europe Scientific Foresight Study. Brussels, Belgium. Available from: http://www.europarl.europa.eu/RegData/etudes/STUD/2016/581892/EPRS_STU(2016)581892_EN.pdf [Accessed: 19 April 2017].

Sengupta, S. & Lee, W.S. (2014). Identification and determination of the number of immature green citrus fruit in a canopy under different ambient light conditions. Biosystems Engineering. 117. pp. 51–61.

Sepúlveda-Reyes, D., Ingram, B., Bardeen, M., Zúñiga, M., Ortega-Farías, S. & Poblete-Echeverría, C. (2016). Selecting canopy zones and thresholding approaches to assess grapevine water status by using aerial and ground-based thermal imaging. Remote Sensing. 8 (10). p. 822.

Smart, R. & Robinson, M. (1991). Sunlight into wine; A handbook for winegrape canopy management. Adelaide: Winetitles.

Smit, J.L., Sithole, G. & Strever, A.E. (2010). Vine signal extraction and application of remote sensing in precision viticulture. South African journal of enology and viticulture. 31 (2). pp. 65–74.

Sonka, M., Hlavac, V. & Boyle, R. (2008). Image processing, analysis, and machine vision. 3rd Ed. H. Gowans (ed.). Toronto, Ontario: Thomson Learning.

D.W. Sun (ed.) (2016). Computer vision technology for food quality evaluation. 2nd Ed. Amsterdam: Elsevier.

Szeliski, R. (2011). Computer Vision: Algorithms and Applications. 1st Ed. D. Gries & F. B. Scheneider (eds.). London: Springer-Verlag London.

Tagarakis, A.C., Koundouras, S., Fountas, S. & Gemtos, T. (2017). Evaluation of the use of LIDAR laser scanner to map pruning wood in vineyards and its potential for management zones delineation. Precision Agriculture. pp. 1–14.

Tang, J., Woods, M., Cossell, S., Liu, S. & Whitty, M. (2016). Non-productive vine canopy estimation through proximal and remote sensing. In: 5th IFAC Conference on Sensing, Control and Automation Technologies for Agriculture AGRICONTROL 2016. 2016, Seattle, WA, USA: IFAC, pp. 398–403.

Tardaguila, J., Baluja, J., Arpon, L., Balda, P. & Oliveira, M. (2011). Variations of soil properties affect the vegetative growth and yield components of 'Tempranillo' grapevines. Precision Agriculture. 12 (5). pp. 762–773.

Tisseyre, B., Mazzoni, C., Ardoin, N. & Clipet, C. (2001). Yield and harvest quality measurement in precision viticulture—application for a selective vintage. In: G. Grenier & S. Blackmore (eds.). Proceedings of the 3rd European Conference on Precision Agriculture. 2001, Montpellier, France: agro-Montpellier, pp. 133–138.

Tregoat, O., Ollat, N., Grenier, G. & Van Leeuwen, C. (2001). Etude comparative de la précision et de la rapidité de mise en oeuvre de différentes méthodes d'estimation de la surface foliaire de la vigne. Journal International Des Sciences de La Vigne et Du Vin. 35 (1). pp. 31–39.

Wample, R.L., Mills, L. & Davenport, J.R. (1999). Use of precision farming practices in grape production. In: R. P.C., R. R.H., & L. W.E. (eds.). Proceedings of the IV international conference on precision agriculture. 1999, Minneapolis: American Society of Agronomy, Crop Science Society of America, Soil Science Society of America, pp. 897–905.

Wang, Q., Nuske, S., Bergerman, M. & Singh, S. (2012). Automated crop yield estimation for apple orchards. Proceedings of International Symposium of Experimental Robotics. (ISER).

Wolpert, J.A. & Vilas, E.P. (1992). Estimating vineyard yields: Introduction to a simple, two-step method. American Journal of Enology and Viticulture. 43 (4). pp. 384–388.

Zarco-Tejada, P.J., Hubbard, N. & Loudjani, P. (2014). Precision agriculture: an opportunity for EU farmers - Potential support with the CAP 2014 - 2020. Brussels, Belgium. Available from: http://www.europarl.europa.eu/RegData/etudes/note/join/2014/529049/IPOL-AGRI_NT(2014)529049_EN.pdf [Accessed: 29 January 2017].

Zerger, A., Rossel, R.A.V., Swain, D.L., Wark, T., Handcock, R.N., Doerr, V.A.J., Bishop-Hurley, G.J., Doerr, E.D., Gibbons, P.G. & Lobsey, C. (2010). Environmental sensor networks for vegetation, animal and soil sciences. International Journal of Applied Earth Observation and Geoinformation. 12 (5). pp. 303–316.

Zhang, N., Wang, M. & Wang, N. (2002). Precision agriculture—a worldwide overview. Computers and Electronics in Agriculture. 36 (2). pp. 113–132.